

**THE USE OF CHEMOSTRATIGRAPHY AND GEOCHEMICAL VECTORING AS AN
EXPLORATION TOOL FOR PLATINUM GROUP METALS IN THE PLATREEF,
BUSHVELD COMPLEX, SOUTH AFRICA:
A CASE STUDY ON THE TWEEFONTEIN AND SANDSLOOT FARMS**

by

Marcelene Andrews



A FULL THESIS SUBMITTED IN FULFILMENT OF THE REQUIREMENTS FOR A
MASTERS DEGREE IN GEOLOGY, FACULTY OF SCIENCES,
UNIVERSITY OF THE WESTERN CAPE

Supervisor: Prof. C. Okujeni

Co-supervisors: Dr. R. bailie and Dr. A. Siad

November 2015

DECLARATION

I declare that *the use of chemostratigraphy and geochemical vectoring as an exploration tool for platinum group metals in the Platreef, Bushveld Igneous Complex, South Africa: a case study on the Tweefontein and Sandsloot farms* is my own and unaided work. It has not been submitted before for any degree or examination in any other university. All the sources I have used or quoted have been indicated and acknowledged as complete references.

Candidate: Marcelene Andrews



.....
Signature of Candidate

UNIVERSITY of the
WESTERN CAPE

DATE: _____ of _____ **2016**

KEYWORDS

Bushveld Complex

Platreef

Sandsloot farm

Tweefontein farm

Chemostratigraphy

Platinum Group-Elements

Statistical Techniques

PGE Mineralisation

Metasomatism



ABSTRACT

The Platreef is known for its complexity and its heterogeneous lithologies, coupled with an unpredictable PGE and BMS mineralisation. The motivation behind this study was to aid mining geologists in targeting mineralisation irrespective of the farm. It is known that the Platreef generally overlies different footwall lithologies at individual farms. Thus, the aims of this study were firstly to investigate the potential of chemostratigraphy by delineating indices indicative of distinctive lithological layers. These indices were then tied to the second aim; which were to use geochemical vectoring, which is process-based, to target the PGEs at two different farms.

This study included three drillcores: from the farms Sandsloot (SS339) and Tweefontein (TN754 and TN200). The footwall units at Tweefontein are shales of the Deutschland Formation and the Penge banded iron formation; and at Sandsloot it is the Malmani Subgroup dolomites. Samples included 121 quarter cores, used for petrographical and geochemical studies. The elemental rock composition was determined by XRF and ICP-OES analyses. The approach also included statistical and mass balance methods to understand the geological and geochemical controlling processes.

Initially, the Platreef package at both farms was petrographically divided into three main layers: pyroxenite, and two distinctive feldspathic pyroxenites (FP-I and FP-II). However, the pyroxenites were also further separated as P-I and P-II, because of a higher notable difference in the degree of alteration within P-I. Progressive degrees of metasomatism were further observed in the lithologies, e.g. within the Platreef package, where feldspathisation was potentially the main metasomatic process.

Many geochemical plots (corroborated by the petrographical and mass balance results) illustrated that the feldspathisation were linked to an increase in the content of Al_2O_3 and CaO , and coupled with a decrease in content of Fe_2O_3 and MgO . Together with other geochemical trends, geochemically distinct units of the Platreef package could be discriminated with a metasomatism index (MI; $\text{CaO} + 10\text{Na}_2\text{O} / \text{CaO} + 10\text{Na}_2\text{O} + \text{Fe}_2\text{O}_3 + \text{MgO}$). The ensuing MI is lowest for the P-II pyroxenite and shows a progressive increase through FP-I, P-I to the highest values in FP-II. Geochemical layering were also observed in the calcsilicates and hornfels; e.g. a progressive decrease in the content of Fe_2O_3 , Al_2O_3 , Ce, Co, Cu, Ni, Zn, Zr, Au, Pd and Pt from the hornfels subunits H-I, H-II to H-III and an increase in of SiO_2 , Fe_2O_3 , TiO_2 , SO_3 , Co, Cu, Ni, Rb, V and Zn content from CS-I, CS-II to

CS-III. Correlating the pyroxenites and feldspathic pyroxenites spatially from one drillcore to another were hindered, hence, chemostratigraphy were not completed.

In terms of vectoring, it was essential to establish a possible link between the metasomatism index and the nature and style of the PGE and/or BMS mineralisation. The Hornfels subunit H-I and calcsilicate subunit CS-III were the main carriers of BMS and PGE. The Platreef package were more complicated: P-I (low PGE, low BMS); P-II (low PGE, high BMS); FP-II (high PGE, low BMS); and FP-I (high PGE, high BMS).

Element indices (e.g. Cu+Ni and Co+Zn) were developed to define a consistent gradient indicative of these ore subunits. A validation process to assess the metasomatism index (MI), base metal indices and PGE distribution within the individual drillcores (TN754, TN200 and SS339) were then undertaken. The results were that the MI ranges were similar in all drillcores, and discriminated the subunits of the Platreef package, gabbro-norites and even the calcsilicates. The base metal ratios (e.g. Ni/Co and Cu/Co) were indicative of the PGE rich zones. Trends of the base metal ratios reflected a strong positive relationship with the MI within the Platreef package and the calcsilicates. However, the opposite trend is observed with the hornfels.

In conclusion, the MI could potentially be a strong vector of high PGE and BMS mineralisation. It is also possible to discriminate lithologies within the Platreef package with the MI. However, it should be noted that the limitation of this study is that the results are based on three drillcores. The Platreef is heterogeneous at individual farms and extremely diverse across the northern limb. Therefore, future research could be undertaken to validate these findings, by using a bigger drillcore database.

ACKNOWLEDGEMENTS

A special thanks to AngloPlatinum and its staff for making the drillcore information and samples available for this study. This study was funded by the National Research Foundation and later by Inkaba yeAfrica, which is highly appreciated.

My gratitude is further extended to my supervisor, Prof. Okujeni, for his academic guidance. Special thanks to my co-supervisors, Dr. Bailie and Dr. Siad, and each staff member in the Earth Sciences Department at the University of the Western Cape. My acknowledgments are also extended to Ms. Crowley and Mr. Meyer for the XRF analysis and the thin sections preparation. I appreciate all my colleagues, Tshipeng Mwenze, Yafah Williams and Janine Becorney, who have been motivating influences.

I have countless appreciations for Prof. Holtman who has been a different pillar of support. Thank you for the guidance and support.

Lastly, but definitely not the least, a special thanks to my family and husband, Velasco, for their continuous support, patience and love.

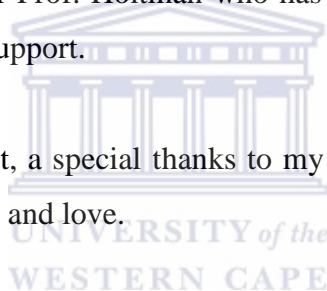



TABLE OF CONTENTS

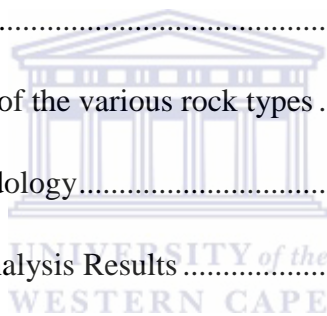
Declaration.....	ii
Keywords.....	iii
Abstract.....	iv
Acknowledgements.....	vi
Table of contents.....	vii
List of figures.....	xii
List of tables.....	xv
 The logo of the University of the Western Cape, featuring a classical building with columns and a pediment, with the text 'UNIVERSITY of the WESTERN CAPE' below it. CHAPTER 1.....	1
1. INTRODUCTION.....	1
1.1 Background.....	1
1.1.1 Preamble.....	1
1.1.2 Bushveld Complex (BC).....	2
1.1.3 Platreef.....	4
1.2 Problem statement.....	4
1.3 Aims / objectives.....	5
1.4 Approach.....	6
1.5 Chemostratigraphy and geochemical vectoring.....	7
1.6 Study Area.....	8
CHAPTER 2.....	9

2. REGIONAL AND LOCAL GEOLOGY	9
2.1 Regional Geology.....	9
2.1.1 Historical overview (Bushveld Complex)	9
2.1.2 Bushveld Complex	10
2.1.3 Rustenburg Layered Suite	11
2.1.4 Northern Limb of the Bushveld Complex	12
2.1.5 The Platreef.....	13
2.2 Local Geology	17
 CHAPTER 3	 19
3. METHODOLOGY	19
3.1 Field methodology.....	19
3.1.1 Core logging and sampling.....	19
3.2 Petrography	19
3.3 Chemical analysis.....	20
3.3.1 Sample preparation	20
3.3.2 X-Ray Fluorescence Spectrometry (XRF) Analysis	20
3.3.3 ICP-MS (Fire Assay) Analysis	21
3.3.4 QA / QC.....	21
3.4 Data evaluation.....	23



CHAPTER 4	24
4. LITHOLOGIES AND PETROGRAPHY.....	24
4.1 Introduction	24
4.2 Platreef nomenclature.....	24
4.3 Lithologies.....	25
4.4 Petrography	27
4.1.1 Platreef package.....	27
a. Pyroxenite subunit I (P-I)	27
b. Pyroxenite subunit II (P-II).....	30
c. Feld. Pyroxenite I (FP-I).....	30
d. Feld. Pyroxenite II (FP-II)	31
4.1.2 Metasedimentary rocks.....	32
a. Hornfels subunit I (H-I)	32
b. Hornfels subunit II (H-II)	34
c. Hornfels subunit III (H-III).....	35
d. Calcsilicate subunit I (CS-I)	35
e. Calcsilicate subunit II (CS-II).....	36
f. Calcsilicate subunit III (CS-III).....	36
4.1.3 Main zone gabbronorite.....	38
4.5 Stratigraphy	39
4.5.1 TN200.....	39
4.5.2 TN754.....	41
4.5.3 SS339.....	43

4.6 Summary	45
CHAPTER 5	46
5. GEOCHEMISTRY	46
Preamble.....	46
i. Geochemical classification of the rock subunits	47
ii. Geochemical characterisation of the rocks and subunits.....	47
iii. Mass Balancing	49
iv. Chemostratigraphy	49
v. Geochemical vectoring	49
5.1 Geochemical classification of the various rock types	50
5.1.1 Cluster analysis methodology.....	50
5.1.2 Hierarchical Cluster Analysis Results	51
5.2 Geochemical characterisation of the various rock types	53
5.2.1 Introduction	53
a. Statistical summary.....	54
b. Box and whisker plots	54
c. Spider diagrams	55
5.2.2 Hornfels	57
5.2.3 Calcsilicates	61
5.2.4 Platreef package.....	65
5.2.5 Gabbronorite	65
5.2.6 Summary.....	72



5.3 Metasomatic studies at the farms Tweefontein and Sandsloot	74
5.3.1 Introduction	74
5.3.2 Principles of the mass balance study	75
5.3.3 Mass-balance evaluation.....	78
a. EASYGRESGRANT software	79
5.3.4 Mass balance in the hornfels and pyroxenite subunits at Tweefontein	82
5.3.5 Mass balance of the calcsilicates and pyroxenite subunits at Sandsloot	85
5.3.6 Mass balance in the pyroxenite subunits at Tweefontein and Sandsloot	88
5.3.7 Summary.....	89
5.4 Chemostratigraphy and Vectoring	92
5.4.1 Introduction	92
5.4.2 Geochemical Indices.....	94
5.4.3 Feldspathisation or metasomatic index.....	95
5.4.4 Relationships between the feldspathisation index and the BMS mineralisation	96
5.4.5 Vectoring towards PGE mineralisation	97
5.4.6 Downhole plots:.....	101
 CHAPTER 6	 105
6. DISCUSSION AND CONCLUSIONS	105
6.1 Discussion	105
6.1.1 Introduction	105
6.1.2 Chemostratigraphy.....	106
a. Platreef package.....	106

b. Cyclic layering.....	107
c. Metasomatism index	109
d. Floor rocks	110
6.1.3 Vectoring	112
6.1.4 Shortcomings and recommendations.....	113
a. Shortcomings	113
b. Recommendations	113
6.2 Conclusions	114
REFERENCES	116
APPENDICES	131



LIST OF FIGURES

Figure 1.1: A geological map of the Bushveld Igneous Complex (Reczko et al, 1995; Cawthorn and Lee; Barnes and Maier, 200)	1
Figure 1.2: A geological map of the Platreef, northern limb, Bushveld Igneous Complex. Illustrating the various floor rocks, the extent of the Platreef and with the overlying hangingwall rocks (modified from van der Merwe, 1978; Ashwal et al., 2005, Kinnaird and McDonald, 2005).	3
Figure 3.1: The above diagrams illustrate the precision control scatter plots of the analytical data. A and B: Scatter plots of the major elements SiO ₂ and MgO (in wt %). C and D: Scatter plots of the trace elements Sr and Rb (in ppm).	22
Figure 4.1: Photomicrographs of pyroxenites encountered at both farms.	29
Figure 4.2: Photomicrographs of hornfels encountered at the farm Tweefontein. Panel (A and B): Hornfels subunit I from drillcore TN200. Where A is under plane polarised light and B under crossed polars. Panel (C and D): Hornfels subunit II, from drillcore TN754. Where C is under plane polarised light and D under cross polars . Panel (E and F):	

Hornfels subunit III from the drillcore TN754. Where E is under plane polarised light and F is under crossed polars.	33
Figure 4.3: Photomicrographs of calc-silicates encountered at the farm Sandsloot. Panel (A and B): Calc-silicate subunit I from drillcore SS339. Where A is under plane polarised light and B under crossed polars. Panel (C and D): Calc-silicate subunit II, from drillcore SS339. Where C is under crossed polars, and D under plane polarised light . Panel (E and F): Calc-silicate subunit III from the drillcore SS339. Where E is under crossed polars, and F under plane polarised light.	37
Figure 4.4: Photomicrographs of gabbronorite encountered at the farms Sandsloot and Tweefontein. Panel (a): illustrates the Main zone gabbronorite at Sandsloot under crossed polars, and panel (b) illustrates the Main zone gabbronorite found at Tweefontein.....	38
Figure 4.4: Stratigraphic logs of the drillcores studied on the farms Tweefontein 238 KR (TN754 and TN200) and Sandsloot 236 KR (SS339). The figure illustrates the floor rocks; calc-silicate and hornfels at Sandsloot and Tweefontein respectively. The Platreef lithologies occur in varying thicknesses, and the drillcores are capped by the hanging wall gabbronorite. Later granitic veins cut across the Tweefontein drillcores.	44
Figure 5.1: Dendrogram illustrating clusters of samples from the data of boreholes TN754, TN200 and SS339. These clusters represent all samples from all rock types, where annotations show the respective subunits.....	52
Figure 5.2: Box and whisker plots showing the variation of major elements for the three subunits of the hornfels (i.e. subunits H-I, H-II and H-III).....	58
Figure 5.3: Trace-element compositions of the hornfels subunits, where each sample in the subunit is plotted (primitive mantle normalization values from McDonough and Sun, 1989)	60
Figure 5.4: Box and whisker plots of various major elements for the three subunits of the calc-silicates (i.e. CS-I, CS-II and CS-III).	63
Figure 5.5: Trace-element compositions of the calc-silicate subunits and their individual samples (primitive mantle normalization values from McDonough and Sun, 1989).	64
Figure 5.6: Box and whisker plots for the pyroxenite subunits, showing the various major elements. These pyroxenites are also compared with the gabbronorites.	68

Figure 5.6: Trace-element compositions of pyroxenite subunits and their individual samples (primitive mantle normalization values from McDonough and Sun, 1989).	69
Figure 5.8: Trace-element compositions of gabbro-norites (primitive mantle normalization values from McDonough and Sun, 1989).	72
Figure 5.9: An example of the isocon diagram. Here the least altered pyroxenite (P-II) is plotted against the more altered pyroxenite (FP-II). The lines represent the constant mass (CM) and the constant volume (CV). The figure reflects two different scales: (A) the original view or scale; and (B) represents the extended view (in a stacked manner).	76
Figure 5.10: Is an example of the isocon diagrams of the hornfels subunit H-I (least altered) relative to the more altered hornfels subunit H-III.	77
Figure 5.11: An example of the isocon diagrams of the calc-silicates subunit CS-I (least altered) relative to the more altered calc-silicate subunit CS-III.	84
Figure 5.12: Illustrates bivariate plots of the immobile and mobile elements. (A) the immobile elements TiO ₂ against Zr; (B-F) the immobile Zr against the mobile major elements; SiO ₂ , Al ₂ O ₃ , Fe ₂ O ₃ , MgO and CaO. It is evident how Al ₂ O ₃ and CaO are clear indicators of feldspathisation.	93
Figure 5.13: Illustrates bivariate plots of the Zr against Ba and Sr respectively	95
Figure 5.14: Illustrates the index $(CaO + 10Na_2O / CaO + 10Na_2O + Fe_2O_3 + MgO)$ against (A) SiO ₂ ; (B) validation of the index against Al ₂ O ₃ ; and (C-E) BMS mineralisation.	95
Figure 5.15: Illustrates the feldspathisation index against ratios of Ni/Cu, Cu/Co, Ni/V, Ni/Co, Cu/Zn and also Cu+Ni.	98
Figure 5.16: Ratios created against PGEs, with the aim of targeting the PGE mineralisation. 99	
Figure 5.17: Downhole plot of borehole SS339. This plot shows the down hole geochemical variations in this drillcore.	100
Figure 5.18: Downhole plot of borehole TN754. This plot shows the down hole geochemical variations in this drillcore.	103
Figure 5.19: Downhole plot of borehole TN200. This plot shows the down hole geochemical variations in this drillcore.	104

LIST OF TABLES

Table 4.1 List of igneous and metasedimentary rocks sampled at the two farms (Tweefontein and Sandsloot). The list include the number of samples per rock type	27
Table 4.2 A petrographical summary of the lithologies of interest: subunits of the hornfels (H-I, H-II and H-III), subunits of the calc-silicates (CS-I, CS-II and CS-III) and the subunits of the Platreef package (P-I, P-II, FP-I and FP-II).....	44
Table 5.1: Statistical summary of oxides (wt. %), trace elements (ppm) and PGE (g/t) for hornfels accompanied by a summary of anomalies MN for hornfels.....	56
Table 5.2: Statistical summary of oxides (wt. %), trace elements (ppm) and PGE (g/t) for calc-silicate rocks.	62
Table 5.3: Statistical summary of oxides (wt. %), trace elements (ppm) and PGE (g/t) for Pyroxenites	66
Table 5.4: Statistical summary of oxides (wt. %), trace elements (ppm) and PGE (g/t) for gabbro-norites. Mean values for feldspathic pyroxenite, pyroxenite, hornfels and calc-silicates are included for comparison.	71
Table 5.5: Shows the median concentrations of hornfels and pyroxenite subunits from the samples of Tweefontein. This is together with the median concentrations of the calc-silicates and the pyroxenite subunits from samples at Sandsloot. All the oxides are in wt. % and trace elements in ppm.	77
Table 5.6: Shows the mass balance calculations for median concentrations for the hornfels and their accompanied pyroxenites (at Tweefontein) by using the clustering of slopes method (oxides are in wt% and trace elements in ppm).	81
Table 5.7: Shows the mass balance calculations for median concentrations for the calc-silicates and their accompanied pyroxenites (at Sandsloot) by using the clustering of slopes method (oxides are in wt% and trace elements in ppm).	84
Table 5.8: Shows the mass balance calculations for median concentrations for pyroxenites (at Tweefontein vs Sandsloot) by using the clustering of slopes method (oxides are in wt% and trace elements in ppm).	87

CHAPTER 1

1. INTRODUCTION

1.1 Background

1.1.1 Preamble

The last two decades has seen an increase in exploration for Platinum-group element (PGE) mineralisation within the Platreef, in the northern limb of the Bushveld Complex (BC), in South Africa (Armitage et al., 2002; McDonald et al., 2005; Kinnaird and McDonald, 2005; Holwell and McDonald, 2006; Hutchinson and McDonald, 2008). The Bushveld Complex (see Fig. 1.1) serves as the largest single reserve in South Africa, and hosts approximately 89% of world's platinum-group metal reserves (U.S. Geological Survey, Mineral Commodity Summaries, 2007).

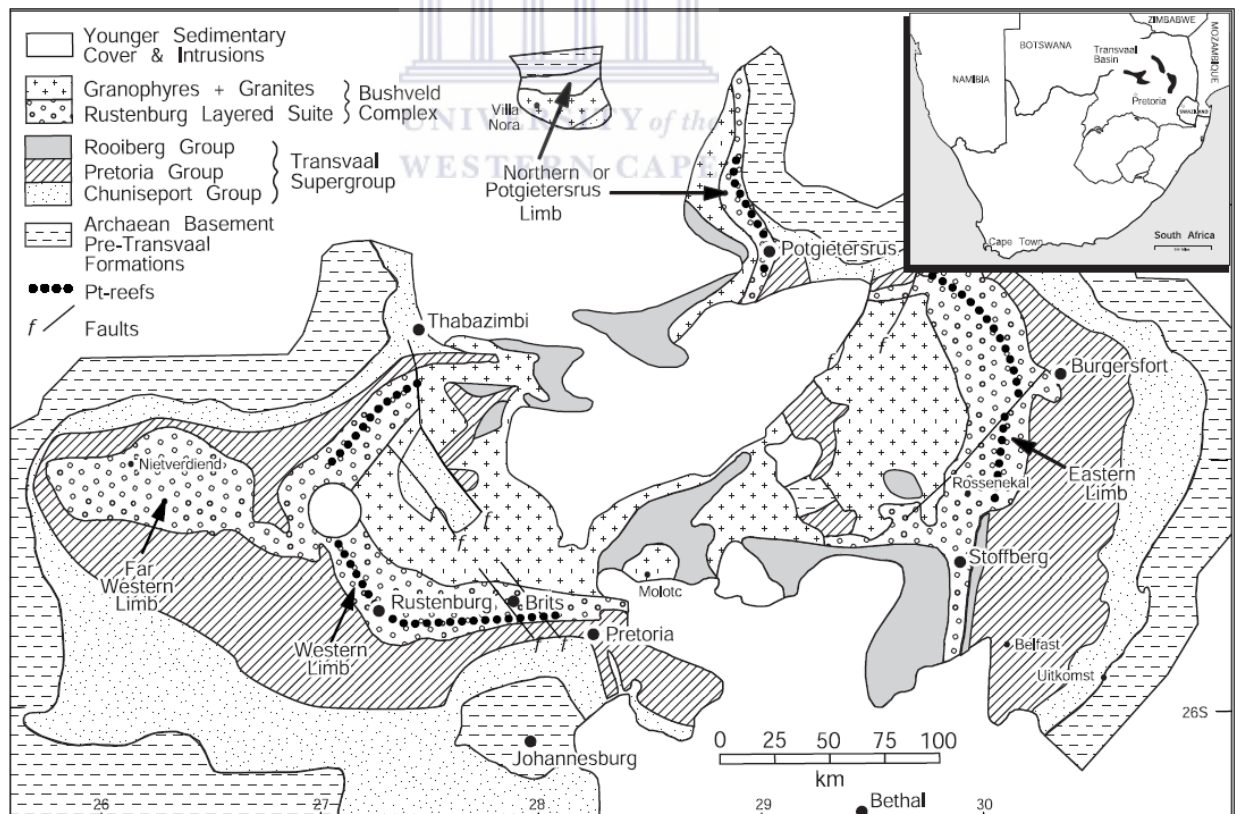


Figure 1.1: A geological map of the Bushveld Complex (Reczko et al., 1995; Cawtorn and Lee, 1998; Barnes and Maier, 2002).

The BC contains the most abundant Pt (75%), Pd (52%) and Rh (82%) resources of the world (Naldrett et al., 2009). The Platreef (see Fig. 1.2) may be less important than the other reefs in the BC, that is in term of total reserves and mining activity; but is still one of the world's largest PGE deposits in its own right (Pronost et al., 2008).

The renewed demand for Pt ores in the last 10 years has focussed exploration interest on the Platreef. The Platreef is geologically more complex than any of the PGE-bearing horizons (or reefs) in the BC (Viljoen and Schürmann, 1998; Bye, 2001; Kinnaird and Nex, 2003). It has been the focus of intense studies by many researchers. Today the Platreef is being exploited for PGE, Cu, Ni and Au mineralisation (Kinnaird et al., 2005; Holwell and McDonald, 2006).

There have been serious challenges in locating the PGE mineralisation in the Platreef using the traditional mineral exploration methods. New practical tools, approaches and solutions are needed for the multifaceted Platreef.

1.1.2 Bushveld Complex (BC)

The BC is ~2.06 Ga old (Walraven et al., 1990) and located in the northeastern part of South Africa. It has an extent area of ~ 65,000 km², with 9 km maximum thickness of rocks (Eales et al., 1993; Kruger, 2005). It has layered mafic and ultramafic rocks also known as the Rustenburg Layered Suite (RLS; South African Committee on Stratigraphy, 1980). The BC is a magmatic-type deposit predominantly hosted within a package of pyroxenites. Processes of chemical and physical fractionation led to the concentration of important platinum group element (PGE) deposits (Boorman and Boudreau, 2002). The RLS is exposed in three main limbs referred to as the Eastern, Western and Northern limbs. The PGE mineralisation is hosted within these three layers: The Merensky Reef and the Upper Group 2 (UG-2) chromitite, from the upper part of the Critical Zone (CZ), which occur in the Eastern and Western limbs of the Complex; and the Platreef, which occurs at the base of the igneous sequence in the Northern limb of the BC (Lee, 1996; Barnes and Maier, 2002). The term “reef” is a mining rather than a lithological term, and refers to a layer which is sufficiently enriched in PGE to be exploited (Barnes and Maier, 2002).

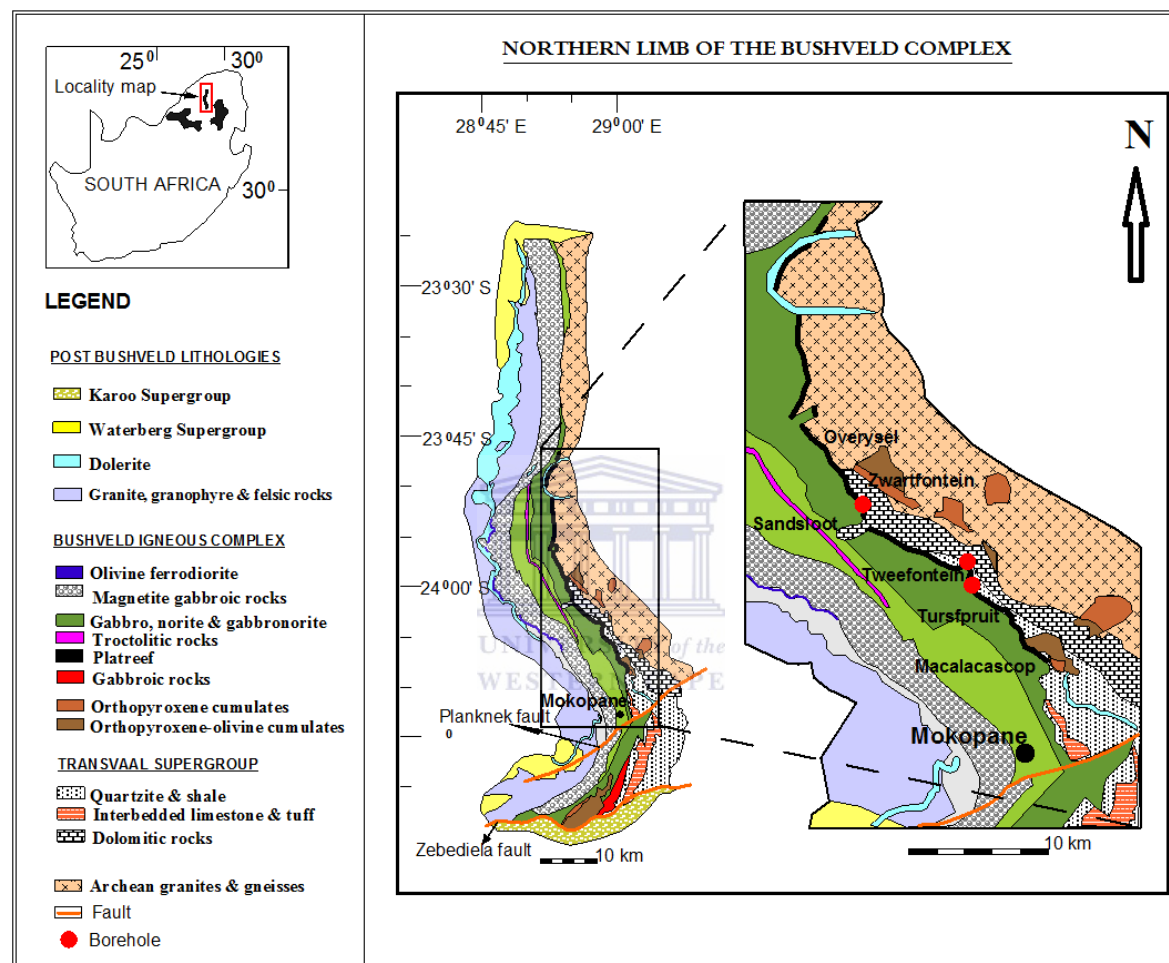


Figure 1.2: A geological map of the Platreef, northern limb, Bushveld Complex. This map illustrates the various floor rocks, the extent of the Platreef and the contact with the overlying hanging wall rocks (modified from van der Merwe, 1976; Ashwal et al., 2005; Kinnaird and McDonald, 2005).

1.1.3 Platreef

The Platreef (see Fig. 1.2) is a PGE deposit in the form of a mafic to ultramafic, tabular body at the base of the northern limb of the Bushveld Complex. It is comprised of a 10 to 400 m thick package (Kinnaird et al., 2005; Pronost et al., 2008; Ihlenfeld and Keays, 2011). The Platreef rocks are dominated by variable proportions of norites, gabbros, peridotite, serpentinite, pyroxenites, rare dunites, and xenoliths of meta-sedimentary rocks (Armitage et al., 2002; McDonald et al., 2005; Kinnaird et al., 2005; Hutchinson and Kinnaird, 2005). The Platreef stretches ~ 30 km north-west of Mokopane, and is overlain by the Main Zone (MZ) of the BC (Armitage, 2011). It rests north of the town of Mokopane (formerly Potgietersrus), upon a succession of progressively older sedimentary units of the Proterozoic Transvaal Supergroup (McDonald et al., 2009 and its references). Lithologies include quartzite, shale, iron formation and dolomite. The footwall transgresses into Archaean granites-gneisses northwards (Cawthorn and Walraven, 1998).

Mineralisation of PGE and Base Metal sulphide (BMS) are sporadic and occur over a zone up to 400 m in width (Gain and Mostert, 1982; Holwell and McDonald, 2006). PGE mineralisation in the Platreef is the result of a complex interplay between magmatic, syn- and post magmatic processes (Hutchinson and Kinnaird, 2005). Previous researchers have noted an abundance of dolomite xenoliths in the Platreef, where the xenoliths are evidence for interaction between the local footwall rock and the magma in the Platreef (Buchanan et al., 1981; Gain and Mostert, 1982; Cawthorn et al., 1985; Barton et al., 1986; Harris and Chaumba, 2001).

1.2 Problem statement

There are many challenges where the Platreef is concerned. Pronost et al. (2008) have outlined the various issues relevant to the formation of the Platreef, which are discussed within the research community. These issues are still a subject of debate, and are as follows: The sequence of intrusive events between the Platreef pyroxenite and the Main Zone magma. The overall effect of these intrusive events on the nature, style and grade of the mineralisation (Harris and Chaumba, 2001; Hutchinson and Kinnaird, 2005; Mayneruke et al., 2005; Kinnaird et al., 2005; Holwell and Jordaan, 2006; Howell and McDonald, 2007; and Pronost et al., 2008).

There is an uncertainty of the genesis of the Platreef, and its relationship with the rest of the Rustenburg Layer Suite of the BC (McDonald et al., 2005; Kruger, 2005; Pronost et al., 2008 and Reisberg et al., 2011). The nature and amount of crustal contamination, and the relationship between contamination and PGE mineralisation is also uncertain (Buchanan et al., 1981; Cawthorn et al., 1985; Barton et al., 1986; Harris and Chaumba, 2001; McDonald and Holwell, 2007; Pronost et al., 2008).

For the purpose of this thesis, certain problems regarding the Platreef have been emphasised and discussed. These highlighted problems are: The Platreef displays complex and heterogeneous lithology and mineralisation patterns that distinguish its genesis from that which was proposed for the Merensky Reef and UG-2 (Lee, 1996; Cawthorn and Lee, 1998; Barnes and Maier, 2002; Kinnaird, 2005). The style and grade of mineralisation varies not only in different regions of the Platreef, but also within different pyroxenitic packages from the same region (Hutchinson and Kinnaird, 2005; Yudovskaya and Kinnaird, 2010). This makes it difficult to predict mineralisation as it may occur anywhere within the succession (Cawthorn et al., 2006). Studies have also shown that the amount of associated fluid activity has had variable impact on the base sulphide mineralisation and PGE mineralogy, and spatial distribution as well as a decoupling or fractionation of the PGE relative to the position of the floor rocks (Gain and Mostert, 1982; Holwell and McDonald, 2006). The geological and geochemical controls of the mineralisation are poorly understood and this therefore remains a subject debated amongst numerous researchers.

1.3 Aims / objectives

The above mentioned problems indicate the factors that have caused difficulties for most companies mining PGEs in the Platreef. It is difficult to define and target the PGE mineralisation within the Platreef. The ultimate aim of this thesis is to investigate the potential of chemostratigraphy and vectoring as significant tools for PGE mineralisation within the complex Platreef. The foundation behind this is to find efficient and feasible ideas by using simple inexpensive and fast methods. The methods should be unambiguous and straightforward, as new and effective exploration tools are needed to target the irregular mineralisation.

The first objective is to investigate the potential of chemostratigraphy by using the major and trace element geochemistry and identifying geochemically distinct layers and correlating them between the Sandsloot and Tweefontein farms. The second objective is to develop cost-effective geochemical vectors that locate PGE mineralised sections / rocks. Below is a detailed outline of the necessary approach that will lead to chemostratigraphy and vectoring in the Platreef.

1.4 Approach

Petrographical studies: The aim here is to identify, classify and characterise in detail the rock units found at the farms Tweefontein and Sandsloot by using core logging and optical microscopy. This chapter is the foundation for all other chapters. The objectives are to represent the three drillcores studied, to identify the mineralogy and various mineral abundances within the rock sequences, to identify their alteration and textural patterns, and their associated base metal sulphide (BMS) mineralisation.

Geochemical classification and characterisation of rocks studies: This section aims at classifying the rocks geochemically by using their chemical composition and the statistical method of hierarchical cluster analysis. The objectives are to enable confirmation of the major rock lithologies identified and observed in the petrography section, and to identify the individual samples that are associated with each rock lithology. The groups or clusters created will then be the foundation to characterise these rock types. Characterisation is done by using descriptive statistical analysis, box-whisker-plots and spider diagrams. This will enable the description of the variability of elements within each lithology and to graphically show comparison of the different rocks.

Mass balancing studies: The aim in this section is to launch a lithological investigation that uses immobile elements to calculate the mass changes that occur within the alteration zones, thus, it describes the chemical changes which took place in a rock after its formation. The idea is to assess the effect of interaction between the Platreef magma and the floor rocks at Sandsloot and Tweefontein, and to later establish chemostratigraphic units in altered and unaltered sequences.

This is to further aid in identifying distinctive rock units, and to assess the levels and effects of crustal contamination of the Platreef magma, and to show how this impacted the grade and style of mineralisation in the pyroxenite packages in various regions and along the strike of the Platreef.

Chemostratigraphy and vectoring: This section will focus on identifying geochemically distinct units, and correlating them by recognising the geochemical signatures between the two farms in the altered and unaltered rocks. It will develop element ratios, pathfinder elements or trace element signatures that are able to define a consistent gradient indicative of ore zone for mineral exploration. This will help to distinguish mineralised from barren geological complexes and will identify geochemical trends. The idea is to illustrate and define relationships between: (1) BMS mineralisation (i.e. Cu and Ni) and PGE (Pt and Pd); (2) define the relationships between the BMS and/or PGE with the most influential trace elements; and (3) define the relationship with the BMS and/or PGE with the rock layers at each farm. The ultimate aim is to vector towards the PGE mineralisation at both farms.

1.5 Chemostratigraphy and geochemical vectoring

The applications of chemostratigraphy and geochemical vectoring have been used as tools for exploration in a number of other studies (e.g. Large and Goldrick, 1998; Brand, 1999; Pearce, 1999; Ramkumar and Sathish, 2006; Urqueta et al., 2009). To date there is very little and no detailed published information reported on the Platreef using these tools.

Chemostratigraphy is the study of the variations in the chemical compositions of strata. It involves the use of multi-elements to characterise these strata into geochemically distinct units. These units are then correlated by recognising the comparison of the geochemical signatures in neighbouring sections (Pearce, 1999; Monterro et al., 2010). It is also used where other stratigraphic methods failed or may have restrictions (Ramkumar and Sathish, 2006). Chemostratigraphy has been implemented successfully in other complex geological areas (Pearce et al., 2010; Ratcliffe et al., 2010). Closest literature available to using these tools for PGE exploration is from Ames et al (2007) and Maier et al (2008).

Geochemical vectoring entails developing quantifiable element ratios, pathfinder elements or trace element signatures that are able to define a consistent gradient indicative of an ore zone

for mineral exploration. It can help to distinguish mineralised from barren geological complexes (Brand, 1999; Eilu et al., 2001; Ames et al., 2007) and it identifies geochemical trends (Rollinson, 1993). The development of alteration indices (e.g. Ishikawa et al., 1976) related to hydrothermal fluid - rock interaction surrounding massive sulphide deposits have proved very useful in mapping alteration zones and providing vectors to ore to assist mineral exploration. Recent studies on the Zn–Pb–Ag deposit at Lady Loretta, Queensland (Large and McGoldrick, 1998) have enabled the development of a lithogeochemical halo model including quantifiable geochemical vectors. Eilu and Mikucki (1998) used geochemical anomalies to vector towards gold mineralisation within the Bulletin lode-gold deposit. Brand (1999) used the element ratios in fresh komatiite rocks to point towards ore environments in nickel sulphide exploration.

1.6 Study Area

A suite of samples were taken from three drillcores (SS339, TN200 and TN754) across the Platreef in the Sandsloot and Tweefontein farms from the AngloPlatinum Mogalakwena mines (see Fig 1.2). These mines are situated near Mokopane in the Limpopo Province of South Africa. The Platreef, from south to north, consists of varying floor rocks at the different farms. Yudovskaya and Kinnaird (2010) have outlined the various floor rocks found at the farms located along the Platreef. This and more on the study area are discussed in detail within the next chapter.

CHAPTER 2

2. REGIONAL AND LOCAL GEOLOGY

2.1 Regional Geology

2.1.1 Historical overview (Bushveld Complex)

South Africa hosts the Bushveld Complex (BC; see Fig. 1.1) which is the largest layered igneous intrusion in the world (Vermaak and Von Gruenewaldt, 1986; Cawthorn, 1999; McDonald et al., 2009).

The first mention of platinum in the Bushveld Complex were in 1906, and by 1908, Hall and Humphrey reported that there are PGEs in the chromitite layers in the Rustenburg area (Viljoen and Schurmann, 1998). However, the Geological Survey of South Africa initially reported these amounts of platinum in the chromitite layers as uneconomic (Cawthorn, 1999). There have also been other PGE recoveries in South Africa (by 1919), for example in the Witwatersrand basin (Viljoen and Schurmann, 1998). By 1924, the discovery of the Merensky Reef (eastern Bushveld) was made by Dr. H. Merensky and Andries Lombaard (Cawthorn, 1999).

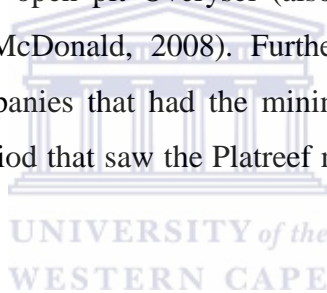
Merensky also identified the Platreef in 1925 (Cawthorn, 1999; Maier et al., 2012), and the first detailed geological descriptions of the Platreef were by Wagner (1929; Maier et al., 2012). De Villiers later remapped the entire northern limb during the years 1967 to 1970. He had previously mapped the Grasvally and Zoetveld (south of Mokopane) geology that concentrated on the chromite mineralisation, leading to the exploration events at that time (Van der Merwe, 2008).

Later, studies by Hulbert and von Gruenewaldt (1986) gave detailed petrological and whole rock chemical analysis of the Critical and Lower Zones at the Grasvally farm (Yudovskaya and Kinnaird, 2010; Maier et al., 2012). Together with others such as Van der Merwe (1976), Kinloch (1982), Cawthorn et al. (1985), Lee and Parry (1988); and Mitchell (1990), a significant amount of studies on the Northern Limb were undertaken.

Literature on the Northern Limb and active platinum productions were directly related to the platinum demand and price. However, there were also periods where mining ceased because of the lapse in platinum prices, e.g. in 1930 (Kinnaird and McDonald, 2005).

Most of the literature we have today started when Anglo American started its Platreef mining (Holwell et al., 2011). The platinum mining at the Anglo Platinum's Sandsloot open pit commenced in 1991. This was after significant mineralisation was described northwest of Mokopane (van der Merwe, 1976; White, 1994, van der Merwe, 2008). The expansion of exploration from other surrounding companies also aided the growing number of studies on the Northern Limb and thus the Platreef (Kinnaird and McDonald 2005; Holwell et al., 2011).

By 2008, only open pits by Anglo Platinum (e.g. Sandsloot and Zwartfontein) were producing ore. At this time, the open pit Overysel (also by Anglo Platinum) was under development (Hutchinson and McDonald, 2008). Further reading is found in Armitage (2011), which includes the companies that had the mining rights on the Platreef, and the details regarding the dormant period that saw the Platreef mining production being ceased in 1930.



2.1.2 Bushveld Complex

The BC is ~2.06 Ga old (e.g. Walraven et al., 1990; Scoates & Friedman, 2008; McDonald et al., 2009; Maier et al., 2012) and located in the northeastern part of South Africa where it has been emplaced into the Kaapvaal craton (e.g. Walraven et al., 1990; Cawthorn and Walraven, 1998; Scoates and Friedman, 2008; McDonald et al., 2009; Scoates et al., 2011). The BC has an extension of 450 km width along the east-west direction and 350 km length along the north-south axis (Naldrett et al., 2009).

The BC covers an area of approximately 65,000 km² (Kruger, 2005) and is comprised of four distinctive igneous suites. They are the early mafic sills (Uitkomst Complex), the Rooiberg felsites, the Rustenburg Layered Suite (RLS), and the younger Lebowa Granite Suite (Naldrett et al., 2009; 2012). The BC is spatially divided into five limbs; eastern-, western-, southeastern- (Bethal), far western- and northern limb (Wilson and Chunnnett, 2006; McDonald et al., 2009; Maier et al., 2013). The eastern and western limbs are roughly

symmetrical (McDonald et al., 2009), the northern limb is a sinuous outcrop, and the Bethal limb is covered by Karoo sedimentary rocks (Buchanan 1981; Eales and Cawthorn, 1996). The Paleaeoproterozoic Transvaal Supergroup sediments and the Archaean basement rocks were intruded by the igneous rocks of the BC (Walraven et al., 1990; Buick et al., 2001; Scoates and Friedman, 2008; McDonald et al., 2009).

Reisberg et al. (2011) summarises the controversy regarding the form and connection between these limbs. Based on gravity data and stratigraphic correlation, the western and eastern limbs show the most evidence of connectivity as interpreted by Cawthorn and Webb (2001). It was previously reported that the limbs are considered disconnected (Sharpe et al., 1980; Hatton and Schweitzer, 1995). The giant lopolithic form for the intrusion as suggested by Cawthorn et al. (1998) and Webb et al. (2004) coincided with the initial work by Hall (1932). However, differences with the far western, northern and southeastern limbs, in comparison to the eastern and western limbs are more pronounced (Eales and Cawthorn 1996). Thus, the connectivity between all the limbs should be considered as speculative (Cawthorn and Webb, 2001).



2.1.3 Rustenburg Layered Suite

The RLS is typically composed of ~8 km thickness of layered mafic – ultramafic rocks (Cawthorn et al., 2006, Naldrett et al., 2009). The RLS can be subdivided into five stratigraphic zones (where it is complete); Marginal Zone, Lower Zone, Critical Zone, Main Zone and Upper Zone (Hall, 1932; Eales and Cawthorn, 1996).

Generally, the zones are composed of the following; plagioclase to orthopyroxene cumulates (Marginal zone); harzburgite, dunite and bronzitite (Lower Zone); the Critical Zone is mainly orthopyroxenite, chromitite, pyroxenite, harzburgite, norite and anorthosite (Yudovskaya et al., 2013); the Main Zone can be gabbronorite, norite or anorthosite (Holwell et al., 2013); the Upper Zone consists of plagioclase, magnetite and iron-rich pyroxenes and olivine (Eales et al., 1993; Eales and Cawthorn, 1996; Barnes and Maier, 2002). More detailed descriptions and characteristics of these zones, and other general stratigraphy of the Bushveld Complex can be found in Maier et al. (2013) and all their references within.

The Critical Zone hosts the platineferous layers known as the Platreef (northern limb), the Upper Group Chromitite No. 2 (UG-2) and the Merensky Reef layers in the western and eastern limbs (e.g. Vermaak, 1976; McLaren, 1980, 1982; Lee, 1996; Schouwstra and Kinloch, 2002; Barnes and Maier, 2002). These layers contain the largest concentration of the PGEs in the world.

Many authors (see Reisberg et al., 2011 and their references) have considered the Merensky Reef and the Platreef to be equivalent because of petrographic resemblances. E.g., the mineralisation occurs in a coarse-grained feldspathic pyroxenite. However, there have been notable differences also, as the Platreef has higher nickel and sulphur contents than both the more sulphide-poor mineralisation in the UG-2 and Merensky Reef (Kinnaird et al., 2005; Hutchinson and McDonald, 2008; Yudovskaya and Kinnaird, 2010). The UG-2 is a chromitite layer, and the Merensky Reef is bounded by a top and bottom thin chromitite layers. The UG-2 generally consist of 60-90% chromite, and silicate minerals. PGMs present in the UG-2 Reef are highly variable, but generally consists of PGE sulphides; laurite, cooperite, braggite, and an unnamed PtRhCuS (Schouwstra and Kinloch, 2002). The UG-2 can be located 20 to 400m below the Merensky Reef (e.g. Vermaak, 1976; McLaren, 1980, 1982; Schouwstra and Kinloch, 2002). According to literature the vertical and lateral distribution of PGE in both the Merensky and UG-2 chromitite reefs are highly variable (see Cawthorn, 2010 and its references within). The Critical Zone is also host to all the 14 chromitite layers of the Bushveld Complex (Yudovskaya and Kinnaird, 2010). A more detailed summary of the Merensky Reef, the UG-2 and their differences with the Platreef is given by authors such as Naldrett et al., (2009); Maier et al. (2013) and Lomberg (2014). More detailed literature on the chromitites of the BC can be found by authors such as McCandless et al (1999); Yudovskaya and Kinnaird (2010); Naldrett et al (2011) and Yudovskaya et al (2013).

2.1.4 Northern Limb of the BC

The sinuous northern limb has a north to south orientation, and is separated from the rest of the eastern and western limbs by the Thabazimbi–Murchison Lineament (TML; Kinnaird et al., 2005; McDonald et al., 2009). The TML is a fault zone, which has been active from the Archaean till recent times (Good and de Wit, 1997; Yudovskaya and Kinnaird, 2010). The Zebediela fault and Ysterberg-Planknek faults forms part of the TML, which cuts the

northern limb in the southern part (McDonald et al., 2009; Yudovskaya and Kinnaird, 2010). The Zebediela fault is a prominent feature extending approximately 500 km in a NNE-SSW direction across the Kaapvaal Craton (Harris and Chaumba, 2001). Van der Merwe (1976) estimated the extent of the northern limb, to be 7,275 km², based on gravity data.

The RLS in the northern limb is subdivided into four units (Reisberg et al., 2011). The other zones consist of; pyroxenites and harzburgites, which are partly developed in the southern part of the northern limb (Lower Zone). The Critical Zone shows cyclic units of chromitite, pyroxenite, and norite cyclic. The Main Zone gabbro-norite and Upper Zone anorthosite, gabbro-norite and magnetite are all well developed in the northern limb (Holwell et al., 2013).

2.1.5 The Platreef

The Platreef is a PGE deposit in the form of a mafic-ultramafic, tabular body at the base of the northern limb of the BC (van der Merwe, 1976; Walraven et al., 1990). The Platreef extends for almost 30 km, and its variable thickness can range from <50 m to 400 m (Kinnaird et al., 2005; Armitage, 2011). The Platreef has a general strike of north to northwest at the surface, with a moderate dip of 40 - 45° to the west and southwest (Van Der Merwe, 1976; Viljoen and Schürmann, 1998, McDonald et al., 2009). However, the overall geometry appears to have been controlled by irregular floor topography (Kinnaird et al., 2005; Yudovskaya and Kinnaird, 2010; Armitage et al., 2011).

The Platreef is composed of heterogeneous and altered lithologies, comprising of pyroxenites with norites, peridotites and gabbros. The Platreef has variable footwall lithologies along its strike. These footwall rocks get successively older northwards and include the Transvaal Supergroup metasedimentary footwall units, and the oldest Archaean granite footwall (Kinnaird, 2005; and all its references). The horizon may be traced along the northern limb, until covered by sediments of the 1800-m.y Waterberg Group (White, 1994).

The Platreef is also devoid of any regular layering, contains minimal chromite, and has a mineralisation that may occur anywhere within the succession (Cawthorn et al., 2006). Holwell et al. (2005) describe in detail the relationship between the pyroxenites of the Platreef and the overlying gabbro-norites of the hangingwall. The sequence of intrusive events that affects the Platreef and the Main Zone magma; and the effect of these events on the

nature, style and grade of the mineralisation has been a subject of debate over the years (e.g. Harris and Chaumba, 2001; Hutchison and Kinnaird, 2005; Manyeruke et al., 2005; Kinnaird et al., 2005; Holwell and Jordaan, 2006; Howell and McDonald, 2007; and Pronost et al., 2008). Manyeruke et al. (2005) and Kinnaird et al. (2005) have suggested that the Platreef was intruded as a sill or series of sills (Pronost et al., 2008). McDonald and Holwell (2007) suggested that the Platreef sill network was without an overlying magma column initially. Manyeruke et al. (2005), Kinnaird et al. (2005), Maier et al. (2008), and Yudovskaya and Kinnaird (2010) suggest that these sill-like intrusions are composed of three geochemically distinct pyroxenites. However, it is normally not possible to distinguish between the different sills in core visually, but they can be separated on element ratios (e.g. Ni/Cu ratio; Yudovskaya and Kinnaird, 2010).

Yudovskaya and Kinnaird (2010) have outlined the Platreef nomenclature of these pyroxenites as initially proposed by Kinnaird et al. (2005). The Platreef host rocks are predominantly coarsegrained feldspathic pyroxenite (30 to 70 vol. % of cumulus orthopyroxene; 10 to 30 vol. % of intercumulus plagioclase; up to 20 vol. % post-cumulus clinopyroxene; together with minor phlogopite, quartz and accessory phases). Olivine pyroxenite and feldspathic harzburgite contain variable amounts of olivine (5 to 70 vol. %), and their plagioclase content may reach up to 10 to 15 vol. %. Yudovskaya and Kinnaird (2010) also further outline the geochemical characterisation of these pyroxenite sills. For example; in the southern sector, an upper pyroxenite will have higher MgO, and lower Al₂O₃ and CaO values than a lower pyroxenite (which is characterised by higher plagioclase content, with chemical heterogeneity).

Yudovskaya and Kinnaird (2010) further used the chromitite layers in the Platreef to ascertain whether any correlation can be made with the chromitite layers of the Bushveld Complex. This was to contribute to the debate on the correlation of the Platreef with the Critical Zone of the eastern and western limbs (see also van der Merwe, 1976; Kinnaird et al., 2005; Kruger, 2005; McDonald et al., 2005; Maier et al., 2008). They also used the chromitite correlation study to explain the relationship between the successions of the intrusive sills.

Kinnaird et al. (2005) further signifies the Platreef package is composed of an upward succession of dunite, serpentinitised peridotite, pyroxenite and feldspathic pyroxenite, to

melanorite through leuconorite to anorthosite. The feldspathic pyroxenite is considered the dominant rock type. Kinnaird et al. (2005) further mentions norite cycles. These include repetitive cycles of mafic-rich to mafic-poor layers that occur in the mid to upper portion of the Platreef. Typically, a cycle (from the base upward) is pyroxenite, feldspathic pyroxenite, melanorite, leuconorite with anorthosite. However, the cyclic packages are limited to correlation at short segments, and they are also more common in the southern sector of the Platreef.

The findings by Kinnaird et al., (2005) suggested that the Platreef is a result of multiple magmatic pulses of different compositions. Studies by McDonald and Holwell (2007) illustrated geochemical data showing trends appearing to be inconsistent with a single magma. McDonald and Holwell (2007) further concluded that the Platreef pyroxenite intruded as a crystal mush. They further suggested that PGE mineralisation in the Platreef originated from sulphides (PGE-rich) formed in magma conduits that fed magma chambers, and which were then transported by a later magma into the Platreef (Van der Merwe et al., 2012). Recently, Holwell et al. (2013) and their references (Holwell et al., 2005 and Holwell and Jordaan, 2006) suggested that there have been a magmatic break between the Platreef and the Main Zone intrusions. There is now a possibility that the Main Zone in the north may have been emplaced as a PGE-fertile magma, and had the potential to form the ore deposit.

Hutchinson and Kinnaird (2005) proposed a petrogenetic model that generally described the sequence of events and the distribution of mineralisation (Ni, Cu, PGE) of the northern limb. This model describes the formation of immiscible sulphide droplets. These sulphides scavenged for PGEs from a parental mafic magma before its emplacement. The post emplacement processes (country rock assimilation, footwall and magma interaction) resulted in the present distribution of sulphides and PGEs.

The isotopic study by Harris and Chaumba (2001) suggested that the Platreef shows evidence for post-magmatic fluid interaction, and that the assimilation of the floor rocks played a vital role in the origin and mineralisation. The variability of PGM assemblages, due to the nature of the floor rocks have also been discussed by other authors (e.g. Kinloch, 1982; Kinloch and Peyerl, 1990; Lee 1996; Viljoen and Schürmann, 1998; Holwell and McDonald, 2006, 2007; Hutchinson and McDonald, 2008; Holwell and McDonald, 2010).

Hutchinson and Kinnaird (2005) also suggest other processes in this petrogenetic model; such as devolatilisation and partial melting, infiltration of felsic magmas, contamination, variations in fS₂, later alteration processes, hydrothermal processes which remobilised the PGEs.

Kinnaird et al. (2005) suggested that the hydrothermal fluids redistributed the PGEs and this will explain the decoupling of base metal from PGE abundances in their study. They also distinguish between two types of pyroxenite (at Sandsloot) with a difference in mineralisation type. E.g. the mediumgrained pyroxenite is primary; however, the pegmatoidal pyroxenite contains mobilised sulphides. The mineralisation is not limited to a specific Platreef lithology, and good grade can occur anywhere in the Platreef package (e.g. either pegmatitic pyroxenite; feldspathic pyroxenite, or serpentinised peridotite).

Van der Merwe et al. (2012) explains the mineralogical distribution of the PGM is highly variable throughout the Platreef, a widespread prevalence, and general dominance, of PGE tellurides and bismuthotellurides is apparent (Lee 1996; Viljoen and Schürmann 1998; Schouwstra et al. 2000; Armitage et al. 2002; Cawthorn et al. 2002; Holwell and McDonald 2006; 2007; McDonald and Holwell 2011; Yudovskaya et al. 2013). Van der Merwe et al. (2012, and all references within), further explains that the extensive assimilation of floor rocks have played a role in the variability of PGM assemblages in the Platreef, and probably controlled the proportion of semimetals within the mineralising sulphide liquid as well as the amount of hydrothermal activity in the magmatic system. This contamination resulted in the local development, and the redistribution, of a variety of high- and low-temperature semi-metal alloys of the PGE. Van der Merwe et al, (2012) concluded that the PGMs are associated to a varying extent with BMS, suggesting the PGM genesis model, which involved the exsolution of the PGM from the BMS during cooling. Some PGE were redistributed and recrystallised during hydrothermal alteration, and hence the observed association of these minerals with secondary silicates. This contamination also explains why the Platreef deviates from the Merensky Reef and the UG-2 of the Bushveld Complex, in terms of PGE abundance. Also this will explain the decoupling of PGE from Cu and Ni (or sulphides) at some farms (Holwell and McDonald, 2007 and their references within).

Pronost et al. (2008) and its references (e.g. Harris and Chaumba, 2001; Holwell and McDonald, 2006) explains the composition and source effects of these fluids. Penniston-Dorland et al. (2008) and McDonald and Holwell (2011) proposed that the sulphur isotope

data reflect a dominantly magmatic signature for S in the Platreef. Ihlenfeld and Keays (2011) and Van der Merwe et al. (2012) concluded that it is possible that the pre-Platreef magmas may have undergone significant fractionation at the time they became sulphur-saturated, perhaps resulting in the concentration of semi-metals such as bismuth and tellurium (see also Hutchinson and Kinnaird, 2005; Hutchinson and McDonald 2008). Penniston-Dorland et al. (2012) suggested that the igneous rocks from the eastern and western Bushveld had a homogeneous magma prior to its emplacement in the upper crust. The possible sources for surface-derived sulphur were the Transvaal Supergroup sedimentary rocks, lower crustal metamorphosed sedimentary rocks, and sub-continental lithospheric mantle. Annotated by various authors (Sharpe et al., 1980; Cawthorn and Davies, 1983; Eales et al., 1996; Cawthorn and Walraven, 1998; Kruger, 2005), the RLS did not result from the crystallization of a single magma, but was emplaced as multiple influxes (Yudovskaya et al., 2013).

2.2 Local Geology

Two drillcores were sampled from the farm Tweefontein 238KR; namely, TN754 and TN200. This farm is located 14 km NNW of Mokopane. At this locality, the thickness of the Platreef ranges from 100 to 200 m (Nyama et al., 2005) and has a sharp contact with the overlying gabbro-norites of the Main Zone. The immediate footwall to the Platreef at this locality is rocks of the Deutschland Formation, which consists of predominantly shales that have undergone metamorphism. Banded ironstone of the Penge Formation underlies the Deutschland shales.

A comprehensive study on the Platreef's platinum group minerals at Tweefontein was completed by McCutcheon (2012). Platreef rocks that were observed in this study were composed of pyroxenites and norites with minor harzburgitic lithologies. These lithologies also contained numerous cross-cutting granitic veins. The Penge BIF consists of alternating magnetite and chert-rich layers, and occurs with ferruginous shale and quartzite at its base (Nex, 2005; references within).

The mineralisation style of the PGE grade profiles can vary from Tweefontein Hill southwards (McCutcheon, 2012), as the mineralisation becomes generally more bottom loaded, compared to the top loaded profiles at for example the northern farms like Overysel. The PGM assemblage, hosted by base metal sulphides and magmatic silicates, is dominated

by Pt-and Pd-bismuthides and -tellurides with minor PGE-sulphides and Pt-arsenides. It is thought that the PGE mineralisation at this locality is more closely associated with a pegmatoidal pyroxenite unit, which is generally below a thin chromitite layer from the top Platreef contact (White, 1994; Nichol and Kinnaird, 2008). In local depressions (e.g. at Tweefontein Hill), accumulations of massive sulphides has also been observed (White, 1994), which possibly affected the distribution of mineralisation (Kinnaird, 2005).

Armitage (2011) further gives a very detailed description and history of the Sandsloot open pit platinum mine. Here, together with other literature, a summary is given. At Sandsloot there is a mix of lithologies broadly described as gabbros and pyroxenites in variable states of alteration, overlain by a hangingwall of norites and gabbro-norites belonging to the Main Zone (Armitage, 2011). At this locality, the footwall consists of siliceous Malmani Dolomite of the Transvaal Supergroup (e.g. Holwell et al., 2007). The footwall has been subjected to variable degrees of retrograde alteration, where it has been metamorphosed to calcsilicate hornfels and metasomatised to clinopyroxenites (Wagner 1929; Armitage, 2011). Metasomatised dolomite xenoliths also occur, and are a significant component of the Platreef at Sandsloot, and may not be applicable regionally (Mitchell and Scoon, 2012).

Detailed studies of these variable lithologies are given by; e.g., Harris and Chaumba, 2001; Armitage et al., 2002; Holwell et al., 2005. Van der merwe et al. (2012), describes the Platreef as generally composed of PGM typically dominated by Pt-Pd tellurides and bismuthotellurides, PGM alloys, arsenides and rare PGE sulphides (Viljoen and Schürmann 1998; Schouwstra et al. 2000; Armitage et al. 2002; Holwell et al. 2006).

More detailed descriptions based on literature are given in Chapter 4 regarding the lithologies.

CHAPTER 3

3. METHODOLOGY

3.1 Field methodology

3.1.1 Core logging and sampling

The initial step of this investigation included logging, examination and sampling of three drillcores drilled at the Anglo - Mogalakwena Platinum Mines near Mokopane, in the Limpopo Province. Drillcores TN200 and TN754 were selected from the Tweefontein 238KR farm, and drillcore SS339 was selected from the Sandsloot 236KR farm. These drillcores intersected the Malmani dolomite floor at Sandsloot, and the Penge BIF at Tweefontein respectively. On these two farms, 122 quarter-core samples were collected. The lengths of drillcores; SS339, TN754 and TN200 are 229m, 225m and 175m respectively. Samples were selected at intervals according to localities of particular interest, which included areas: of abrupt lithological variation, lithological boundaries, alteration differences and zones, and where BMS occurs in the samples. Samples were stored in individual plastic sample bags to prevent contamination between samples of the various rock types. Core samples were divided into three parts. One part was used for thin sections, another part was used for X-Ray Fluorescence Spectrometry (XRF) preparation and Fire assay analysis, and the remaining part of the core sample was used for microscopic descriptions.

3.2 Petrography

Detailed descriptions of these three drillcores were completed with the aid of core samples and polished thin sections. Sixty six samples were selected from the 122 rock samples for thin section cutting. Thin sections were studied with the aid of a microscope at the University of the Western Cape. The petrographical descriptions on each rock type studied included: the identification of the various minerals and their abundances; identifying the alteration and textural patterns; and also identifying the associated base metal sulphide (BMS) contents in each rock type.

These descriptions were further used to identify, classify and characterise in detail the different rock units found at the farms Tweefontein and Sandsloot. The lithological log was produced using Earthworks® (Downhole Explorer) software.

3.3 Chemical analysis

3.3.1 Sample preparation

Samples were prepared for all the laboratory analysis at the University of the Western Cape. The initial step included the washing and drying of samples to remove dirt and other contaminants. The core samples were crushed in a 5x3 inch Dickie & Stockler® jaw crusher machine. Crushed samples were then milled for five minutes into a fine powder in a *T-S 250 MILL* Dickie & Stockler® machine. The mill was cleaned thoroughly after each sample. This cleaning process removed the remaining residue in the milling pot by adding and milling quartz grains. To avoid contamination of the next sample, the milling pot was washed with distilled water, cleaned and dried. All samples were milled in this manner.

3.3.2 X-Ray Fluorescence Spectrometry (XRF) Analysis

(a) XRF sample preparation

Sample preparation for XRF analysis included 9g of sample added to a 2g wax binding material. This mixture was pressed (at 15 kilobars) into powder discs (pellets) which were used during XRF analysis for both major and trace elements (example of this method: Norrish and Hutton, 1969).

(b) XRF analysis

Samples were prepared for whole-rock XRF analysis, to provide data to evaluate any systematic geochemical changes with lithological variation or to indicate any abrupt changes in composition through the stratigraphy (Stevens, 2007). The methods used for XRF analysis follow those of Norrish and Hutton (1969). XRF analysis were processed at the geochemistry laboratory of the University of The Western Cape (Earth Sciences department), which were used to obtain major and trace element chemistry.

Elements include: SiO₂, Al₂O₃, Fe₂O₃, MnO, MgO, CaO, Na₂O, K₂O, P₂O₅, TiO₂, SO₃, As, Ba, Ce, Co, Cu, Nb, Ni, Pb, Rb, Sr, V, Y, Zn, Zr, Mo, U and Th. The major elements are expressed in weight percentage (wt. %) while the trace elements in part per million (ppm). The samples were analysed by a Phillips PW Model 1480 XRF spectrometer. XRF results are given in Appendix I.

(c) Loss on Ignition

Samples with high moisture and volatile contents can easily lose their volatiles because of the high temperatures the samples are accompanied with during XRF analysis. The loss is referred to as Loss on Ignition (LOI). Following the methods of Potts (1987), a test has been undertaken and designed to assess the amount of loss in each sample. The percentage of LOI is calculated based on the original weight of a sample (~0.5g were used), together with the weight of the sample after drying at 100° C (for 30min), and the weight of the sample after ignition at 1000° C (for 45min). These calculations were completed at the University of the Western Cape, and the samples were ignited in a Labcon[®] L-1200 furnace.



3.3.3 ICP-MS (Fire Assay) Analysis

Forty-five samples (50g each) were analysed for platinum-group elements Pt, Pd and Au by fire assay at the Scientific Services Laboratory in Cape Town. The chemical data is represented in Appendix II. Fire assay was used to dissolve samples prior to Graphite furnace atomic absorption spectrometry (GFAAS) and inductively coupled plasma emission mass spectrometry (ICP-MS) analysis. Details of this procedure are given in Bédard and Barnes (2002). The reference standard ST 265 was used.

3.3.4 QA / QC

Quality Control (QC) in exploration geochemistry often refers to the processes and procedures that are followed for sampling and its planning. QC procedures are necessary to monitor accuracy, precision and contamination. Quality Assurance (QA) is more a demonstration of the results obtained and their reliability. They are also important because large errors in geological databases can be prevented (Stevens, 2007).

XRF is a sensitive technique and samples must be clean, as even fingerprints on a sample can affect the results. For accurate results the spectrometer is tuned to the elements to be analysed. Bad settings can lead to poor results (Stevens, 2007). For this reason duplicate analyses were performed on fifteen randomly selected samples across the three drillcores. Certified reference standards were used to assess the quality and accuracy of the analysis. Duplicate samples assure the reproducibility and precision of the instrument. These standards are SARM-50 (S-18), SARM-48 (S-16), SARM-72, NIM-L and NIM-P.

Fig. 3.1 illustrates the quality control of the geochemical data that was determined using duplicate samples plotted on a scatterplot. The XLStat® statistical software package was used. As examples, the instrument is precise for up to 5% and 10% for the major elements SiO₂ and MgO respectively. The trace elements Sr and Rb are precise for up to 5% and 25% respectively.

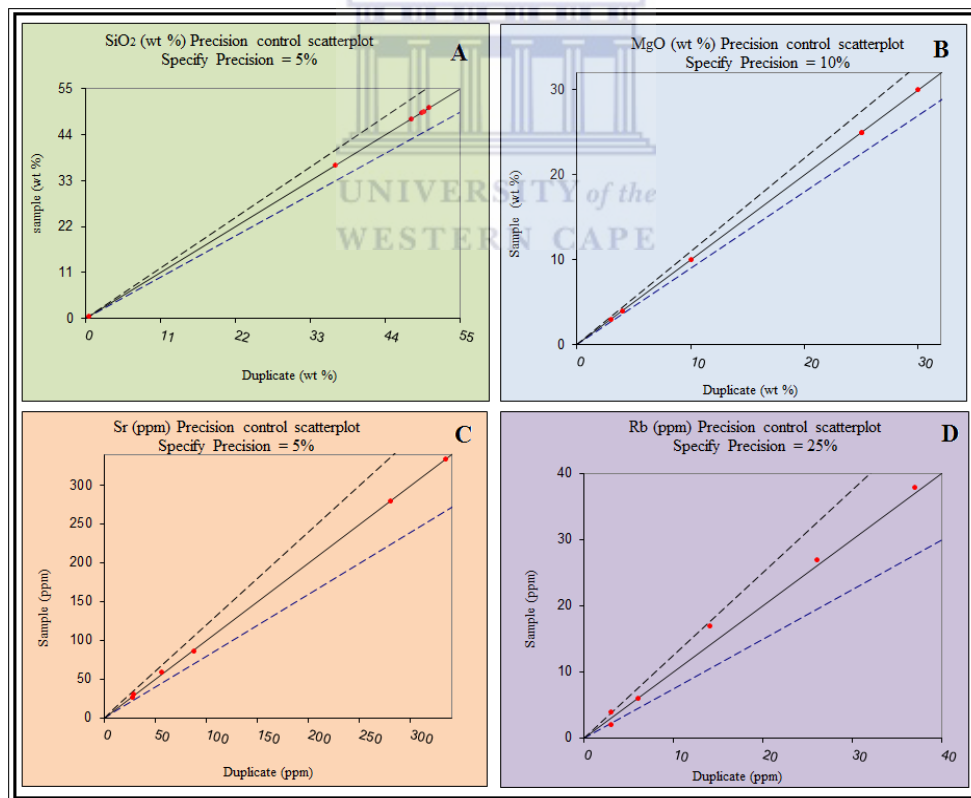


Figure 3.1: The above diagrams illustrate the precision control scatter plots of the analytical data. A and B: Scatter plots of the major elements SiO₂ and MgO (wt. %). C and D: Scatter plots of the trace elements Sr and Rb (in ppm).

3.4 Data evaluation

Cluster analysis was applied to the geochemical data using SPSS 19[®]. The cluster analysis results are presented as a graphic called a dendrogram, a tree-like diagram that illustrates the arrangement of the cluster solutions (e.g. Kaufmann and Rousseeuw, 1990, 2005).

The geochemical data were further subjected to descriptive and multivariate statistical analysis using Microsoft Excel software package. Descriptive statistical analysis was completed on the geochemical data set based on the cluster analysis and petrography results. Box-and-whisker plots were used to graphically show comparison of the different rocks. Spider diagrams have been used where geochemical data are presented on normalised multi-element diagrams using the normalizing values of McDonough and Sun (1989) and processed by the GCDkit 2.3.

This study uses the method proposed by Grant (1986) for all mass balance calculations because of its simplicity and adaptability as reported by Mukherjee and Gupta (2008). By using EASYGRESGRANT, the clusters and slopes of volume factors were determined (Grant, 2005; Mukherjee and Gupta, 2008). EASYGRESGRANT is a friendly interactive Microsoft Excel spreadsheet program that quantifies volume changes and performs mass-balance modeling in metasomatic systems (López-Moro, 2012). The program performs mass-balance calculations considering all possible reference frames between the unaltered rocks and their altered counterpart.

Downhole Explorer was used to plot the varying geochemical trends of elements down hole for each drillcore; i.e. for SS339, TN754 and TN200.

CHAPTER 4

4. PETROGRAPHY

4.1 Introduction

This chapter focuses on identifying the mineralogy and various mineral abundances within the rock sequences; their alteration and textural patterns; as well as their associated base metal sulphide (BMS) mineralisation. The goal is to use the petrographical descriptions as a foundation for all the geochemical studies. The descriptions of the rock units found at the Tweefontein 238KR and Sandsloot 236KR farms are based on three drillcores. Drillcores TN754 and TN200 were sampled from Tweefontein; and drillcore, SS339 was sampled from Sandsloot. Core logging and microscopy were used for detailed descriptions of the rock types in this study. This was attained by using 122 quarter core samples and 86 polished thin sections across these three drillcores.

Mineral abundances were estimated by using the percentage of volume that each mineral occupies within the rock sample. Each drillcore was individually described before any correlation was attempted because of the major variations within stratigraphic Platreef lithologies as well as along the strike of the Platreef farms. The three drillcores are described individually in section 4.3 and the various lithologies are described petrographically in section 4.4.

4.2 Platreef Nomenclature

The Platreef has a complex intercalation of markedly different lithological units (Mitchell and Scoon, 2012). Generally rock nomenclature for the Platreef is based on the IUGS Rock Classification Scheme (Streckeisen, 1976); however, there is also local Bushveld nomenclature as used by mining geologists. These terminologies should also be included (e.g. nomenclature in Kinnaird et al., 2005). The term “feldspathic pyroxenite” for example, will be used to describe the lithology comprising of cumulus orthopyroxene with significant intercumulus feldspar. Kinnaird et al. (2005) also mentions the repetitive norite cycles which include mafic-rich to mafic-poor layers, which occur in the mid to upper portion of the

Platreef. Typically, a cycle (from the base upward) is pyroxenite, feldspathic pyroxenite, melanorite, leuconorite with anorthosite. However, the cyclic packages are limited to correlation at short segments (Kinnaird et al., 2005).

Over the years, the classification scheme by White (1994) has been generally used. This scheme focuses on dividing the Platreef stratigraphic sequence into three pyroxenitic units termed the A, B and C reefs (McCutcheon, 2012; and its references). These units are considered to be a series of successive and upward younging units (McDonald et al., 2005). Later, Manyeruke et al. (2005) and Kinnaird et al. (2005) have suggested that the Platreef was indeed intruded as a sill or series of sills (Pronost et al., 2008). Manyeruke et al. (2005), Kinnaird et al. (2005), Maier et al. (2008), and Yudovskaya and Kinnaird (2010) suggested that these sill-like intrusions are composed of three geochemically distinct pyroxenites.

At Akanani, this is not applicable (Mitchell and Scoon, 2012) as the stratigraphic sequence does not constitute a simple upward younging sequence. They further challenge the common view that the Platreef package is made up of three reefs emplaced in stratigraphic sequence. They thought the alternative to solving the complexities in the Platreef package, is to group the rocks into a new broad and generic classification. It can be agreed that the Platreef show complexities, and in this thesis, it should be emphasised that a criteria is used to characterise zones of greatest similarity to simplify the heterogeneity.

4.3 Lithologies

A variety of lithological units are encountered in the drillcores, which can be divided into igneous and metasedimentary lithologies. These lithologies have been classified based on the IUGS scheme, it also incorporated commonly used local terms (Kinnaird et al., 2005), as well as allowing for new terminologies (Mitchell and Scoon, 2012). Subsequent to the literature, the heterogeneous Platreef package has initially been divided into three main layers: pyroxenite and two distinctive feldspathic pyroxenites (named in this thesis as FP-I and FP-II). However, the pyroxenites were also further separated and named as P-I and P-II, because of a notable difference in the degree of alteration.

The main metasedimentary rocks observed at Tweefontein included the hornfels, and at Sandsloot, the calcsilicate and parapyroxenite. It should be noted that samples that included xenoliths or granitic veins (e.g. Tweefontein drillcores) were excluded from this study. The ultimate aim of this study is to seek potential vectors that locate the PGE mineralisation. Therefore, the granitic veins and xenoliths could not be used as training samples. Training samples were considered those samples that represented the lithologies of interest (e.g. pyroxenite, feldspathic pyroxenite, hornfels and calcsilicates). After carefully selecting the training samples, only 86 samples were used out of the original 122 core samples for hand specimen descriptions and a petrographic investigation (see Table 4.1 for sample list per farm).

The pyroxenite subunit **P-I** is based on descriptions by Kinnaird et al. (2005); Reisberg et al. (2011) and Armitage (2011) which is considered as typical pyroxenites in the southern sectors of the Platreef.

The feldspathic pyroxenite subunit **FP-I** was named in line with Kinnaird et al. (2005), i.e. cumulus orthopyroxene and intercumulus plagioclase (norite on the IUGS scheme). The subunit **FP-II** is described by Reisberg et al. (2011), where they are called leuconorites or Platreef norites (Harris and Chaumba, 2001; McCutcheon, 2012).

The Platreef magma interacted with variable footwall lithologies to form hybrid rock types (McDonald et al., 2005). Furthermore, thermal metamorphism resulted in clinopyroxenite (locally termed “parapyroxenite”) and calcsilicate hornfels (Harris and Chaumba, 2001; Armitage et al, 2002; Armitage, 2011). These are typical footwall lithologies at Sandsloot. At Tweefontein, the footwall lithologies are the banded ironstone which was metamorphosed to magnetite bearing hornfels (White, 1994; McCutcheon, 2012). Shales of the Deutschland formation can also form the footwall, e.g. at Tweefontein Hill (Nex, 2005; Nyama et al, 2005).

The Tweefontein drillcores (TN754 and TN200) include metasedimentary rocks composed of hornfels. Three different and distinct zones of hornfels were identified based on their varying mineral abundance, textures, alteration and their contents of sulphide mineralisation. This study also includes drillcore SS339, from the farm Sandsloot. The floor rocks consist of the Malmani Dolomite. The metasedimentary rocks were subdivided into three subunits of calcsilicate, based on the same criteria.

Table 4.1: List of igneous and metasedimentary rocks sampled at the two farms, Tweefontein and Sandsloot. This list also includes the number of samples selected per rock type.

Lithologies	Tweefontein	Sandsloot
P-I	9	1
P-II	4	2
FP-I	4	8
FP-11	8	2
CS-I		5
CS-II		7
CS-III		5
H-I	7	
H-II	13	
H-III	6	

4.4 Petrography

Thin sections were petrographically described using transmitted and reflected light. Differentiations were made based on mineralogical abundance of certain minerals and the overall textures of all the samples. The modal percentages, textures, alteration and BMS association based are given below for the subunits:

4.4.1 Platreef package

a. Pyroxenite subunit I (P-I)

The specimens representing this pyroxenite are generally medium to coarse-grained (grain sizes are ~ 5mm and up to 10mm) and are equigranular and holocrystalline (see fig. 4.1 A and B). Orthopyroxene can range between 30 – 70 modal %, clinopyroxene range between 5 – 30 modal %, and plagioclase range between 10 – 35 modal %. These rocks contain average modal percentages of 56 % orthopyroxene, 22% clinopyroxene, 15% plagioclase, 2% olivine, 3% sulphides and 2% accessory minerals.

Orthopyroxene is 1 mm up to 10 mm in size. It is extensively fractured, mostly rounded and anhedral grains, and can be subhedral in towards the top of a drillcore. It can be partly skeletal in texture, with embayments both along grain boundaries and internally. The orthopyroxene fractures are filled by chlorite veining and fine-grained sericitisation. Clinopyroxene grains are larger than the orthopyroxene grains (~7 mm). They are anhedral, embayed and skeletal and can include small rounded orthopyroxene within it. Minor plagioclase occurs interstitially to the pyroxenes as 0.5 to 1 mm anhedral grains. Sulphides are present as disseminated blebs 1 - 4 mm. The sulphides are predominantly pyrrhotite with smaller chalcopyrite blebs (~0.3 mm).



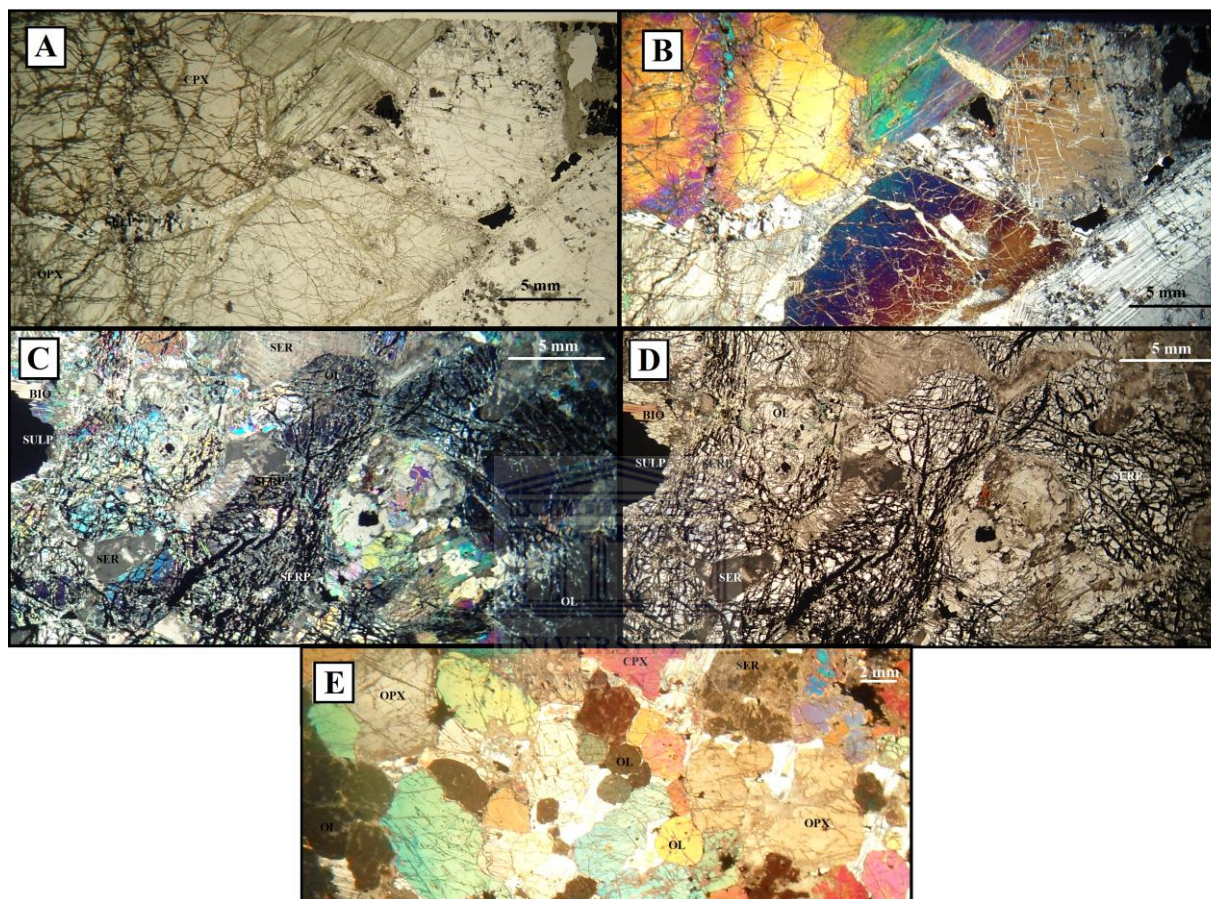


Figure 4.1: Photomicrographs of pyroxenite subunits from the Platreef at Tweefontein and Sandsloot. Panel A and B: pyroxenite subunit I under plane polarised light (A) and under crossed polars (B). The rock is predominantly made up of orthopyroxene (30 – 70 modal %), clinopyroxene (5 – 30 modal %), and plagioclase (10 – 35 modal %). Panel C, D and E: Pyroxenite subunit II, under plane polarised light (A) and under crossed polars (D and E) and contains; orthopyroxene (35 – 75 modal %), olivine (10 – 15 %), clinopyroxene (5 – 30 modal %), and plagioclase (2 – 8 modal %).

b. Pyroxenite subunit II (P-II)

The specimens representing this pyroxenite are generally medium-grained (grain sizes < 5mm) and are equigranular and holocrystalline (see Fig. 4.1; C, D and E). These rocks contain average modal percentages of 50% orthopyroxene, 20% clinopyroxene, 4% plagioclase, 17% olivine, 6% sulphides and 3% accessory minerals. Orthopyroxene can range between 35 – 75 modal %, olivine can range between 10 – 35 %, clinopyroxene range between 5 – 30 modal %, and plagioclase range between 2 – 8 modal %. Orthopyroxenes are anhedral, rounded, and fractured (~3mm in size). Clinopyroxenes (~6mm in size) are subhedral and larger than the orthopyroxenes. Olivines are rounded, anhedral and fractured. It is in some areas extensively serpentinised. Plagioclase is totally altered to sericite. Sulphides occur as tiny disseminated blebs throughout this lithology, and also as stringers and veins. Sulphides are predominantly pyrrhotite and chalcopyrite and can have blebs of up to 6mm in highly altered areas.

c. Feldspathic pyroxenite subunit I (FP-I)

The specimens representing this pyroxenite are generally fine to medium-grained (~4mm in grain sizes) and are inequigranular and holocrystalline. These rocks contain average modal percentages of 77% orthopyroxene, 10% clinopyroxene, 5% plagioclase, 7% sulphides and 1% accessory minerals. Orthopyroxenes can range between 78 – 85 modal %, clinopyroxene range between 4 – 15 modal %, and plagioclase range between 3 – 8 modal %. Orthopyroxene occurs as large subhedral grains which are up to 10 mm in size and poikilitically has inclusions of smaller 1 mm sized subhedral pyroxene and plagioclase grains. Where clinopyroxene grains occur, it is as large as 8 mm and poikilitically includes orthopyroxene and plagioclase grains within it. Pyroxenes are fractured with the fractures filled with fine-grained amphibole. Sulphides are interstitial to the pyroxenes, with mostly pyrrhotite, with some chalcopyrite margins. Small anhedral, rust red brown biotite grains (0.5 mm in size) occur in close proximity to the sulphides. Overall the texture shows interlocking, sutured grain boundaries, orthocumulate texture.

d. Feldspathic pyroxenite subunit II (FP-II)

The specimens representing this pyroxenite are generally medium to coarse-grained, inequigranular and holocrystalline, with grain sizes up to 12mm. These rocks contain average modal percentages of 17% orthopyroxene, 25% clinopyroxene, 50% plagioclase, 1% olivine, 4% sulphides and 3% accessory minerals. Orthopyroxenes can range between 9 – 35 modal %, clinopyroxene range between 3 – 35 modal %, and plagioclase range between 42 – 55 modal %. Pyroxene grains are up to 10 mm in diameter and are fractured and show alteration (uralitisation) along cleavage planes. Alteration by micas and carbonates also occurs sporadically. Pyroxenes show grain boundaries that are irregular and embayed. Cumulus plagioclase grains are up to 10 mm in size and are extensively sericitised and show deformation twinning.

Pleochroic brown biotite grains occur within the pyroxenes. Clinopyroxene grains are less abundant and are subhedral, reaching sizes of up to 5 mm. Sulphide blebs ~2 mm, are irregularly shaped as well as disseminated minor sulphide blebs (~0.5 mm) are also present interstitially and associated with the pyroxenes.

Orthopyroxene are 1 mm up to 10 mm in size. It is extensively fractured, mostly rounded and anhedral grains, and can be subhedral in towards the top of a drillcore. It can be partly skeletal in texture, with embayments both along grain boundaries and internally. The orthopyroxene fractures are filled by chlorite veining and fine-grained sericitisation. Clinopyroxene grains are larger than the orthopyroxene grains (~7 mm). They are anhedral, embayed and skeletal and can include small rounded orthopyroxene within it. Minor plagioclase occurs interstitially to the pyroxenes as 0.5 to 1 mm anhedral grains. Sulphides are present as disseminated blebs 1 - 4 mm. The sulphides are predominantly pyrrhotite with smaller chalcopyrite blebs (~0.3 mm).

4.4.2 metasedimentary rocks

a. Hornfels subunit I (H-I)

The specimens representing this hornfels subunit are fine to medium-grained with crystal sizes < 4 mm (see Fig. 4.2 A and B). These rocks contain average modal percentages of 35 % iron oxides, 48% quartz, 15% plagioclase, and 2% accessory minerals. Iron oxide minerals ranges between 10 - 45 modal %, plagioclase ranges between 2 – 30 modal %, and quartz ranges between 10 - 60 modal %. These rocks show a granoblastic texture, with typical layering (banding) of distinguishable bands of clinopyroxene and iron oxides. Clinopyroxene grains are idioblastic to subidioblastic. They are of two sizes; finer <1.5 mm sized and coarser ~ 4mm sized. The latter is more unaltered and pristine. The iron oxides are more xenoblastic and where plagioclase and quartz occur; they are small euhedral to subhedral laths (~1 mm). Alteration includes minor sericitisation, where plagioclase is altered to sericite. Pyroxene grains can be chloritised.



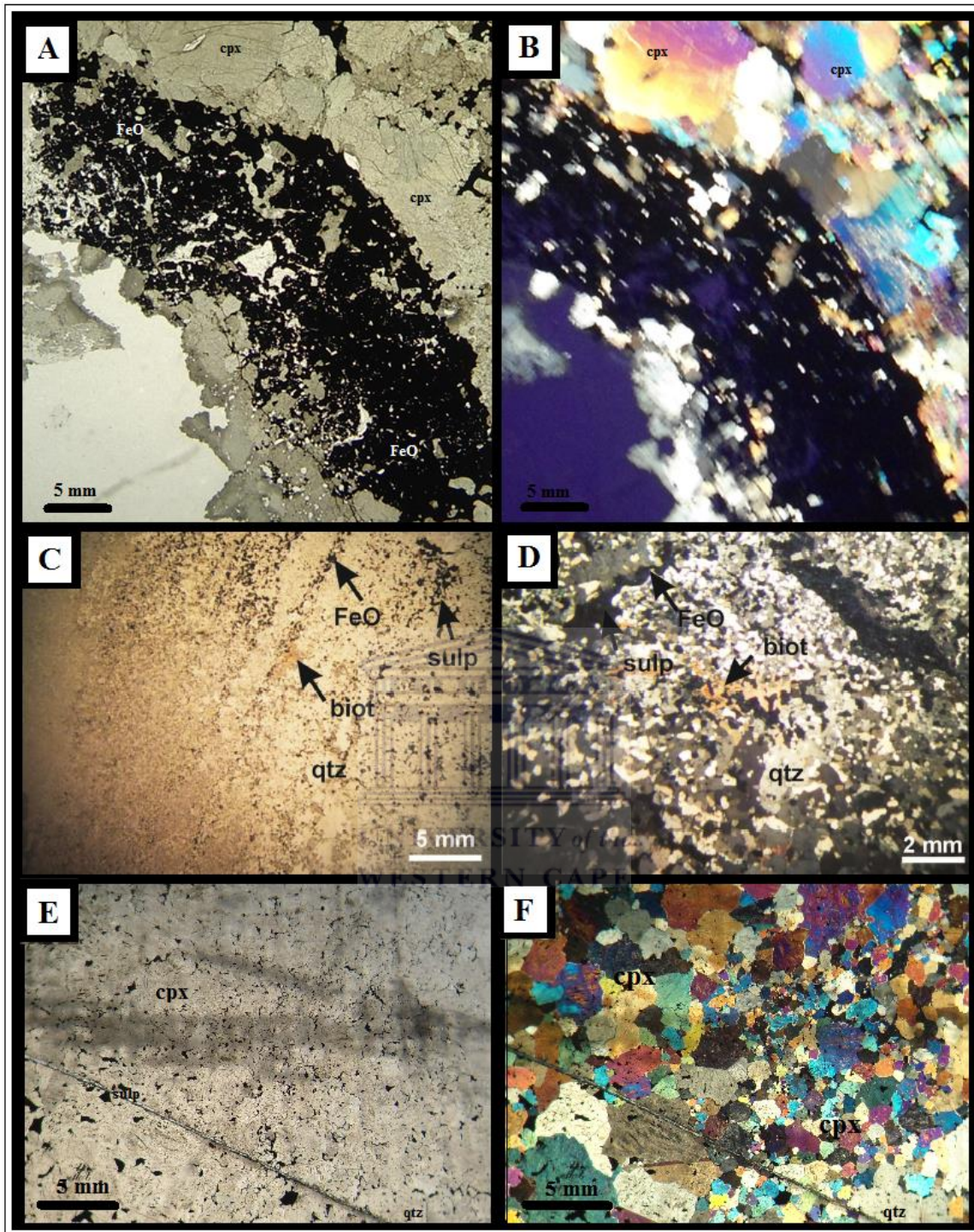


Figure 4.2: Photomicrographs of the hornfels encountered at the farm Tweefontein. Panel (A and B): Hornfels subunit I from drillcore TN200, where A is under plane polarised light and B under crossed polars. Panel (C and D): Hornfels subunit II, from drillcore TN754, where C is under plane polarised light and D under cross polars. Panel (E and F): Hornfels subunit III from the drillcore TN754, where E is under plane polarised light and F is under crossed polars.

Sulphides (predominantly pyrrhotite with chalcopyrite margins) generally occur as irregular disseminated and tiny blebs throughout these rocks (< 3 mm in size). The sulphides are associated with the quartz grains, where they occur interstitially and can make up almost 4% of the sample. Remobilised sulphide veinlets also occur as sulphide stringers of up to 10 mm in length and ~ 0.5 mm thick. The remobilised sulphides are more chalcopyrite and minor pyrite.

b. Hornfels subunit II (H-II)

The specimens representing this hornfels subunit are not homogeneous, and can alternate between two main heterogeneous types.

The specimens representing this type are fine to medium-grained with crystal sizes ranging between 0.1 and 5 mm. These rocks contain average modal percentages of 32 % iron oxides, 60% clinopyroxene and 8% accessory minerals. Iron oxide minerals range between 10 - 45 modal % and clinopyroxene ranges between 40 - 80 modal %. These rocks show a granoblastic texture, with typical layering (banding) of distinguishable bands of either clinopyroxene or iron oxides; or coarser and finer clinopyroxene bands. Clinopyroxene grains are idioblastic to subidioblastic. They are of two sizes; very fine <0.8 mm sized and coarser ~ 3mm sized. The iron oxides are more xenoblastic and where plagioclase and quartz occur; they are in accessory amounts, interstitial to the pyroxenes, and small euhedral to subhedral laths (~1 mm). Alteration includes minor sericitisation, where plagioclase is altered to sericite. Pyroxene grains are extensively chloritised and serpentised. Sulphides (predominantly pyrrhotite with chalcopyrite margins) generally occur as irregular disseminated and tiny blebs throughout these rocks (< 3 mm in size). These sulphides are associated with the clinopyroxene bands, and are mostly pyrrhotite and chalcopyrite.

Specimens can also be fine-grained hornfels that have crystal sizes of < 1mm (see Fig. 4.2 C and D). These rocks contain average modal percentages of 30 % iron oxides, 10% clinopyroxene, 45% quartz, 10% plagioclase, and 5% accessory minerals.

Iron oxide minerals ranges between 20 - 45 modal %, plagioclase ranges between 5 – 15 modal %, and clinopyroxene ranges between 5 - 20 modal %. These rocks show a typical hornfelsic texture, with typical layering (banding) of distinguishable bands of predominantly quartz and iron oxides. Quartz grains are idioblastic to subidioblastic, and < 1mm in size.

Clinopyroxene and iron oxide grains are xenoblastic. Alteration includes minor sericitisation, where plagioclase is altered to sericite. Sulphides are present as irregularly shaped pyrrhotite blebs mostly oriented parallel to the banding in the rock. Sulphides vary from small, finely disseminated grains to concentrated along iron oxides and then defining the banding within the rock.

c. Hornfels subunit III (H-III)

The specimens representing this hornfels subunit are medium-grained with crystal sizes < 5 mm (see Fig. 4.2 E and F). These rocks contain average modal percentages of 15 % iron oxides, 65% clinopyroxene, 10% plagioclase, 5% quartz and 5% accessory minerals. Iron oxide minerals ranges between 5 - 15 modal %, plagioclase ranges between 5 – 30 modal %, and clinopyroxene ranges between 40 - 80 modal %. These rocks show an interlobate granoblastic texture, where the layering (banding) are not as well defined as in the other two hornfels zones (no clear banding of iron oxides with clinopyroxene). Clinopyroxene grains are subidioblastic to xenoblastic and occur in varying grains of: finer grains (~0.5mm) as well as coarser grains (~5mm). Clinopyroxene are extensively chloritised, where abundant chlorite occurs as veinlets around sutured and irregular grain boundaries. Plagioclase, quartz and iron oxides are anhedral. Plagioclase has been altered extensively to sericite. Pyrrhotite is the dominant sulphide occurring as small, irregular and disseminated ~1mm anhedral sulphide blebs.

d. Calcsilicates subunit I (CS-I)

The specimens representing this calcsilicate subunit are generally medium-grained with crystal sizes of 2 to 5mm (see Fig. 4.3 A and B). These rocks contain average modal percentages of 90% dolomitic / calcitic (carbonate) minerals, 6% orthopyroxene, 2% plagioclase and of 2% accessory minerals. They contain carbonate minerals ranging in 80 – 95 modal %, orthopyroxene ranging in 3 – 10 modal %, and plagioclase with 1 - 3 modal %. These rocks have a predominantly intergranular and relict texture. Carbonate grains are idioblastic to subidioblastic and ~3.5 mm in size. Orthopyroxene grain shapes are xenoblastic and < 2mm in size. Where plagioclase occurs it forms small euhedral laths (~1 mm) and overgrow the orthopyroxene grains. Chlorite, talc and minor iron oxides occur in accessory amounts. Alteration includes chloritisation, minor sericitisation and serpentinisation. Olivine

is totally serpentinised and plagioclase is sericitised. Sulphides are rare and almost none and where they occur, they are disseminated and tiny blebs (< 0.3mm in size).

e. Calcsilicates subunit II (CS-II)

The specimens representing this calc-silicate subunit are slightly more finer-grained than the calc-silicates in zone I (see Fig. 4.3 C and D). Crystal sizes in these rocks are fine to medium-grained (ranges between 0.3 and 5mm). These rocks contain average modal percentages of 75% dolomitic / calcitic (carbonate) minerals, 20% orthopyroxene, 3% plagioclase and of 2% accessory minerals. They contains carbonate minerals ranging in 60 – 80 modal %, pyroxene ranging in 15 – 40 modal %, and plagioclase with 1 - 5 modal %. These rocks have a general amoeboid granoblastic texture. Carbonate grains are subidioblastic and ~2 mm in size. Orthopyroxene grain shapes are idioblastic to subidioblastic and ~2 mm in size. Where plagioclase occurs, it forms small euhedral laths (~1 mm) and is overgrown by orthopyroxene grains. Alteration includes minor sericitisation and more prominent serpentinisation. Olivine is totally serpentinised and plagioclase is sericitised. Sulphides (predominantly pyrrhotite) occur as disseminated and tiny blebs (< 1 mm in size).

f. Calcsilicates subunit III (CS-III)

These rocks contain average modal percentages of 50% carbonate minerals, 20% orthopyroxene, 20% clinopyroxene, 6% plagioclase and of 4% accessory minerals (see Fig. 4.3 E and F). They contain carbonate minerals ranging in 40 – 60 modal %, pyroxenes ranging in 10 – 40 modal %, and plagioclase with 4 - 15 modal %. The specimens representing this calcsilicate subunit are of two types: (1) finer-grained and have crystal sizes < 2mm; and (2) medium-grained and have crystal sizes of up to 4mm. Where the samples are more fine grained, the rocks have a general porphyroclastic (superimposed) texture. Carbonate and pyroxene grains are xenoblastic (<2 mm in size). Alteration includes sericitisation and chloritisation, where plagioclase is sericitised. Sulphides occur as disseminated and tiny blebs (< 1 mm in size). Where the samples are more medium-grained, the rocks have a granoblastic texture. Grain forms of carbonates and pyroxenes are subidioblastic. Alteration includes major serpentinisation, chloritisation and sericitisation. Sulphides can occur in extensive amounts; in specific samples it can be as high as 15% of the specimen. Sulphides are predominantly pyrrhotite with a chalcopyrite margin.

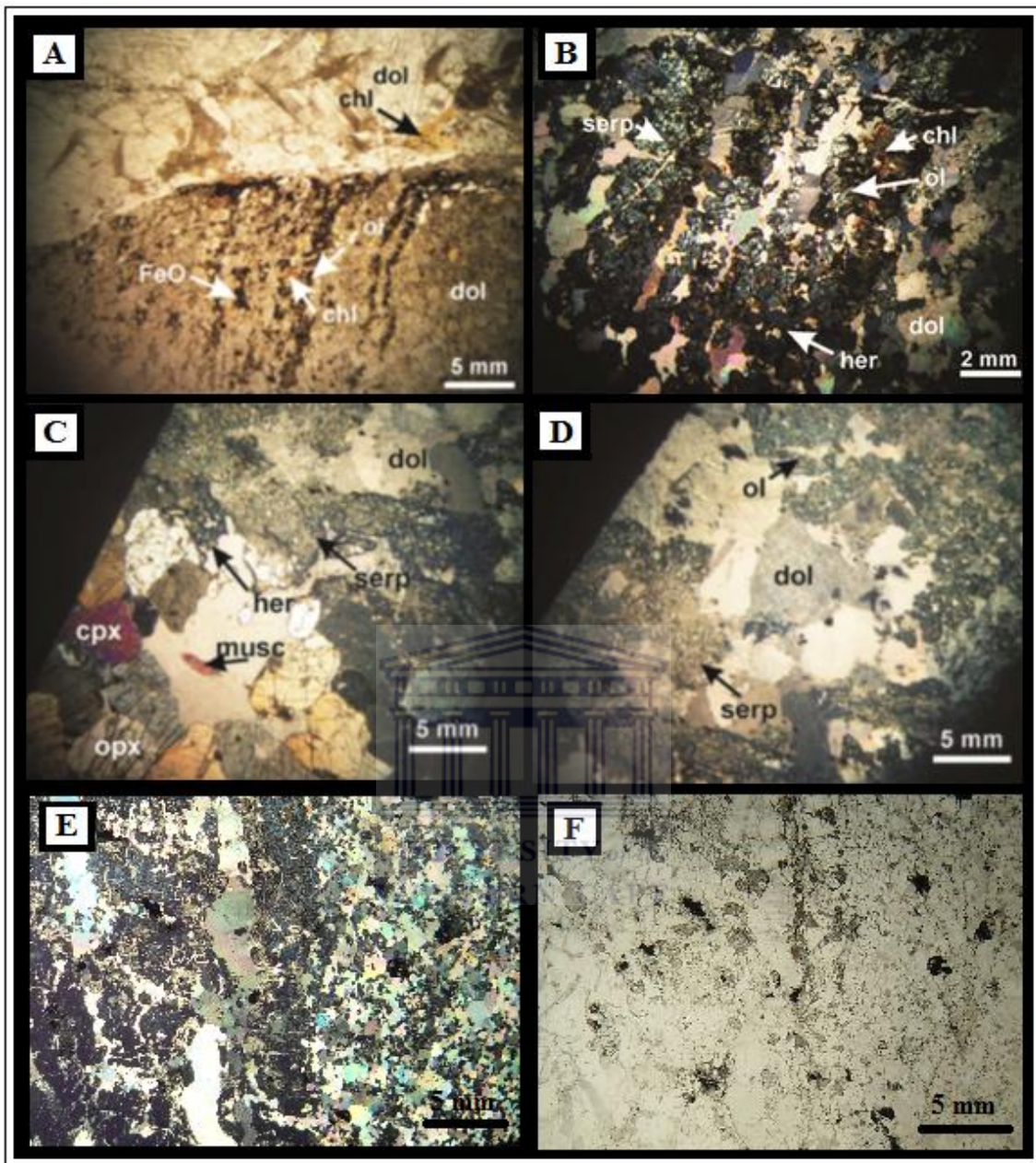


Figure 4.3: Photomicrographs of calcisilicates encountered at the farm Sandsloot. Panel (A and B): Calcisilicate subunit I from drillcore SS339, where A is under plane polarised light and B under crossed polars. Panel (C and D): Calcisilicate subunit II, from drillcore SS339, where C is under crossed polars, and D under plane polarised light. Panel (E and F): Calcisilicate subunit III from the drillcore SS339, where E is under crossed polars, and F under plane polarised light.

4.3.3 Main zone gabbronorite

The gabbronorite is medium-grained with grain sizes ranging between 2 – 5mm in diameter (see Fig. 4.9). They are very feldspathic and contain 50 – 75 modal % plagioclase and 20 – 45 % pyroxene. Minor minerals include amphibole, chlorite and biotite. Plagioclase laths are up to 3 mm in diameter, and along with irregularly shaped anhedral, skeletal ~5 mm olive green orthopyroxene grains, with lesser ~3mm clinopyroxene grains which poikilitically include and envelope subhedral to anhedral ~2 mm plagioclase laths within it. Plagioclase is partly sericitised and show deformation twinning in places. The pyroxenes are relatively pristine, but in places, particularly the clinopyroxene grains, are altered and replaced by fine-grained amphibole with some pyroxenes showing some twinning. The presence of deformation twinning in the plagioclase indicates a degree of later deformation after crystallisation which may be related to later local serpentinisation of the Platreef package. No sulphides are present, but Fe oxides occur as grains ~0.5 mm in size, and are disseminated throughout the rock.

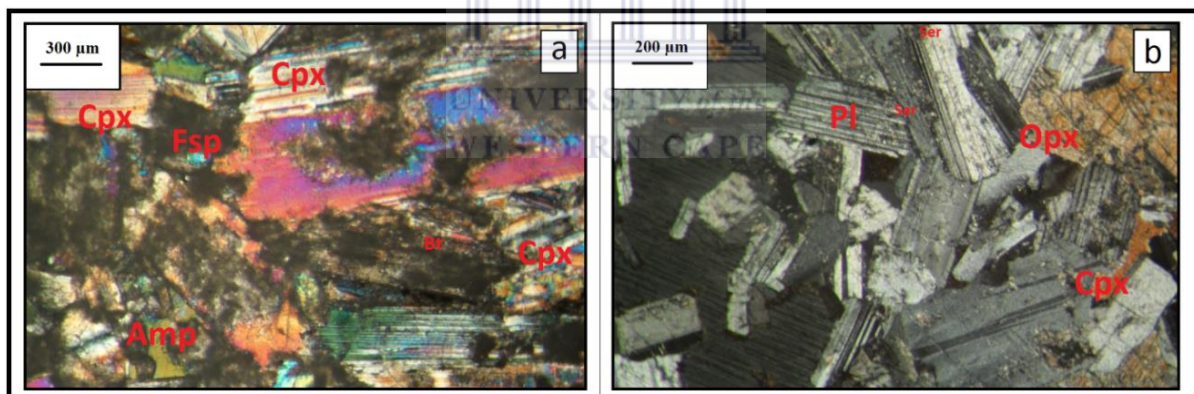


Figure 4.9: Photomicrographs of gabbronorite encountered at the farms Sandsloot and Tweefontein. Panel (A): illustrates the Main zone gabbronorite at Sandsloot under crossed polars, and panel (B) illustrates the Main zone gabbronorite found at Tweefontein (plagioclase ranges from 50 – 75 modal % and pyroxene ranges from 20 – 45 modal percentage).

4.5 Stratigraphy

A detailed stratigraphy is given below for each drillcore (see Fig. 4.4). The rock types included below are based on the outlined nomenclature and petrographical studies as described above.

4.5.1 TN200

Drillcore TN200 was logged from a drill depth of 365.73 to 190m, and has a length of ~170m. From the end of the drillcore at 365.73 to 312m is a package of hornfels which is ~53m thick.

- Hornfels subunit II (H-II) is found at the base of the drillcore for ~10m (depths of 365.73 – 355.73m). This subunit is fine to medium-grained in hand specimen. It is predominantly iron oxides and pyroxene, with a distinctive banding between these two minerals. These rocks are moderately altered by chloritisation and serpentinisation.
- At the top of the hornfels unit from depths of 355.73 to 312m is a layer of hornfels subunit III (H-III). This subunit is more highly altered with a thickness of ~43m. It is predominantly highly chloritised pyroxene, with less iron oxides and plagioclase (sulphides occur as small tiny disseminated blebs).

The Platreef package within this drillcore is ~107m thick, and alternate between feldspathic pyroxenite and pyroxenite layers.

- This Platreef package has a ~10m fine to medium-grained pyroxenite layer at the base from depths of 312 to 304.25m. This pyroxenite (type I) is predominantly pyroxene with minor plagioclase and tiny disseminated sulphides.
- The Platreef rocks then grade into a more sulphide-rich pyroxenite (type II) that is ~2m in thickness. These rocks are highly serpentinised, and dominantly pyroxenes, olivine and minor plagioclase.
- The Platreef package then gradually progresses into a thick package of alternating feldspathic pyroxenite and pyroxenite layers between depths of 302 and 200m.
- The feldspathic pyroxenite (type II) has high contents of plagioclase (half the specimen), is very coarse-grained, and with visible biotite and sulphides blebs.

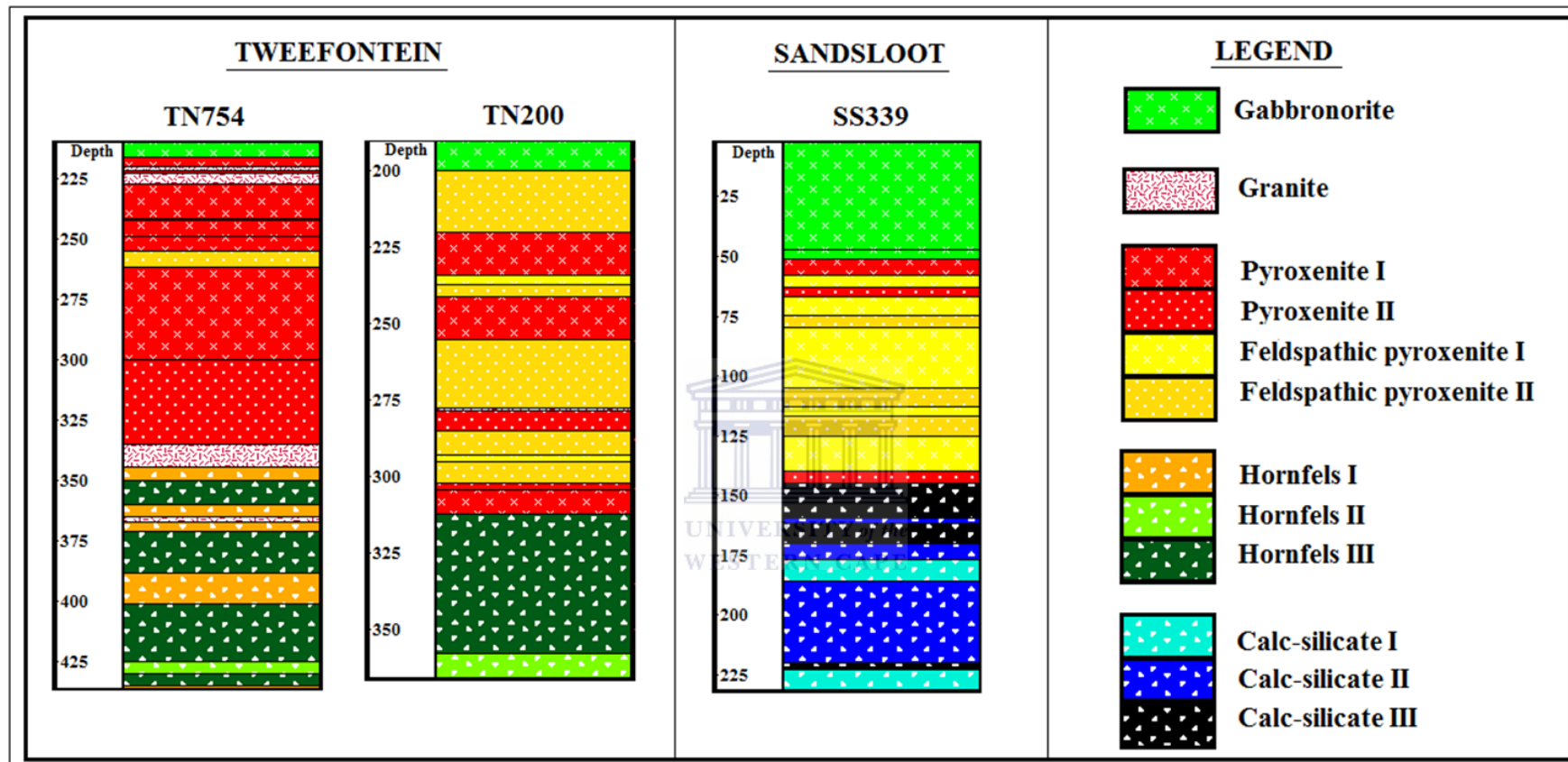


Figure 4.4: Stratigraphic logs of the drillcores studied on the farms Tweefontein 238 KR (TN754 and TN200) and Sandsloot 236 KR (SS339). The figure illustrates the floor rocks; calcsilicate and hornfels at Sandsloot and Tweefontein respectively. The Platreef lithologies occur in varying thicknesses, and the drillcores are capped by the hanging wall gabbronorite. Later granitic veins cut across the Tweefontein drillcores.

- The pyroxenite is fine to medium-grained in hand specimen. It is predominantly pyroxenes with minor plagioclase and tiny disseminated sulphides (i.e. type I is repeated).

A later granite layer of ~2m cuts across this Platreef package at a depth of 277 – 279m. The drillcore is capped by a 10m thick gabbro-norite layer. All boundaries between the granites and gabbro-norites with other rocks are sharp contacts.

4.5.2 TN754

Drillcore TN754 was logged from a drill depth of 436m to 210, and has a length of ~226m.

From the end of the drillcore at 436m to 344m is a package of hornfels which is ~92m thick.

This package alternates between subunits of various hornfels. These hornfels were classified into three subunits (i.e. subunits H-I, H-II and H-III).

- At the base of the hornfels package is the more medium-grained (H-I) occurring for ~1m. This subunit is the least altered hornfels, with minor chloritisation and sericitisation. It is comprised of predominantly iron oxides, pyroxenes and plagioclase. It is highly mineralised with massive sulphides.
- The hornfels gradually grade into a fine to medium-grained hornfels subunit II with a thickness of ~5m (between depths of 430 to 425m). This subunit is moderately altered by chloritisation and serpentinisation. It is predominantly iron oxides and pyroxene with distinctive banding between these two minerals.
- Between depths of 403 and 425m are alternating subunits of weakly (H-I) and highly altered (H-II) hornfels. Here the H-II is characterised by bands of alternating quartz and iron oxides, and the hand specimen is very fine-grained. With minor sulphides disseminated throughout the rock. This subunit is derived from the Deutschland shales which were metamorphosed to hornfels.
- The hornfels further progresses into hornfels subunit III at the top of the hornfels package. These hornfels are highly altered and predominantly chloritised pyroxene, with less iron oxides and plagioclase (sulphides occurring as small tiny disseminated blebs).

The Platreef package of drillcore TN754 is ~120m thick and occurs between depths of 335 to 216m. This package alternates between feldspathic pyroxenite and pyroxenite layers.

- The Platreef package has a ~35m pyroxenite layer at the base, which is a sulphide rich pyroxenite (type II). It is highly serpentinised, predominantly pyroxenes, olivine and minor plagioclase.
- The pyroxenite rocks progresses into a pyroxenite (type I) which is fine to medium-grained in hand specimen. This pyroxenite is predominantly pyroxenes with minor plagioclase and tiny disseminated sulphides.
- The pyroxenitic rocks gradually progresses into a feldspathic pyroxenite layer (~7m in thickness). This feldspathic pyroxenite (type II) has high contents of plagioclase, very coarse-grained, with visible disseminated sulphide blebs.
- The top of the Platreef is dominated by pyroxenite type I layers (between depths of 255 and 216m). This part of the Platreef package has a thickness of ~39m. This pyroxenite is fine to medium-grained and predominantly pyroxene with minor plagioclase and tiny disseminated sulphides.

The Platreef lithologies are intersected by granite layers with thicknesses varying from 1 to 10m, and at depths of ~340, 248m, 241m, 224 and 221m respectively. The Platreef is capped by a 10m thick gabbronorite layer. All boundaries between granites and gabbronorites with other rocks are sharp contacts.

4.5.3 Sandsloot

From the end of the drillcore at 231.56m to 145m is a package of calcsilicates (see Fig. 4.3) which is ~86m thick. This package alternates between subunits of various calcsilicates (i.e. calcsilicate subunits I, II and III).

- The base of the drillcore starts with a weakly altered coarse-grained calcsilicate subunit (CS-I) for an approximate thickness of 8m.
- The calcsilicates gradually progresses into medium-grained subunit that is moderately altered (CS-II) with a thickness of ~37m.
- The calcsilicates then progresses into a highly altered and fine grained subunit (CS-III) with a thickness of ~25m.

The Platreef package in this drillcore is ~105m thick and has alternating pyroxenite and feldspathic pyroxenite layers.

- The base of the Platreef package is comprised of a ~5m thick pyroxenite layer (pyroxenite type II). This pyroxenite is more sulphide rich which is highly serpentinised, and dominantly pyroxenes, olivine and minor plagioclase.
- The Platreef package then progresses into a feldspathic pyroxenite package with a thickness of ~73m (between depths of 140 to 58m). This unit alternates between two types of feldspathic pyroxenite: (1) feldspathic pyroxenite type I, which is cumulus orthopyroxene with interstitial plagioclase (noritic appearance in hand specimen) and (2) feldspathic pyroxenite type II, which has high contents of plagioclase (half the specimen), very coarse-grained, with visible biotite and sulphides blebs.
- The top of the Platreef package is composed of a pyroxenite layer (pyroxenite type I) of ~ 16m (between depths of 58 to 47m). The pyroxenite is fine to medium-grained in hand specimen. It is predominantly pyroxenes with minor plagioclase and tiny disseminated sulphides.

The Platreef is capped by a ~50m thick gabbro-norite layer. The boundary between the gabbro-norite with the Platreef is a sharp contact.

Table 4.2: A petrographical summary of the lithologies of interest: subunits of the hornfels (H-I, H-II and H-III), subunits of the calcsilicates (CS-I, CS-II and CS-III) and the subunits of the Platreef package (P-I, P-II, FP-I and FP-II).

LITHOLOGIES		TEXTURES and ALTERATION	MINERAL ASSEMBLAGE AND ABUNDANCE
Hornfels	H-I	Fine to medium grained	Iron oxides (35%), clinopyroxene (48%) , plagioclase (15%), and accessory minerals (2%)
		Granoblastic texture	Accessory: chlorite
			Sulphides: massive
	H-II	Fine to medium grained	Iron oxides (30%), clinopyroxene (10%) , plagioclase (10%), Quartz (45%) and accessory minerals (5%)
		Granoblastic texture and typical layering	Accessory: sericite
		Serpentinisation, chloritisation and minor sericitisation	Sulphides: Irregular disseminated, tiny blebs, also more extensive massive, veining
		Accessory: chert	
H-III	Medium grained with no clear banding	Iron oxides (15%), clinopyroxene (65%) , plagioclase (10%), quartz (5%) and accessory minerals (5%)	
	Interlobate granoblastic texture	Accessory: chlorite, sericite	
	Extensive chloritisation and sericitisation	Sulphides: Small, irregular and disseminated	
Calc-silicates	CS-I	Generally medium grained	Dolomitic / calcitic minerals (90%), orthopyroxene (6%), plagioclase (2%) and accessory minerals (2%)
		Oolitic and intergranular relict texture	Accessory: Chlorite, talc and minor iron oxides
		Minor sericitisation, serpentinisation and chloritisation	Sulphides: almost none
	CS-II	Fine to medium grained	Dolomitic / calcitic minerals (75%), orthopyroxene (20%), plagioclase (3%)and accessory minerals (2%)
		Amoeboid granoblastic texture	Sulphides: disseminated and tiny blebs
		Minor sericitisation and prominent serpentinisation	
CS-III	Porphyroclastic (superimposed) texture	Dolomitic / calcitic minerals (50%), orthopyroxene (20%), clinopyroxene (20%), plagioclase (6%) and accessory minerals (4%)	
	Major serpentinisation, chloritisation and sericitisation.	Sulphides: disseminated, extensive and massive	
Pyroxenites	P-II	Medium grained, with major serpentinisation and sericitisation	Orthopyroxene (50%), clinopyroxene (20%), plagioclase (4%), olivine (17%), sulphides (6%) and accessory minerals (3%)
	FP-I	Fine to medium grained and minor sericitisation	Orthopyroxene (77%), clinopyroxene (10%), plagioclase (5%), sulphides (7%) and accessory minerals (1%)
	P-I	Coarse grained	Orthopyroxene (56%), clinopyroxene (22%), plagioclase (15%), olivine (2%), sulphides (3%) and accessory minerals (2%)
		Sericitisation and chloritisation	Accessory: chlorite
FP-II	Generally medium to coarse grained	Orthopyroxene (17%), clinopyroxene (25%), plagioclase (50%), olivine (1%), sulphides (4%) and accessory minerals (3%)	
	Major sericitisation	Accessory: amphibole, biotite	

4.3.6 Summary

The petrographical rock classification and characterization has predominantly been based on changes in modal layering and the grain size variation. Particularly for the Platreef lithologies there is a distinct difference between the pyroxenite subunits P-I, P-II, FP-I and FP-II.

The subunit P-II is characterised by predominantly serpentinised orthopyroxene and olivine. The subunit P-I is characterised by predominantly orthopyroxene, clinopyroxene, and plagioclase. The FP-I is characterised by predominantly cumulus orthopyroxene and interstitial plagioclase. And the FP-II is characterised by predominantly cumulus plagioclase and clinopyroxene, with lesser orthopyroxene. Table 4.2 shows the grain size and modal percentage variation of feldspars are significant and occurs in an increasing order from P-II, FP-I, P-I and FP-II. Feldspars changes from finer-grained to coarser grained in the same sequence.

A close examination of the stratigraphic logs in Fig 4.1 shows a predominance of P-II and P-I in TN754. This is also coupled with an upward thickening of P-I layers in this drillcore. In SS339 there is a rhythmic interlayering of predominantly FP-I and FP-II. There appear to be a cyclic pattern of P-II, to FP-I to FP-II. Where P-I occurs, the pattern is P-II, FP-I, P-I and FP-II. Thus, the layers generally grade from orthopyroxene and olivine; into predominantly orthopyroxene; then into orthopyroxene, clinopyroxene and plagioclase; and then into predominantly plagioclase rich (and clinopyroxene) layers.

Spatially, TN754 is located furthest away from Sandsloot, followed by TN200 which is closer to Sandsloot.

CHAPTER 5

5. GEOCHEMISTRY

Preamble

The objectives of this thesis are twofold: 1.) to identify petrographic and geochemically distinct layers which can be correlated between the Sandsloot and Tweefontein farms. Furthermore, to identify vectors or indices that discriminate between BMS and PGE mineralised and barren rocks.

Petrographically distinct layers of hornfels, calcsilicates, pyroxenites and gabbro-norites were identified in the previous chapter on petrography. This petrographic classification serves as a basis for chemostratigraphic correlation, and this classification is as follows:

- Only one of the drillcores located at Sandsloot contained calcsilicates, which can be subdivided into three subunits namely; calcsilicate subunit I (CS-I), calcsilicate subunit II (CS-II) and calcsilicate subunit III (CS-III). The intensity of contact metasomatism progresses from CS-I through CS-II to CS-III. This is coupled with a decrease in the average modal percentages of the dolomitic / calcitic (carbonate) minerals and an increase in orthopyroxene and plagioclase minerals in the order from CS-I, to CS-II to CS-III.
- Three subunits of the hornfels were identified in the two drillcores at Tweefontein, namely; hornfels subunit I (H-I), hornfels subunit II (H-II) and hornfels subunit III (H-III). The intensity of contact metasomatism progresses from the subunit H-I through to H-II to H- III. This is accompanied by a decrease in the average modal percentage of the iron oxide and quartz, as well as an increase in clinopyroxene contents from the H-I to H-II, to H-III.
- The pyroxenites in all drillcores can be broadly classified into: 1.) the medium to coarse grained pyroxenite type I (P-I) that features orthopyroxene, clinopyroxene and plagioclase; 2.) The medium grained pyroxenite type II (P-II), composed of

orthopyroxene and clinopyroxene, together with olivine; 3.) The fine to medium grained feldspathic pyroxenite type I (FP-I) with cumulus orthopyroxene and interstitial plagioclase; and 4.) The coarse grained feldspathic pyroxenite type II (FP-II) which contains predominantly plagioclase, with orthopyroxene and clinopyroxene.

In this chapter, the above subunits of calcsilicates, hornfels and pyroxenites will be geochemically classified and characterised by using the whole rock geochemical data obtained from drillcores TN754, TN200 and SS339. This data includes major oxides, trace elements and PGEs (i.e. Pt, Pd and Au), as presented in Appendix I and II. A detailed description of the approach and the geochemical data evaluation steps are as follows:

i. Geochemical classification of the rock subunits

The petrographical summary outlined above mentions the rock subunits studied in this thesis. Challenges in their petrography included the difficulty in classifying certain samples to a specific rock type. The reasons include the gradational nature of some rock boundaries and the widespread hydrothermal alteration. An unsupervised geochemical classification of these rock types was undertaken with the following goals: 1.) to classify and geochemically associate individual samples with the rock types and their subunits; 2.) to use the ensuing geochemical classification to validate the results of the petrography; and 3.) to establish the geochemical relationships between the rocks and their subunits.

This geochemical classification is achieved by hierarchical cluster analysis by unsupervised clustering the rocks. This creates distinct boundaries between rock types without any interference (thus solely on their geochemical attributes). The groups or clusters created will also be the foundation to characterise the rock types geochemically. The results are presented in section 5.1.

ii. Geochemical characterisation of the rocks and subunits.

Following the geochemical classification, the rock types are geochemically characterised based on the petrography and the validated cluster groupings. The goals of this sub-section are (1) to enable the description of the variability of elements within each lithology and its subunits (2) to graphically show comparison of the

different rock types and their subunits, (3) to establish a link between the element patterns and possible underlying geological processes. This enabled the identification of geochemical indices that interlink the rock types, and the PGEs and BMS mineralisation.

Geochemical characterisation was done by using the major, trace element and PGE data. These data were evaluated in a sequential order using descriptive statistical analysis, box-whisker-plots and spider diagrams. The results are presented in section 5.2. This section is presented in the order of data evaluation sequence as follows:

- First, a statistical summary was used to characterise the geochemical variation of the rock types and their subunits. These summaries allowed the identification of anomalous occurrences of elements in the lithologies. The results are presented for hornfels in section 5.2.2, calcsilicates in section 5.2.3, Platreef lithologies in section 5.2.4 and hanging wall gabbro-norites in section 5.2.5.
- Box-and-whisker plots were used to supplement the statistical summary results. These plots graphically display the differences between elemental distributions in the lithologies and their subunits and to identify any outliers.
- The results are presented for hornfels in section 5.2.2, calcsilicates in section 5.2.3, Platreef lithologies in section 5.2.4 and hanging wall gabbro-norites in section 5.2.5.
- Lastly, spider diagrams were used to study the variation patterns incompatible element in the rock types and their subunits. The incompatible element is presented on normalised multi-element diagrams, in which the abundances of a range of elements are compared with a reference source. Immobile element ratios were calculated and anomalies derived from the spider diagram. These ratios and anomalies provide information about the behaviour of elements within the rock types and the metasomatic subunits (i.e. calcsilicate and hornfels subunits). The results are presented for hornfels in section 5.2.2, calcsilicates in section 5.2.3, Platreef lithologies in section 5.2.4 and hanging wall gabbro-norites in section 5.2.5.

iii. Mass Balancing

The petrography in chapter 4 revealed that the progressive mineralogical and textural changes between calcsilicates and hornfels units have been induced by contact metamorphism and the interaction between the Platreef magma and the floor rocks. A mass balancing study was therefore undertaken to establish, monitor and geochemically characterise element variation patterns in the contact metasomatic subunits. The approach used immobile elements to calculate the mass changes that occurred within the metasomatic subunits (i.e. the hornfels and calcsilicate subunits). The results are presented in section 5.3. and further sub-divided into sections into: 1.) mass transfer between the hornfels (Tweefontein) and the Platreef magma in section 5.3.4; 2.) Between the calcsilicates (Sandsloot) and the Platreef magma in section 5.3.5.; and 3.) Within the pyroxenites, at both localities in section 5.3.6.

iv. Chemostratigraphy

The chemostratigraphy section of this study integrated the results from the geochemical characterisation and the degree of element loss or gain derived from the mass balance calculations for the rocks and subunits. The objective was in establishing chemostratigraphic units, i.e. identifying geochemically distinct units, and correlating them in the three drillcores under study. The goal was to identify element associations for each rock type and discern geochemical indices that characterise them. The results of this section are given in section 5.4.

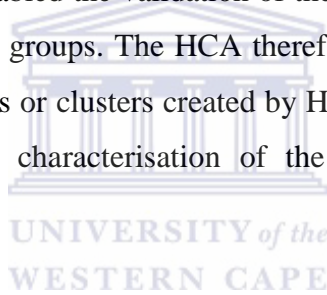
v. Geochemical vectoring

This section looked into the feasibility of using quantifiable element ratios, pathfinder elements in defining a consistent gradient indicative of the ore environment. A major objective was to discern ore environments that are typically BMS or PGE or BMS-PGE mineralisation. The results of this section are given in section 5.4.

5.1 Geochemical classification of the various rock types

A major challenge encountered in the petrography was the inability to clearly demarcate the boundaries of the lithologies and their subunits. This is further exacerbated by pervasive hydrothermal alteration and the occurrence of gradational boundaries between the rock units. The major element chemistry was therefore employed to classify the rocks and validate the petrography results.

Hierarchical cluster analysis (HCA) was undertaken using the major element contents in the samples. The HCA was chosen because it easily groups or clusters the rock types, and can separate samples which are geochemically different from each other. The technique is being used in an unsupervised way, i.e. not pre- grouping the geochemical data according to the rock types and therefore allowing HCA to create distinct boundaries between rock types without any interference. This enabled the validation of the petrography results and allocated marginal samples to distinct rock groups. The HCA therefore aided the petrography and has not substituted it. The rock groups or clusters created by HCA and the petrography served as foundation for the geochemical characterisation of the rock types and the subsequent chemostratigraphy.



5.1.1 Cluster analysis methodology

Cluster analysis was used to arrange the number of observations or measured variables into groups that are similar in their characteristics or behaviour (Hartigan, 1975; Everitt and Dunn, 2001; Kaufmann and Rousseeuw, 2005; Reimann et al., 2008). In an ideal HCA outcome the samples or variables within a cluster should show the closest similarity to each other while the differences between the clusters are preferably as large as possible (Reimann et al., 2008).

Cluster analysis must thus determine the number of groups as well as the memberships of observations or variables in those groups. To determine the group memberships, most clustering methods use a measure of similarity between the measurements. The similarity is usually expressed by distances between the observations in the multivariate data space.

During the application of cluster analysis only major elements were used. The choice of variables used for cluster analysis is an essential step and should be carefully considered. Only major elements were used to reduce the effect of variance by excluding, e.g. trace elements in parts per million from the HCA (Rock, 1988). This is justifiable as the major elements also determine the bulk chemistry of the rock types, which is the objective of the exercise. These data were prepared for cluster analysis by using the appropriate data transformation and standardization (Reimann et al., 2008).

In HCA, a hierarchy of partitions is formed, i.e. grouping the samples into 1 to n clusters (n = number of samples). The first step of HCA is calculating a distance matrix from which the dendrograms are generated. This technique starts with single sample clusters and then the clusters are enlarged stepwise (Reimann et al., 2008). According to a given distance or similarity measure, cases are grouped based on their 'nearness'. For the purpose of this study, the hierarchical clustering is based on the Ward's method, and the distance expansion was performed by the squared Euclidean distance. The first step in the evaluation of the dendrograms was to ascribe the clusters to the rock types, and then identify the individual samples that are associated with these rock lithologies (Kaufmann and Rousseeuw, 1990, 2005). HCA on the data was performed using SPSS 19[®] and the results are presented as a dendrogram.

5.1.2 Hierarchical Cluster Analysis Results

The dendrogram in Fig. 5.1 shows the clustering of samples based on the similarities in their major element chemistry. The dendrogram includes all samples from Tweefontein and Sandstoot. The dendrogram comprise of two major clusters, 1 and 2, and numerous sub-clusters:

- Cluster 1 can be subdivided into sub-clusters A and B. Sub-cluster A is composed of three groups; group (i) and (ii) which appear compositionally more distant from group (iii). Samples in group (i) of the sub-cluster A are FP-I / noritic and P-I. Group (ii) of the sub-cluster A is P-II while group (ii) is composed of FP-II and gabbro-norites samples.
- Group (i) of the sub-cluster A contain the highest pyroxene (orthopyroxene plus clinopyroxene) contents, which decreases through group (ii) to group (iii). The reverse trend is the case for plagioclase. The detailed mineralogy is already given in chapter 4.

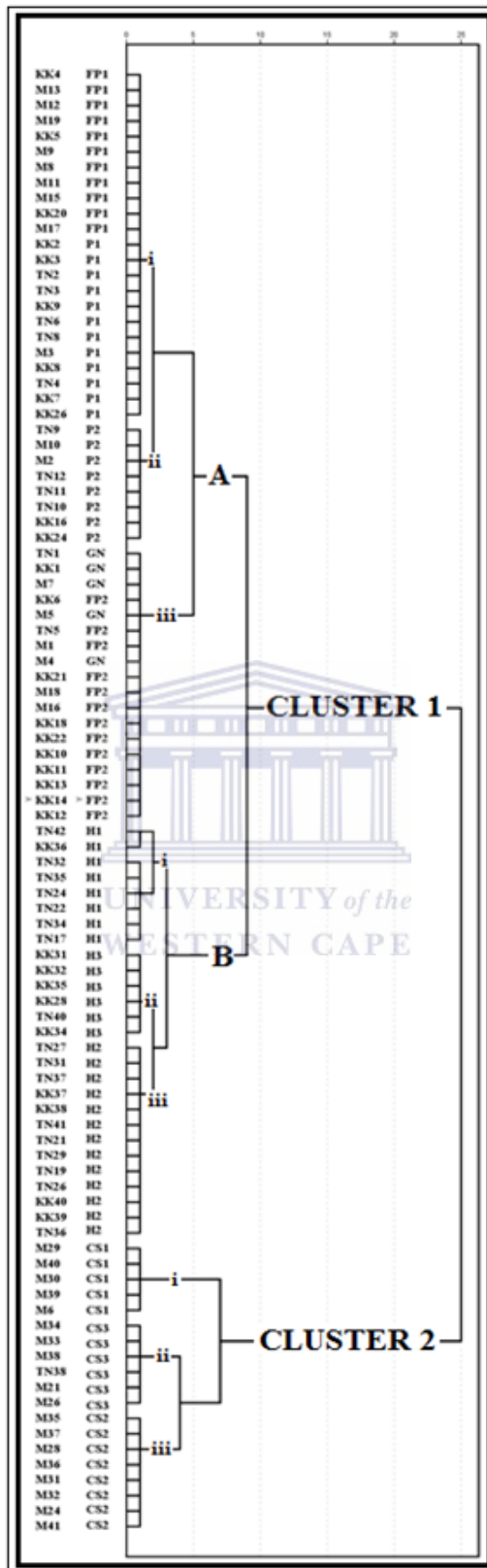


Figure 5.1: Dendrogram illustrating clusters of samples from the data of drillcores TN754, TN200 and SS339. These clusters represent all samples from all rock types, where annotations show the respective subunits.

The Sub-cluster B comprises of three hornfels groups; group B (i) which comprises of samples from H-I followed by B (ii) with samples H-III and B (iii) comprising of samples from H-II.

Group (i) of the sub-cluster B has the lowest pyroxene (mainly clinopyroxene) contents, which increases through group (ii) to group (iii). The reverse trend is the case for plagioclase. The detailed mineralogy is also already given in chapter 4.

Cluster 2 comprises of three calcsilicate groups; group (i) is samples from CS-I followed by (ii) with samples from CS-III and (iii), which are samples from CS-II.

Group (i) of the cluster 2 has the lowest orthopyroxene contents, which increases through group (ii) to group (iii). The reverse trend is the case for the carbonate contents in these calcsilicate subunits. The detailed mineralogy is also already given in chapter 4.

5.2 Geochemical characterisation of rocks

5.2.1 Introduction

The geochemical classification of the various rock types in the previous section supported the petrographical study that was undertaken. The clusters (groups) created represented the various rock types and their samples. This classification effectively confirmed that the rock types were classified correctly and that the borderline samples could be placed accordingly. Together the petrographical and geochemical classification revealed the following rock types: the floor rocks which can be subdivided into three metasomatic subunits of calcsilicates and three metasomatic subunits of hornfels; the Platreef rocks which can be subdivided into the pyroxenite type I (P-I), the pyroxenite type II (P-II), the feldspathic pyroxenite type I (FP-I) and the feldspathic pyroxenite type II (FP-II); and the hanging wall gabbro-norite.

This section describes the patterns of element variation and geochemically characterises these rocks types and their sub-groups. This will be based on the major element, trace element and PGE data. These data will however first be evaluated using descriptive statistical analysis, box-whisker-plots and spider diagrams.

The goals of this section are to identify the magnitude and distribution of the various elements within these rock types; the major and trace element associations for each rock type; and the relationship between these major and trace elements with the PGEs and BMS. It should clearly show which elements control the attributes of the samples in each rock type and subunits.

The statistical summaries will be used to define the magnitude and degree of variation of elements in the rock types and their subunits. The box-and-whisker plots will be used to graphically display the differences in magnitude and degree of variation of elements in the various rock types and subunits. The spider diagrams or normalised multi-element diagrams will graphically display and use the variation patterns of the HFSE and LILE to characterise the rock types and their subunits. Indices derived from the spider diagrams were compared to a reference source.

These rock types and their subunits will be characterised and presented in the following order; i.) Hornfels which includes the three subunits are detailed in section 5.2.2; ii.) Calcsilicates which include the three subunits presented in section 5.2.3; iii.) Platreef package, which incorporates the pyroxenite and feldspathic pyroxenite subunits are detailed in section 5.2.4; iv.) Gabbronorite are characterised and compared to the rocks of the Platreef package in section 5.2.5. Details of the data evaluation procedures are as follows:

a. Statistical summary

Descriptive statistical analysis was performed on the geochemical data subsets for all rock types and their subunits. The data comprise of major element oxides: SiO₂, TiO₂, Al₂O₃, Fe₂O₃, MnO, MgO, CaO, Na₂O, K₂O, P₂O₅ and Loss on Ignition (LOI) and the trace elements Pt Pd, Ba, Ce, Co, Nb, Ni, Pb, Rb, Sr, V, Y, Zn, Zr, Mo, U, Ni, Rb and Zn. The statistical data summaries for the hornfels, calcsilicates, Platreef rocks and their respective subgroups as well as those for the hanging wall gabbronorite have been tabulated in tables 5.1, 5.2, 5.3 and 5.4 respectively.

b. Box-and-whisker plots

Box-and-whisker plots were used to graphically define the magnitude and degree of variability of the elements and compare these for the different rocks types and their subunits.

The idea is to decipher the pattern of variation of major and trace elements amongst a group of rocks (e.g. amongst the three subunits of calcsilicates). The box and whiskers plot combines the minimum and maximum values with the lower and upper quartiles on a useful graph. It consists of a horizontal line, drawn according to scale, from the minimum to the maximum data values, and a box drawn from the lower quartile to the upper quartile with a vertical line within the box marking the median (Myers and Thorbjorsen, 2004). Box-and-whisker plots for the hornfels, calcsilicates and Platreef rocks have been represented in figures 5.2, 5.4 and 5.6 respectively.

c. Spider diagrams

Spider diagrams have been applied with the goal to use normalised HFSE and LILE patterns to define and discriminate the rock types and their subunits. Trace elements, especially the HFSE and LILE are sensitive indicators of petrogenesis, the rock types which share a common source, will most likely plot similarly. Patterns of variation of elements within the rock types and their subunits may also provide information about the extent of fractionation.

Spider diagrams are graphical binary plots of the abundances of a set of elements in an analysed sample relative to their abundance in some standard, e.g. chondritic meteorite. The elemental abundances are adjusted to a variety of normalizing values, e.g. primordial mantle, chondrites, MORB, average upper crust, North American shale. Trace element contents of the rock clusters are presented as primitive mantle normalised plots (see figures 5.3, 5.5, 5.7 and 5.8) using the normalizing values of McDonough and Sun (1989). This normalising values and method were used because it reflects the trace elements that are available in the geochemical data set at Sandsloot and Tweefontein. The geochemical trace element data (see Appendix I) were processed by the GCDkit 2.3.

Table 5.1: Statistical summary of oxides (wt. %), trace elements (ppm) and PGE (g/t) for hornfels subunits. It is accompanied by a summary of anomalies_{MN} for the hornfels subunits (H-I, H-II and H-III).

	Hornfels zone I			Hornfels zone II			Hornfels zone III		
	Min.	Max.	Ave.	Min.	Max.	Ave.	Min.	Max.	Ave.
Major	(N=8)			(N=13)			(N=6)		
SiO ₂	24.87	42.70	35.81	48.50	67.70	56.10	42.95	46.83	44.17
Al ₂ O ₃	0.20	12.97	6.72	0.01	10.09	4.31	1.00	6.63	3.11
Fe ₂ O ₃	26.02	55.41	39.15	13.78	39.09	26.75	15.11	26.43	22.66
MnO	0.20	1.74	0.46	0.05	0.50	0.26	0.32	0.48	0.42
MgO	1.14	9.23	6.04	1.89	6.52	3.79	5.47	10.28	8.51
CaO	2.23	10.51	6.88	1.51	15.17	6.67	14.41	21.53	17.19
Na ₂ O	0.21	1.55	0.77	0.12	1.03	0.46	0.38	0.69	0.48
K ₂ O	0.01	0.93	0.19	0.00	0.98	0.34	0.06	1.25	0.48
P ₂ O ₅	0.02	0.22	0.07	0.01	0.32	0.08	0.01	0.11	0.03
TiO ₂	0.02	1.48	0.51	0.01	0.54	0.19	0.20	0.32	0.26
SO ₃	0.11	5.07	1.27	0.01	1.40	0.28	0.05	1.41	0.77
LOI	0.20	5.00	2.13	0.20	2.60	0.77	1.00	3.40	1.96
Trace	(N=8)			(N=13)			(N=6)		
As	14.21	59.38	34.87	0.50	43.75	14.53	8.98	29.82	23.80
Ba	37.09	262.82	93.69	43.04	193.95	96.54	50.84	156.97	96.64
Ce	265.39	659.55	403.12	114.28	764.86	349.04	124.53	312.28	207.38
Co	1.66	319.92	73.18	0.25	115.81	23.76	0.07	30.03	13.91
Cu	37.13	2330.64	796.51	17.41	1431.81	223.47	18.90	112.32	60.10
Nb	13.99	21.59	17.53	6.06	22.32	16.07	11.26	44.16	19.53
Ni	89.93	8805.97	1869.26	25.80	3534.69	531.40	16.30	225.90	107.25
Pb	0.49	11.92	5.58	0.32	11.73	4.76	0.50	13.58	5.83
Rb	3.45	76.26	19.81	0.55	77.91	29.24	8.77	58.80	24.72
Sr	6.65	114.44	60.34	1.67	143.46	53.53	12.33	134.01	50.46
V	15.70	175.34	84.54	19.49	291.01	70.45	0.45	128.22	77.38
Y	3.18	14.26	7.65	0.50	43.69	8.54	0.62	92.61	17.68
Zn	37.67	141.28	89.12	30.20	119.73	68.37	28.38	53.11	42.35
Zr	1.93	29.84	18.50	0.13	73.62	20.44	0.02	270.07	59.46
Mo	1.83	8.60	5.41	0.38	13.30	6.98	1.83	8.48	4.19
U	0.59	1.00	0.68	-0.01	6.47	1.17	0.42	1.00	0.84
Th	0.25	20.83	6.69	0.25	34.23	9.31	0.25	0.53	0.30
PGEs	(N=5)			(N=4)			(N=3)		
Au	0.05	0.16	0.09	0.05	0.13	0.08	0.05	0.05	0.05
Pd	0.05	1.28	0.47	0.05	1.05	0.44	0.05	0.05	0.05
Pt	0.05	0.88	0.24	0.05	0.39	0.20	0.05	0.05	0.05
Ratios	(N=8)			(N=13)			(N=6)		
Al ₂ O ₃ /TiO ₂	0.56	57.33	20.69	0.13	39.38	15.95	5.00	16.04	10.45
TiO ₂ /Zr	83.03	584.52	299.36	10.42	3846.15	475.73	50.37	120000.00	30200.69
Zr/Y	0.53	29.91	6.17	0.05	21.50	5.25	0.03	21.94	6.83
Anomalies	(N=8)			(N=13)			(N=6)		
K*	0.00	0.28	0.06	0.00	0.42	0.12	0.03	0.22	0.11
Rb*	0.69	5.00	2.38	0.14	9.19	2.55	0.98	6.11	2.60
Ce*	1.78	35.49	10.36	1.17	121.94	24.26	1.05	15.29	7.70
Ba*	0.07	1.54	0.62	0.05	3.24	1.10	0.32	1.69	1.00
Th*	0.09	12.54	3.01	0.08	16.53	3.38	0.09	0.33	0.16
U*	0.22	7.97	2.32	0.00	6.32	2.26	2.12	5.08	3.76
Nb*	0.36	2.00	1.26	0.20	1.89	1.02	0.52	1.32	0.87
Pb*	0.07	2.08	0.90	0.03	2.89	1.02	0.09	3.37	1.14
Sr*	0.01	1.37	0.22	0.02	0.23	0.07	0.07	0.16	0.11
P*	0.25	41.45	5.99	0.12	13.40	3.48	0.15	2.94	1.16
Zr*	0.03	1.95	0.85	0.02	6.42	1.34	0.00	2.71	0.94
Ti*	0.60	10.90	4.22	0.05	23.52	3.59	0.21	150.55	38.69
Y*	0.03	8.67	1.74	0.13	9.61	2.38	0.12	1.54	0.60

Inclusion of HFSE and LILE are particularly useful because their relative immobility and fluid-insoluble nature that results in: (1) a tendency to retain protolith geochemical signature that may prove useful to determine e.g. the protoliths of metasomatised rocks (Dusel-Bacon et al., 2004). Many VMS studies had use HFSE and LILE to identify protolith provenance, for example, Whitford and Ashley (1992).

Anomalies in the spider diagrams were calculated using the method by Taylor and McLennan (1985). Anomalies were calculated for K, Rb, Ce, Ba, Nb, Pb, Sr, P, Zr, Y and Ti and are represented in tables 5.1, 5.2, 5.3 and 5.4. This method uses the adjacent elements in the calculation, e.g. to calculate the Ti anomaly (Ti*): the normalised value of Zr is added to the normalised value of Y, and then divided by 2.

5.2.2 Hornfels

Table 5.1 shows the statistical summary of the major, trace elements, and geochemical indices for the three hornfels subunits; H-I, H-II and H-III. Some of these and the subsequent dataset from Tweefontein compared favourably with published data by Ihlenfeld and Keays (2011). The box and whisker plot in Fig.5.2 graphically shows the magnitude and the elemental variation patterns in the three hornfels subunits.

The hornfels subunit H-I is characterised by the highest average contents of Al₂O₃, Fe₂O₃, Na₂O, MnO, TiO₂, SO₃, LOI, As, Ce, Co, Cu, Ni, V, Sr, Au, Pt and Pd. Conversely, these contain the lowest average contents of SiO₂, K₂O, Ba, Nb, Rb, Y, Zr and U. Subunit H-II has the highest average contents of SiO₂, P₂O₅, Rb, Zn, Mo, U and Th coupled with the lowest contents of MnO, MgO, CaO, Na₂O, SO₃, LOI, As, Pb and V. The subunit H-III show the highest average contents of MgO, CaO, K₂O, Nb, Zn and Zr. These rocks are also characterised by the lowest average contents of as Al₂O₃, Fe₂O₃, P₂O₅, TiO₂, Ce, Co, Cu, Ni, Sr, Y, Mo and Th.

Some elements below are chosen to illustrate the typical compositional variation patterns in the hornfels units. For example, H-I contains SiO₂ (24.87 – 42.7 wt. %); Fe₂O₃ (26.02 – 55.41 wt. %), and CaO (2.23 – 10.51 wt. %). H-II is composed of SiO₂ (48.5 – 67.7 wt. %); Fe₂O₃ (13.78 – 39.09 wt. %), and CaO (1.51 – 15.17 wt. %). H-III has SiO₂ (42.95 – 46.83 wt. %); Fe₂O₃ (15.11 – 26.43 wt. %), and CaO (14.41 – 21.53 wt. %).

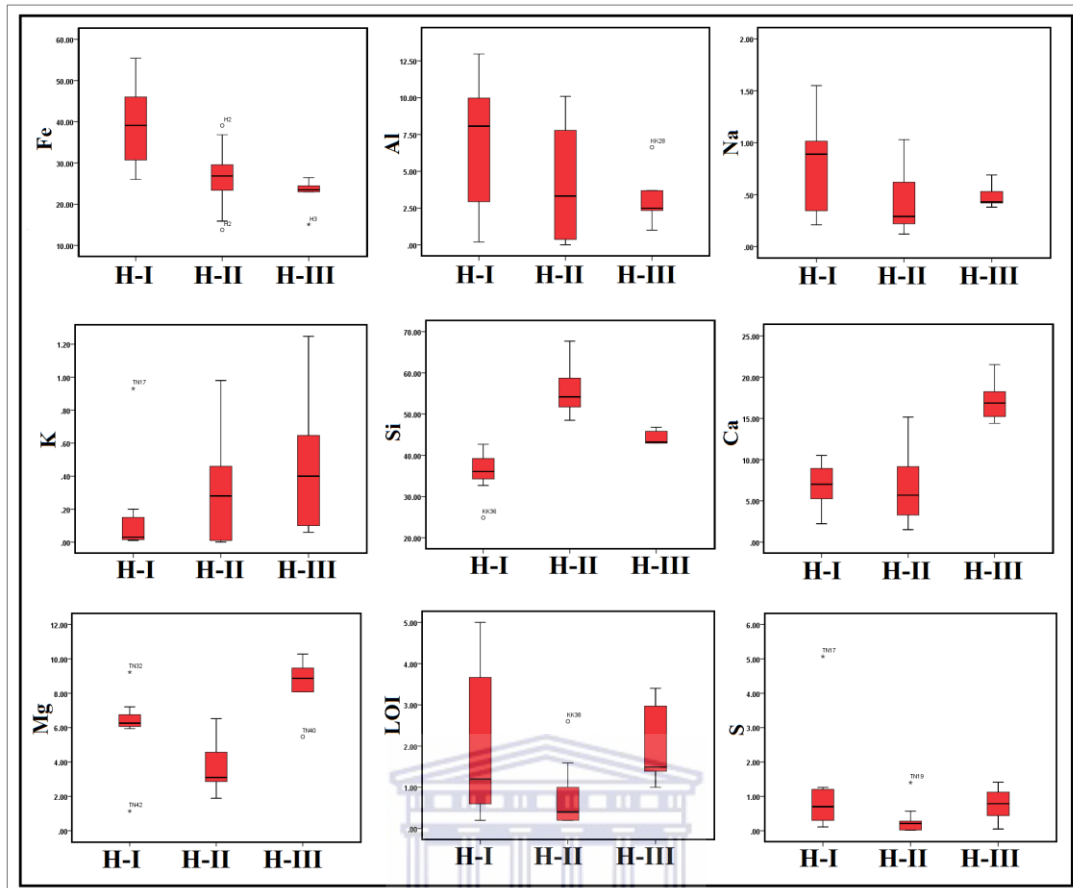


Figure 5.2: Box and whisker plots showing the variation of major elements, for the three hornfels subunits (i.e. subunits H-I, H-II and H-III).

The composition of the base metals also varies between the three subunits: Copper in H-I (37.13 – 2330.64 ppm) and Ni (89.93 – 8805.97 ppm). H- II has lower base metals contents, Cu (17.41 – 1431.81 ppm) and Ni (25.80 – 3534.69 ppm). H-III has the least BMS contents, Cu (18.90 – 112.32 ppm) and Ni (16.30 – 225.9 ppm).

As revealed by the statistical summary table and the box and whisker plots, a decrease in the average contents of Fe_2O_3 , Al_2O_3 , Ce, Co, Cu, Ni, Zn, Zr, Au, Pd and Pt from H-I, H-II to H-III is evident. This is coupled with an increase in the average contents of Zr and Y in the same order. These compositional variations corroborate the results of the petrography and the cluster analysis thus reflecting the inherent mineralogy for these groups; 1.) the iron oxide rich nature of H-I with high BMS and PGE. 2.) the siliceous nature of H-II and 3.) the higher pyroxene contents of H-III.

The three hornfels subunits show variable immobile ratios, e.g. $\text{Al}_2\text{O}_3/\text{TiO}_2$; TiO_2/Zr and Zr/Y . For example, a decrease in the average contents of $\text{Al}_2\text{O}_3/\text{TiO}_2$, this is coupled with an increase in the contents of TiO_2/Zr from H-I, H-II, to H-III. A slightly different trend is shown by Zr/Y from H-II, H-III to H-I with 0.05 – 21.50, 0.03 – 21.94 and 0.83 – 29.91 ppm respectively.

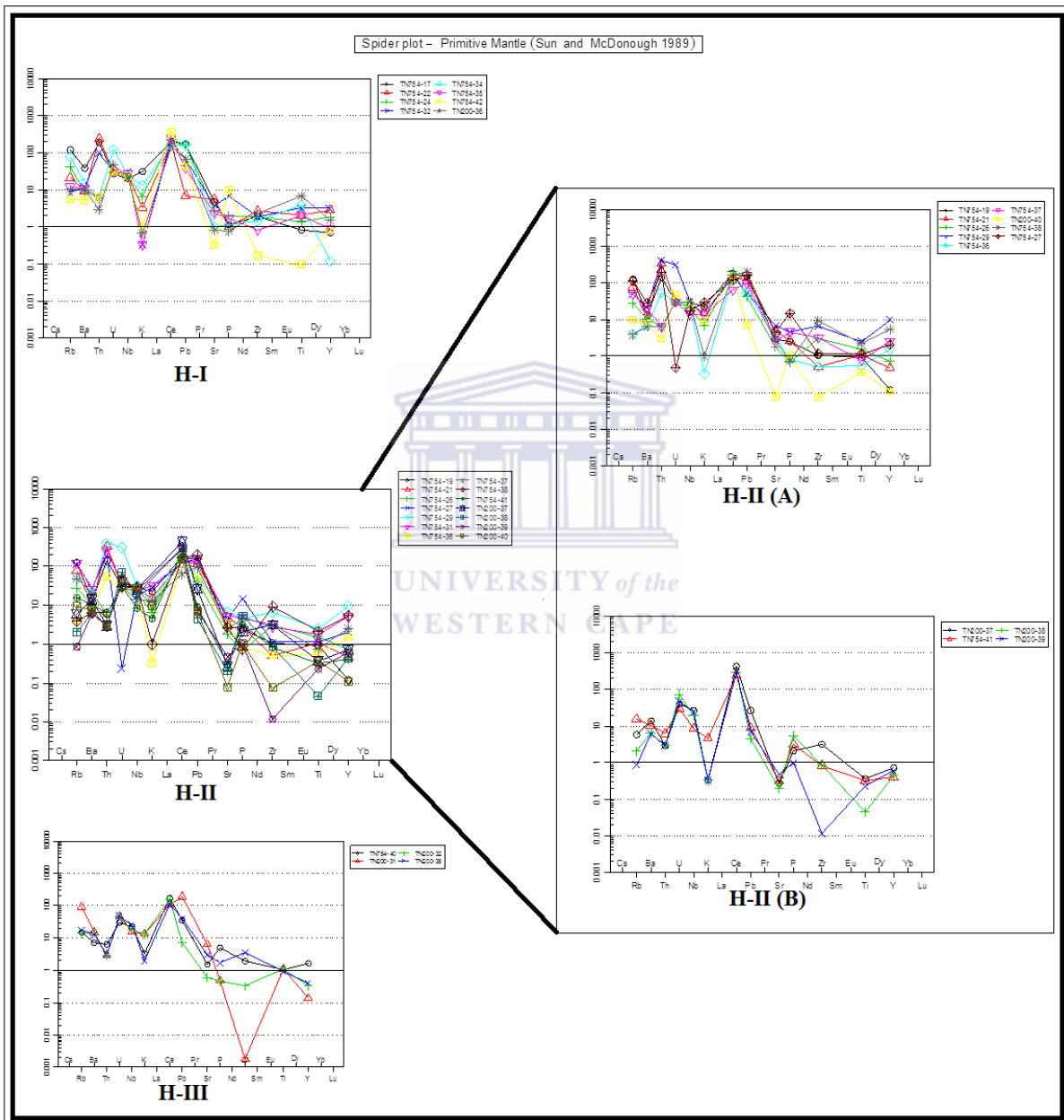


Figure 5.3: Trace-element compositions of the hornfels subunits (primitive mantle normalization values from McDonough and Sun, 1989).

The spider diagrams in Fig. 5.3 can be used to further characterise the hornfels subunits on the basis of their trace element systematics and occurrence of anomalies. They display varying shapes, degree of steepness of curves and patterns of anomalies/ enrichment of the HFSE relative to LILE. The anomalies derived from these diagrams are represented in table 5.1. The anomalies were evaluated following the criteria used by Ordonez-Calderon et al. (2008); values < 1 are qualified as negative; between 1-2 as weakly positive and above 2 as positive etc. The table and the accompanied spider diagram are evaluated as follows:

The LILE (Ba, K, and Sr), thus excluding Rb, in H-I have negative to weakly positive anomalies; K ($K^*_{MN} = 0.002 - 0.27$); Ba ($Ba^*_{MN} = 0.07 - 1.54$); Sr ($Sr^*_{MN} = 0.01 - 1.37$). Highly positive Ce ($Ce^*_{MN} = 1.78 - 35.49$) and Th ($Th^*_{MN} = 0.09 - 12.54$), U ($U^*_{MN} = 0.22 - 7.97$), Ti ($Ti^*_{MN} = 0.6 - 10.9$) dominate the HFSE patterns. Niobium anomaly is positive, Nb ($Nb^*_{MN} = 0.36 - 2.00$) while P ($P^*_{MN} = 0.248 - 41.454$) is also in parts highly enriched in these rocks.

The LILE, especially Rb ($Rb^* = 0.14 - 9.19$) are more enriched in H-II compared to H-I. Others show a negative K ($K^*_{MN} = 0.002 - 0.42$) and Ba ($Ba^*_{MN} = 0.05 - 3.24$) anomaly of a positive value range. The hornfels subunit H-II, display anomalies for Ce ($Ce^*_{MN} = 1.17 - 121.94$), Ti ($Ti^*_{MN} = 0.05 - 23.5$) Y ($Y^*_{MN} = 0.13 - 9.61$) and Th ($Th^*_{MN} = 0.08 - 16.53$), which are more pronounced than those for the H-I hornfels. The anomalies of U ($U^* = 0.0 - 6.23$) and P ($P^*_{MN} = 0.12 - 13.40$) are less pronounced than those in H-I.

As illustrated on Fig. 5.3, the subunit H-II was further subdivided into H-II (A) and H-II (B). The figure illustrates that the subunit H-II (A) shows a spider diagram curve similar in steepness to the subunit H-I. The spider curve for unit H-II (B) which is shales is steeper than H-I and H-II (A). The hornfels subunit H-III is characterised by pronounced anomalies of Ti ($Ti^* = 0.21 - 150$); Ce ($Ce^*_{MN} = 1.05 - 15.29$) and to a lesser extent U ($U^* = 2.12 - 5.08$); Pb ($Pb^* = 0.09 - 3.37$). Other HFSE pattern shows negative to weakly positive anomalies of Nb ($Nb^*_{MN} = 0.52 - 1.32$), and Th ($Th^*_{MN} = 0.09 - 0.33$) as well as P ($P^*_{MN} = 0.15 - 2.94$). Most of the LILE, except Rb, show negative to weakly positive anomalies; K ($K^*_{MN} = 0.03 - 0.22$), Ba ($Ba^*_{MN} = 0.32 - 1.69$).

The hornfels subunit H-II differs distinctly from the subunits H-I and H-III as it features higher HFSE contents. The former is most mineralised with PGEs and BMS but it is least altered.

5.2.3 Calcsilicates

Table 5.2 shows the statistical summary of major, trace elements and geochemical indices for three calcsilicate subunits; CS-I, CS-II and CS-III. The box and whisker plot in Fig. 5.4 graphically demonstrates the magnitude and elemental variation patterns in the three calcsilicates subunits. These and the subsequent dataset from Sandsloot compared favourably to published data by Harris et al. (2011). The calcsilicate subunit CS-I contains the highest average contents of CaO, LOI, As, Ba, Ce, Sr, Y, Zr, U, and Th. Conversely, these also have the lowest average contents of SiO₂, Al₂O₃, Fe₂O₃, P₂O₅, TiO₂, SO₃, Co, Cu, Nb, Ni, Rb, V, Zn and Mo.

In Table 5.2, calcsilicate subunit CS-II feature the highest average contents of Al₂O₃, MnO, MgO, Nb and Au coupled with the lowest contents of CaO, Na₂O, Sr, Zr, As, Ce, Pb and U. The calcsilicate subunit CS-III contains the highest average contents of SiO₂, Fe₂O₃, Na₂O, TiO₂, SO₃, Co, Cu, Ni, Pb, Rb, V, Zn, Mo, Pt and Pd. The CS-III also contains the lowest contents of MnO, MgO, LOI, Ba and Y.

The changing pattern of elements and oxides in the three subunits of the calcsilicate is best illustrated by their contents in SiO₂, CaO, MgO and the base metals. For example, CS-I contains SiO₂ (0.01 – 11.02 wt. %), MgO (3.72 – 23.04 wt. %) and CaO (38.59 – 54.93 wt. %). CS-II is composed of SiO₂ (17.15 – 33.74 wt. %), MgO (25.47 – 42.03 wt. %) and CaO (12.24 – 31.69 wt. %). CS-III has SiO₂ (28.39 – 41.09 wt. %), MgO (8.67 – 15.36 wt. %) and CaO (21.96 – 38.92 wt. %).

For the base metals variation patterns in the calcsilicate subunits, Ni contents in CS-I vary between 12.25 – 53.52 ppm and Cu from 36.16 – 60.73 ppm. Slightly higher is CS-II calcsilicate subunit with base metal contents: Ni (45.01 – 1275.71 ppm) and Cu (23.02 – 785.62 ppm). The calcsilicate subunit CS-III contains the highest BMS contents with Ni (81.3 – 5337.36 ppm) and Cu (55.9 – 3466.15 ppm).

Table 5.2: Statistical summary of oxides (wt. %), trace elements (ppm) and PGE (g/t) for calcsilicate rocks.

ROCKS	Calc-silicate zone I			Calc-silicate zone II			Calc-silicate zone III		
	Min.	Max.	Ave.	Min.	Max.	Ave.	Min.	Max.	Ave.
Major	(N=5)			(N=8)			(N=6)		
SiO ₂	0.01	11.02	4.53	17.15	33.74	26.60	28.39	41.09	35.22
Al ₂ O ₃	0.01	0.76	0.18	0.01	8.43	3.78	0.02	6.35	3.61
Fe ₂ O ₃	0.01	3.71	1.19	0.01	10.26	4.45	0.01	14.27	7.99
MnO	0.31	1.29	0.75	0.38	2.10	1.24	0.20	1.08	0.40
MgO	3.72	23.04	16.67	25.47	42.03	33.14	8.67	15.36	11.77
CaO	38.59	54.93	42.85	12.24	31.69	19.32	21.96	38.92	31.48
Na ₂ O	0.70	1.01	0.79	0.29	0.62	0.46	0.69	2.32	1.35
K ₂ O	0.01	0.01	0.01	0.01	0.01	0.01	0.01	0.01	0.01
P ₂ O ₅	0.01	0.01	0.01	0.01	0.04	0.02	0.01	0.02	0.02
TiO ₂	0.01	0.20	0.07	0.03	0.26	0.16	0.05	0.37	0.17
SO ₃	0.01	0.23	0.11	0.02	0.92	0.29	0.03	1.76	0.84
LOI	29.00	40.00	32.95	2.09	21.60	10.64	2.20	16.47	7.17
Trace	(N=5)			(N=8)			(N=6)		
As	100.75	169.00	116.80	0.50	1.56	0.63	15.20	52.57	30.67
Ba	42.04	88.97	60.11	39.94	59.84	49.10	46.39	64.82	55.58
Ce	158.02	250.09	207.80	39.17	131.24	76.61	73.86	193.77	120.70
Co	3.38	16.15	8.79	1.04	78.49	31.16	12.03	255.59	99.67
Cu	36.16	60.73	45.91	23.02	785.62	265.37	55.90	3466.15	1543.49
Nb	1.77	19.88	10.08	8.44	15.21	12.12	7.31	15.03	10.64
Ni	12.25	53.52	26.15	45.01	1275.71	455.18	81.30	5337.36	2454.44
Pb	0.40	9.39	4.39	0.65	8.01	3.52	0.33	20.08	10.65
Rb	0.84	2.97	1.71	0.61	3.66	2.01	1.58	2.93	2.09
Sr	13.66	87.94	39.09	1.00	8.48	3.26	6.62	62.82	29.30
V	1.43	23.02	12.69	11.56	62.28	33.69	13.00	256.95	94.88
Y	0.19	168.36	37.50	1.39	19.27	8.04	2.14	11.83	5.79
Zn	20.65	39.86	30.93	26.74	78.02	46.13	29.39	77.50	56.10
Zr	12.87	41.10	30.10	3.17	25.59	13.90	3.20	31.62	13.97
Mo	0.80	0.80	0.80	0.04	2.59	1.02	0.80	10.99	4.87
U	0.23	22.54	4.85	0.50	0.50	0.50	0.50	0.73	0.55
Th	0.50	45.41	9.48	0.50	0.50	0.50	0.50	0.50	0.50
PGEs	(N=0)			(N=2)			(N=1)		
Au				0.05	0.14	0.10	0.08	0.08	0.08
Pd				0.32	0.39	0.36	0.75	0.75	0.75
Pt				0.26	0.45	0.36	0.23	0.23	0.23
Ratios	(N=5)			(N=8)			(N=6)		
Al ₂ O ₃ /TiO ₂	0.25	3.80	1.35	0.17	85.60	35.73	0.33	46.83	19.86
TiO ₂ /Zr	2.77	48.66	23.65	72.55	187.05	137.14	62.52	313.59	136.04
Zr/Y	0.21	151.53	33.99	1.43	5.84	2.60	0.54	18.32	4.35
Anomalies	(N=5)			(N=8)			(N=6)		
K*	0.00	0.01	0.01	0.01	0.01	0.01	0.01	0.02	0.01
Rb*	0.14	0.70	0.33	0.29	0.70	0.43	0.15	0.87	0.46
Ce*	2.13	29.84	10.42	0.57	24.30	5.77	0.72	4.65	2.26
Ba*	0.03	2.58	1.63	1.26	2.17	1.76	1.05	2.25	1.61
Th*	0.01	33.89	7.03	0.28	0.39	0.35	0.36	0.40	0.38
U*	0.09	256.66	52.45	1.77	2.95	2.57	1.75	2.69	2.11
Nb*	0.00	2.31	1.30	0.85	1.75	1.13	0.98	1.77	1.41
Pb*	0.13	1.85	0.98	0.15	7.00	4.05	0.83	5.45	2.35
Sr*	0.03	0.21	0.10	0.00	0.24	0.07	0.00	0.03	0.01
P*	0.12	0.51	0.25	0.40	0.96	0.68	0.49	2.26	1.28
Zr*	2.92	16.50	8.12	0.62	2.24	1.38	0.70	3.42	1.67
Ti*	0.00	1.06	0.48	0.47	3.79	1.85	0.24	8.04	3.19
Y*	0.30	804.39	163.83	1.12	2.18	1.70	0.32	4.83	2.51

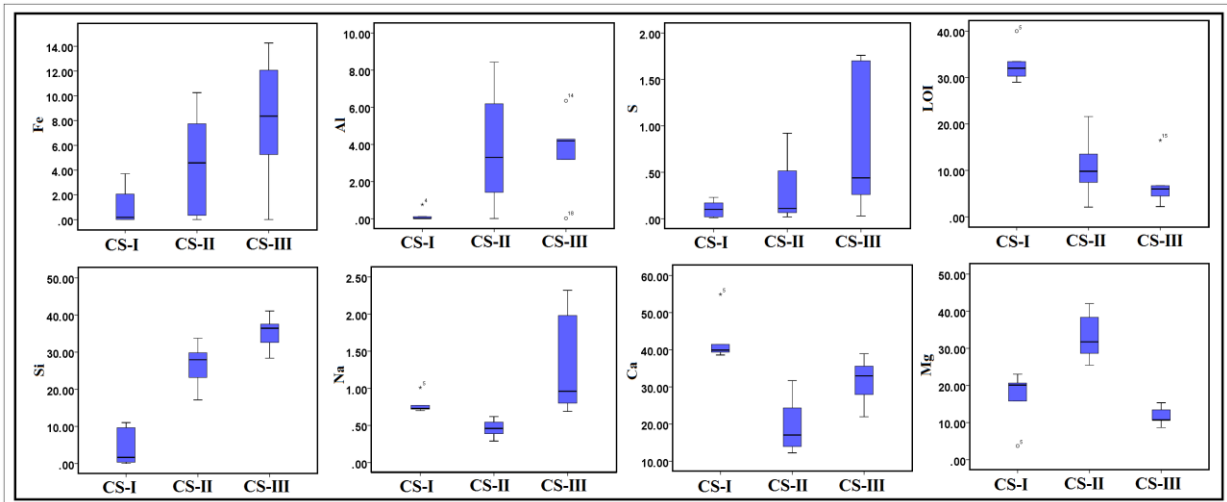


Figure 5.4: Box and whisker plots of various major elements for the three subunits of the calcsilicates (i.e. CS-I, CS-II and CS-III).

The statistical summary is well corroborated by some examples of elements presented in the box and whiskers plot in Fig 5.4. From these, an increase in the average contents of SiO_2 , Fe_2O_3 , TiO_2 , SO_3 , Co, Cu, Ni, Rb, V and Zn from CS-I, CS-II to CS-III is evident. The reverse is the case for LOI and Y contents.

These compositional variations, together with the results in the petrography and the cluster analysis, reflect the inherent mineralogy of these subunits broadly as follows: 1.) CS-I is dominated by a carbonate mineralogy. 2.) Orthopyroxene defines the composition CS-II while 3.) plagioclase and pyroxene (clinopyroxene plus orthopyroxene) control the mineralogy of CS-III where high PGE/ BMS contents also occur.

The compositional variations in the three calcsilicates subunits is also corroborated by immobile element ratios, e.g. highest $\text{Al}_2\text{O}_3/\text{TiO}_2$ in the calcsilicate subunit CS-II compared to the others (Table 5.2), which is rooted in the plagioclase mineralogy. The Zr/Y ratio calcsilicate for the subunit CS-I is most pronounced (0.21 – 151.53) and decreases to (1.43 – 5.84) in CS-II and 0.54 – 18.32 in CS-III. Conversely, CS-I to III subunits show increased TiO_2/Zr values from 2.77 – 48.66 to 72.85 – 187.05, and CS-III has 65.52 – 313.59 respectively. The progressive increase of TiO_2 , Zr and Y from CS-I, to CS-II, to CS-III can be observed.

The spider diagram in Fig. 5.5 can further be used to characterise the calcsilicate subunits on the basis of the trace element systematics and occurrence of anomalies. The three calcsilicate subunits display horizontally undulating or sinuous curves, whose trough and crest are defined by the anomalies of Ce, U, K, Ce and Pb. The anomalies are derived from these diagrams and are represented in table 5.2. This table and the accompanied spider diagram show the following findings:

With the exception of a negative to positive Ba anomaly, Ba ($Ba^*_{MN} = 0.03 - 2.58$), anomalies for the rest LILE (K, Sr and Rb) in CS-I calcsilicate subunit are negative; e.g. K ($K^*_{MN} = 0.002 - 0.1$), Rb ($Rb^*_{MN} = 0.14 - 0.7$). Most HFSE display very pronounced anomalies in this calcsilicate subunit; e.g. Ce ($Ce^*_{MN} = 2.13 - 29.84$); Th ($Th^*_{MN} = 0.01 - 33.89$); Y ($Y^*_{MN} = 0.3 - 163$); U ($U^*_{MN} = 0.09 - 256$) and Nb ($Nb^*_{MN} = 0.00 - 2.31$); Zr ($Zr^*_{MN} = 2.92 - 16.5$). Anomalies of Ti, P and Pb are negative (Table 5.2).

The LILE anomalies in calcsilicate CS-II are similar to those in CS-I. For example, the K ($K^*_{MN} = 0.01 - 0.01$) anomalies in CS-II are negative while Ba ($Ba^*_{MN} = 1.26 - 2.17$) are slightly positive. The HFSE in calcsilicate subunit CS-II, show less enhanced anomalies compared to CS-I; Ce ($Ce^*_{MN} = 0.57 - 24.3$); Y ($Y^*_{MN} = 1.12 - 2.18$); U ($U^*_{MN} = 1.77 - 2.95$) and Nb ($Nb^*_{MN} = 0.85 - 1.75$); Zr ($Zr^*_{MN} = 0.62 - 2.24$). The anomaly of P is negative (Table 5.2).

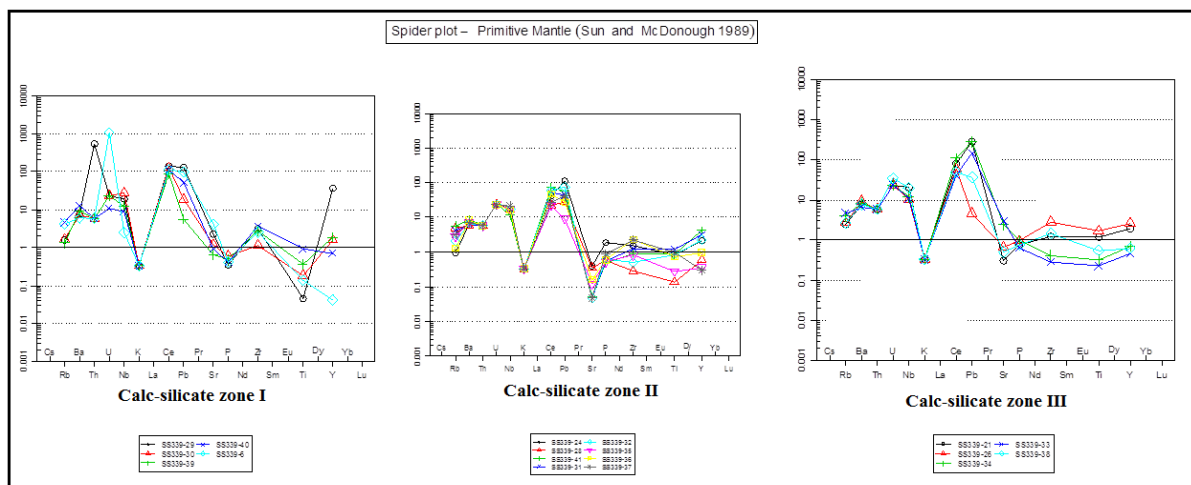


Figure 5.5: Trace-element compositions of the calcsilicate subunits and their individual samples (primitive mantle normalization values from McDonough and Sun, 1989).

Calcsilicate subunit CS-III displays a negative K ($K^*_{MN} = 0.01 - 0.02$) and a positive Ba ($Ba^*_{MN} = 1.05 - 2.25$), similar to units CS-I and CS-II. Unlike the calcsilicate units, CS-I and CS-II, a strong anomaly of Ti dominates the HFSE pattern in this unit; Ti ($Ti^*_{MN} = 0.24 - 8.04$). Otherwise, the anomaly ranges for the rest HFSE are similar to those of the CS-II subunit, though less pronounced compared to those in calcsilicate subunit CS-I. The calcsilicate subunit CS-I, which is the least metasomatised, shows more pronounced Ce, Th, U, Y and Zr anomalies. The LILE show similar levels of anomalies from the CS-I to CS-III subunits. The most pronounced Pb anomaly occurs in subunit CS-II while subunit CS-III shows considerably higher P and Ti anomalies

5.2.4 Platreef Package

A statistical summary of the major, trace elements, and geochemical indices for the four pyroxenite types encountered in the Platreef package, namely: P-I, P-II, FP-I and FP-II are presented in Table 5.3. The box and whisker plot in Fig. 5.6 graphically presents the magnitude and the elemental variation in these four pyroxenite types. These summary data presented in Table 5.3 compare favourably to published data by Ihlenfeld and Keays (2011).

The pyroxenite subunit P-I contains the highest average contents of SiO_2 , TiO_2 , V, Y, Zr and Mo. The reverse is the case for Nb, Th, Au and Pd. Pyroxenite subunit P-II have the highest average contents of Fe_2O_3 , MgO, SO_3 , LOI, As, Ce, Co, Ni, Pb, Rb, Zn and U and also the lowest contents in SiO_2 , Al_2O_3 , CaO, Na_2O , TiO_2 , Sr, V, Y, Mo and Pt contents. The pyroxenite subunit FP-I shows the highest contents of MnO, Cu, Au, Pd and Pt along with the lowest contents of K_2O , As, Ba, Pb, Rb, Zr and U. The pyroxenite subunit FP-II contains the highest average contents of Al_2O_3 , CaO, Na_2O , K_2O , Ba, Nb, Sr and Th and the lowest contents of Fe_2O_3 , MnO, MgO, LOI, Ce, Co, Cu, Ni and Zn.

The changing pattern of elements and oxides in the four subunits of the pyroxenite are best illustrated by their contents Fe_2O_3 , Al_2O_3 , MgO and the base metals. The contents of Fe_2O_3 in pyroxenite P-I varies between (12.11 – 16.68 wt. %); Al_2O_3 (4.83 – 10.97 wt. %), MgO (16.55 – 21.66wt. %) and Na_2O (0.77 – 2.04 wt. %).

Pyroxenite P-II has Fe₂O₃ (14 – 28.80 wt. %), Al₂O₃ (0.81 – 6.0 wt. %), MgO (18.89 – 37.39 wt. %) and Na₂O (0.11 – 0.97 wt. %). The contents of Fe₂O₃ in pyroxenite FP-I is between (11.47 – 16.80 wt. %); Al₂O₃ (2.42 – 6.80 wt. %), MgO (20.80 – 28.23 wt. %) and Na₂O (0.42 – 1.46 wt. %). Pyroxenite FP-II contains Fe₂O₃ (8.28 – 16.19 wt. %), Al₂O₃ (10.65 – 18.39 wt. %), MgO (8.8 – 13.24 wt. %) and Na₂O (0.97 – 2.96 wt. %).

The pyroxenite P-II is defined by the highest contents of Fe₂O₃ and MgO while the highest Al₂O₃ and Na₂O are contained in FP-II. Both are end-members considering their Fe₂O₃, MgO and Al₂O₃ Na₂O contents as illustrated by the box and whiskers plot in Fig 5.6. This corroborates the pyroxene and olivine rich nature of P-II and the feldspathic (high plagioclase) nature of FP-II observed in the petrography. Relative to pyroxenite P-II, the units P-I and FP-I contain lower and almost identical ranges of Fe₂O₃ and MgO contents. The FP-I pyroxenites however show higher Al₂O₃ and Na₂O contents relative to the P-I unit. The diametric relationships in the distribution of the oxide groups Fe₂O₃, MgO, CaO, Al₂O₃ and Na₂O is well illustrated by the box and whiskers plots in Fig. 5.6.

All four types of pyroxenites are further defined by a sharp contrast in immobile ratios: e.g. Al₂O₃/TiO₂ for P-I ranges from 10.80 – 64.53; P-II (12.12 – 31.56) FP-I (14.10 – 42.50 and FP-II (42.60 – 199.00). Similar trends also occur for TiO₂/Zr and Zr/Y ratios and are presented in Table 5.3.

The spider diagrams in Fig. 5.7 display varying shapes, degree of steepness of curves and patterns of enrichment of the HFSE relative to LILE. These trends are best described using the anomalies derived from these diagrams; Table 5.3 as follows:

Pyroxenite unit P-II and FP-II display the steepest curves or enrichment of some elements relative to the others while the curves for the P-I type is the flattest. Amongst the LILE, potassium shows a negative K ($K^*_{MN} = 0.05 – 0.45$) anomaly while Ba anomaly is negative to positive range, Ba ($Ba^*_{MN} = 0.55 – 2.17$). With the exception of Ce and U, other HFSE and phosphorus show a negative to weakly positive anomalies. Cerium and uranium anomalies in the pyroxenite unit P-I ranges are Ce ($Ce^*_{MN} = 0.56 – 7.87$) and ($U^*_{MN} = 1.66 – 6.81$).

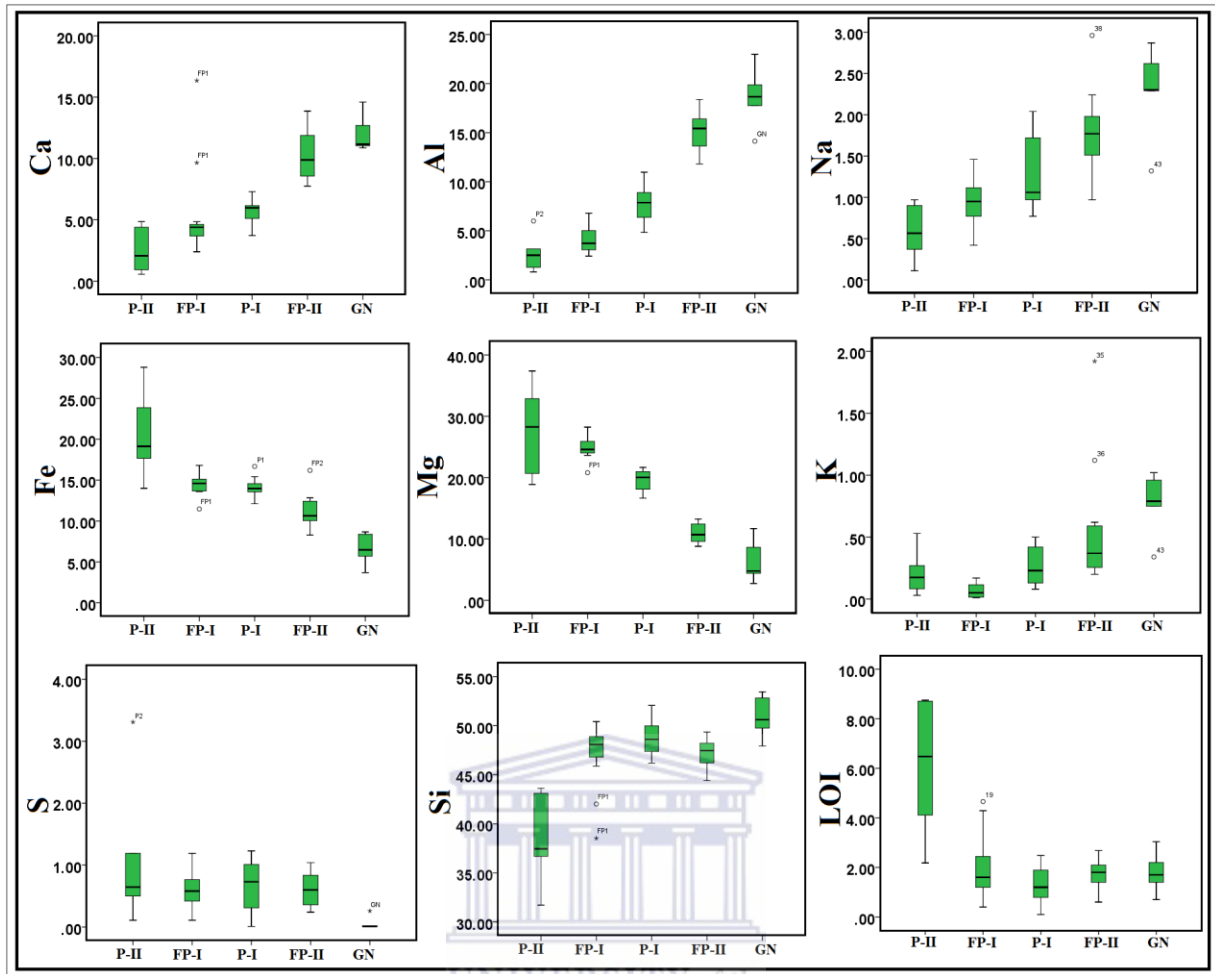


Figure 5.6: Box and whisker plots for the pyroxenite subunits, showing the various major elements. These pyroxenites are also compared with the gabbronorites.

The spider diagram curves for the pyroxenite P-II are steeper than those for the P-I type and are marked by very strong Rb anomalies Rb ($Rb^*_{MN} = 0.88 - 24.34$). Other anomalies for the LILE in the P-II pyroxenite type are negative to weakly positive, e.g. K ($K^*_{MN} = 0.02 - 0.27$) and Ba ($Ba^*_{MN} = 0.08 - 1.79$). The pyroxenite P-II, compared to the P-I variety, is marked by more positive anomalies of Ce ($Ce^*_{MN} = 0.47 - 9.23$) and (U $^*_{MN} = 2.0 - 11.8$) and Pb ($Pb^*_{MN} = 0.4 - 8.17$). The rest HFSE and phosphorus show a negative to weakly positive anomalies (Table 5.3).

The spider diagram curves for the pyroxenite FP-I show similar steepness as the P-II variety. This are however defined by pronounced anomalies of Ce ($Ce^*_{MN} = 0.41 - 22.05$), U ($U^*_{MN} = 1.95 - 5.07$) and Pb ($Pb^*_{MN} = 0.4 - 8.17$) relative to the other elements.

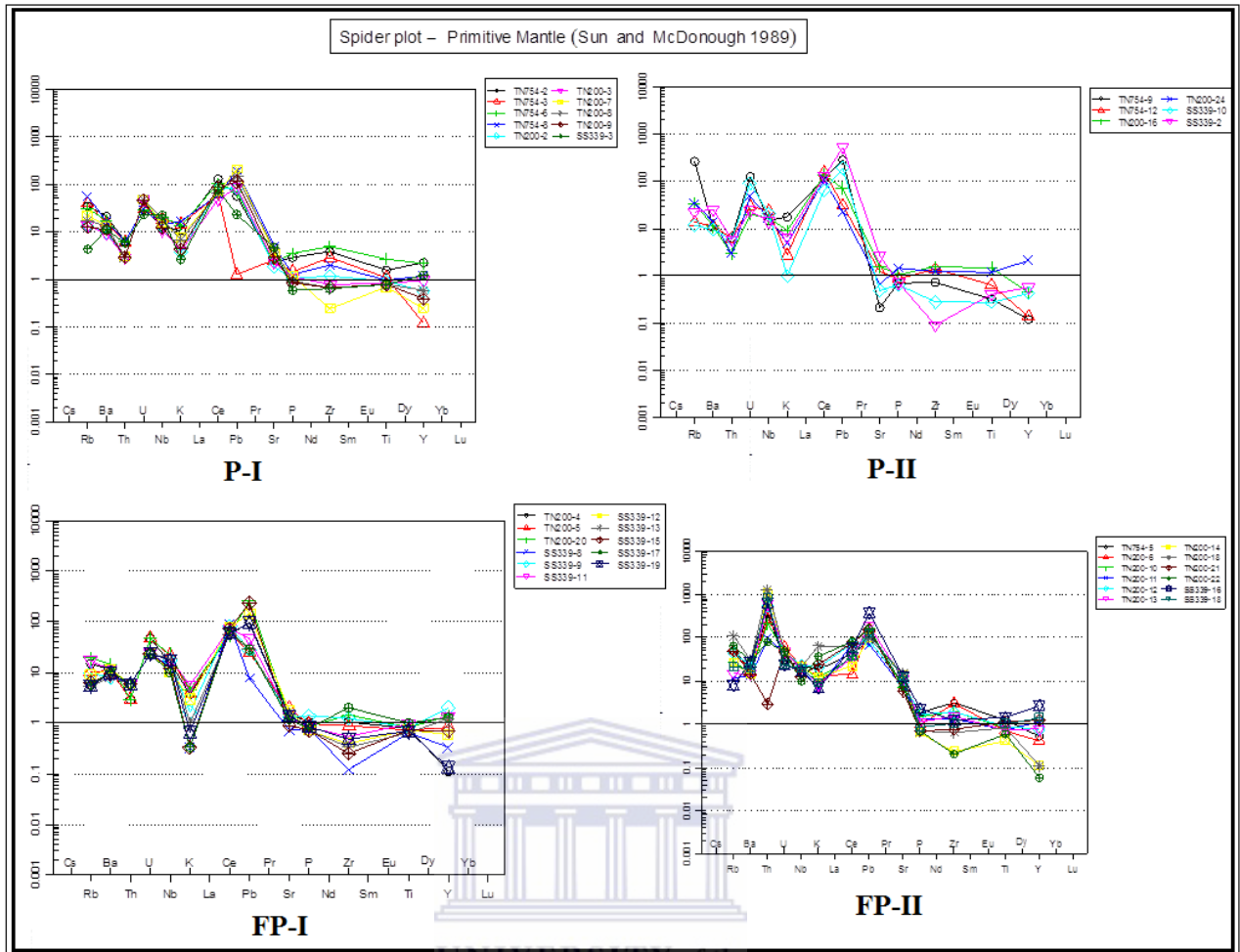


Figure 5.7: Trace-element compositions of pyroxenite subunits and their individual samples (primitive mantle normalization values from McDonough and Sun, 1989).

The LILE generally display a negative to weakly positive anomalies, e.g. K ($K^*_{MN} = 0.01 - 0.13$), Ba ($Ba^*_{MN} = 0.98 - 1.89$) anomalies. Most HFSE, with the exception of Ce and U in the FP-I rocks contain negative to positive anomalies of Nb ($Nb^*_{MN} = 0.62 - 1.52$), Th ($Th^*_{MN} = 0.09 - 0.37$). Phosphorus also shows negative to positive anomaly range; P ($P^*_{MN} = 0.49 - 1.91$). Pyroxenite type FP-II display curves with intermediate steepness compared P-I, P-II and FP-I. The spider curves are shaped by pronounced Th ($Th^*_{MN} = 0.09 - 38.15$), Pb ($Pb^*_{MN} = 1.76 - 15.39$) and weakly positive U ($U^*_{MN} = 0.06 - 6.16$), Rb ($Rb^*_{MN} = 0.29 - 3.64$) anomalies.

The other LILE and HFSE show negative to weakly positive anomalies e.g. K ($K^*_{MN} = 0.15 - 1.58$), Ba ($Ba^*_{MN} = 0.03 - 0.55$), Ce ($Ce^*_{MN} = 0.16 - 1.89$) as well as P ($P^*_{MN} = 0.08 - 0.34$).

Overall, the spider diagrams for the four types of pyroxenites show curves of varying steepness, which can be defined by pronounced anomalies of Ce, Th, Pb, U, Rb and Ba. The anomalies displayed by the pyroxenite varieties are as follows: type P-I (Ba, Ce and U); type P-II (Rb, Ce, U and Pb); type FP-I (Ce, U and Pb) and type FP-II (Th, Pb, and Rb).

5.2.5 Gabbronorite

Table 5.4 shows the statistical summary of the major, trace element and geochemical anomalies for the gabbronorite (GN) unit of the hanging wall. The box and whisker plot in Fig. 5.6 graphically shows the magnitude and the elemental variation patterns between the pyroxenite rocks and the GN. Comparison of the GN unit with the pyroxenite subunits reveals the following element patterns:

The GN is characterised by the highest average contents of SiO₂, CaO, Na₂O, K₂O, Al₂O₃, P₂O₅, TiO₂, Ba, Nb, Sr, Y, Zr and Th coupled with the lowest average contents of SO₃, Fe₂O₃, MgO, MnO, Ce, Co, Cu, Ni, Zn and the PGEs (Pd, Pt and Au).

Elements show a significant variable range in contents of the GN comparative to the pyroxenite subunits. For example, the GN contains Fe₂O₃ (3.69 – 8.67 wt. %), Al₂O₃ (14.13 – 22.99 wt. %), MgO (2.74 – 11.69 wt. %) and Na₂O (1.32 – 2.87 wt. %). The immobile ratios, e.g. Al₂O₃/TiO₂, TiO₂/Zr and Zr/Y shows that the Al₂O₃/TiO₂ ratio is higher in the GN, and the TiO₂/Zr ratio is lower for the GN comparative to all the pyroxenite subunits. The element ranges in the GN for Al₂O₃/TiO₂ is 41.42 – 328.43, and for TiO₂/Zr it is 63.83 – 146.75.

Fig. 5.8 show that amongst the LILE (Ba, K, Sr and Rb) for the gabbronorite unit, potassium shows a negative to positive K ($K^*_{MN} = 0.41 - 3.01$) anomaly, negative Ba ($Ba^*_{MN} = 0.03 - 0.08$) anomaly and also a negative Sr ($Sr^*_{MN} = 0.26 - 0.30$) anomaly. With the exception of Ce, U and Th, the other HFSE (Ti, Nb, Y and Zr) show negative to weakly positive anomalies. Cerium and uranium anomalies in the gabbronorite unit ranges are negative Ce ($Ce^*_{MN} = 0.04 - 0.78$) and negative U ($U^*_{MN} = 0.04 - 0.10$). Thorium show a highly positive anomaly Th ($Th^*_{MN} = 21.69 - 51.80$). And phosphorus show a negative anomaly P ($P^*_{MN} = 0.08 - 0.53$).

Table 5.4: Statistical summary of oxides (wt. %), trace elements (ppm) and PGE (g/t) for gabbro-norites. Mean values for feldspathic pyroxenite, pyroxenite, hornfels and calcsilicates are included for comparison.

ROCKS	Gabbro-norite		
	Min.	Max.	Ave.
Major	(N=5)		
SiO ₂	47.93	53.45	50.91
Al ₂ O ₃	14.13	22.99	18.68
Fe ₂ O ₃	3.69	8.67	6.58
MnO	0.05	0.12	0.09
MgO	2.74	11.69	6.44
CaO	10.86	14.60	12.07
Na ₂ O	1.32	2.87	2.28
K ₂ O	0.34	1.02	0.77
P ₂ O ₅	0.01	0.10	0.04
TiO ₂	0.07	0.48	0.25
SO ₃	0.01	0.26	0.06
LOI	0.70	3.04	1.81
Trace	(N=5)		
As	0.50	18.30	9.70
Ba	143.90	252.20	202.94
Ce	5.00	87.22	40.97
Co	25.95	49.17	34.04
Cu	34.54	624.18	159.30
Nb	14.05	21.03	16.42
Ni	93.54	1531.71	419.88
Pb	6.10	8.32	7.11
Rb	16.96	39.07	30.50
Sr	246.10	354.48	298.34
V	40.89	100.37	73.68
Y	1.73	9.51	6.53
Zn	44.71	67.82	59.48
Zr	4.77	62.82	29.96
Mo	0.65	5.00	2.57
U	0.50	1.00	0.65
Th	65.73	118.84	89.34
PGEs	(N=2)		
Au	0.05	0.09	0.07
Pd	0.05	0.35	0.20
Pt	0.05	0.28	0.17
Ratios	(N=5)		
Al ₂ O ₃ /TiO ₂	41.42	328.43	120.90
TiO ₂ /Zr	63.83	146.75	112.09
Zr/Y	1.05	9.47	4.88
Anomalies	(N=5)		
K*	0.41	3.01	1.37
Rb*	1.14	2.12	1.67
Ce*	0.04	0.78	0.40
Ba*	0.03	0.08	0.06
Th*	21.69	51.80	37.03
U*	0.04	0.10	0.06
Nb*	0.68	1.16	0.84
Pb*	3.03	12.57	6.62
Sr*	0.26	0.30	0.28
P*	0.08	0.53	0.20
Zr*	0.89	3.65	1.73
Ti*	0.50	2.46	1.50
Y*	0.39	3.09	1.59

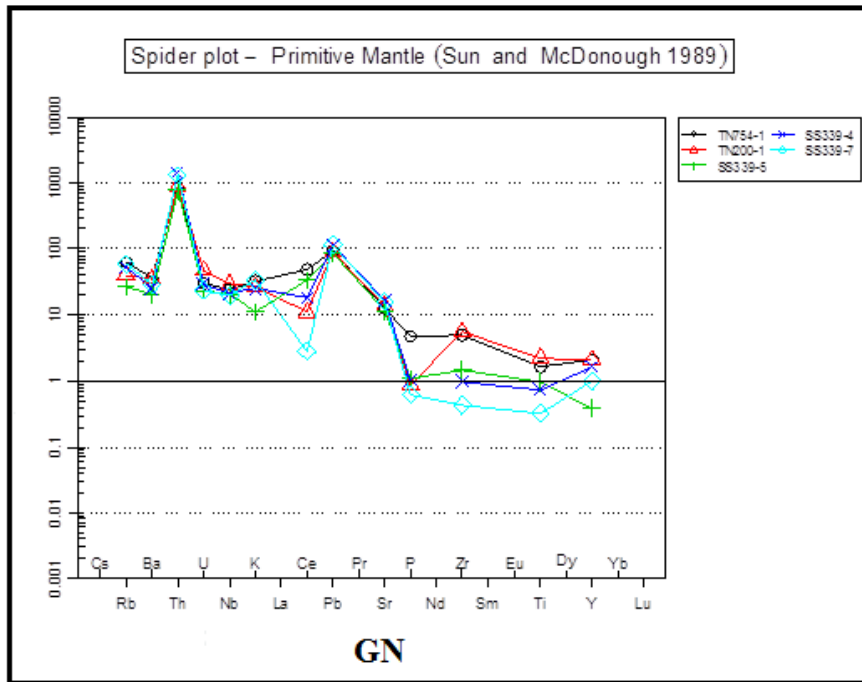


Figure 5.8: Trace-element compositions of gabbronorites (primitive mantle normalization values from McDonough and Sun, 1989).

Comparing the gabbronorite unit to the pyroxenite subunits, the LILE has potassium values which are higher than all the pyroxenite subunits. Sr is also higher than all the pyroxenite subunits with the exception of P-I. Barium values are lower for the GN unit than all the pyroxenite subunits. Rb is also lower than all the pyroxenite subunits with the exception of FP-I. The HFSE for the GN unit has Th and Y which are higher than all the pyroxenite subunits. Zr is also higher for the gabbronorite unit compared to the pyroxenite units with the exception of FP-II. Ce, U, Nb, Ti are all lower in the GN unit than all the pyroxenite subunits.

5.2.6 Summary

There is a decrease in the average contents of Fe_2O_3 , Al_2O_3 , Ce, Co, Cu, Ni, Zn, Zr, Au, Pd and Pt from the hornfels subunits H-I, H-II to H-III coupled with an increase in the average contents of Zr and Y in the same order. Similarly, there is an increase in the average contents of SiO_2 , Fe_2O_3 , TiO_2 , SO_3 , Co, Cu, Ni, Rb, V and Zn from CS-I, CS-II to CS-III with a decrease in contents of LOI and Y in the same order. The three-fold relationship between the major and trace element association with the PGEs and BMS are:

- In the hornfels subunits, the subunit H-I is characterised by the highest PGEs (Au, Pd, Pt) contents together with the BMS mineralisation (Cu, Ni and SO₃). They are accompanied by the major elements Al₂O₃, Fe₂O₃, Na₂O, MnO, TiO₂, LOI and trace elements As, Ce, Co, V and Sr.
- In the calcsilicate subunits, the subunit CS-III is characterised by the highest PGEs (Pd and Pt) contents together with the BMS mineralisation (Cu, Ni and SO₃). They are accompanied by the major elements SiO₂, Fe₂O₃, Na₂O, TiO₂ and trace elements Co, Pb, Rb, V, Zn.
- The pyroxenite subunits show that Cu and Ni reflect highest average concentrations in FP-I, and this is associated with the highest average concentrations of PGEs. However, SO₃ shows the lowest average concentrations in FP-I.

SiO₂, Fe₂O₃ and CaO can be used to discriminate between the three hornfels subunits. As H-I is characterised by Fe₂O₃, H-II by SiO₂, and H-III by CaO and MgO. SiO₂, Fe₂O₃, CaO and TiO₂ can be used to discriminate between the three calcsilicate subunits. As CS-I is characterised by high CaO and low SiO₂, Fe₂O₃ and TiO₂. CS-II is characterised by low CaO and CS-III by high SiO₂, Fe₂O₃ and TiO₂. These elements also show distinctive element ranges indicative of the specific subunit.

The immobile ratios show a progressive trend in the hornfels subunits, from H-I, H-II to H-III: which is a decreasing trend for Al₂O₃/TiO₂ and an increasing trend for TiO₂/Zr in that order. The immobile ratios show no progressive trend from CS-I, CS-II to CS-III: and these ratios are highly variable between the three subunits. The anomalies show a progressive trend from H-I, H-II to H-III where Pb*, P* and Rb* increases, and Nb* decreases. The calcsilicate anomalies also show a progressive trend from CS-I, CS-II to CS-III where Rb*, Nb*, P*, Zr* and Ti* increases, and Ce*, U* and Sr* decreases.

5.3 Metasomatic studies at the farms Tweefontein and Sandsloot

5.3.1 Introduction

The petrography revealed subunits of calcsilicates, hornfels and pyroxenites that have unique mineralogical compositions and textures that are linked to alteration, magmatic processes and related contact metamorphism. The geochemical rock classification in section 5.1 mirrored the petrography results while the rock characterisation defined the compositional differences in between the rock types and their subunits. For example a progressive decrease in the contents of Fe_2O_3 , Al_2O_3 , Ce, Co, Cu, Ni, Zn, Zr, Au, Pd and Pt from the hornfels subunits H-I, H-II to H-III and an increase in of SiO_2 , Fe_2O_3 , TiO_2 , SO_3 , Co, Cu, Ni, Rb, V and Zn contents from CS-I, CS-II to CS-III. Hornfels subunit H-I and calcsilicate subunit CS-III are the main carriers of BMS and PGE at the floor rock pyroxenite interface/ reaction subunit. The pyroxenite subunit FP-I is most enriched in Cu, Ni and PGEs (Au, Pt and Pd).

The results from the previous geochemistry sections point the hornfels and calcsilicate subunits as resulting from a gradational element loss or gain from the protolith. The intensity of the contact metasomatism and therefore element loss and gain in between the hornfels, calcsilicate and the pyroxenite units remains unclear. Mass balance calculations were therefore used to investigate the intensity and pattern of element loss and gain in between the hornfels, calcsilicate and the pyroxenite. The aim is to define patterns that point to interconnected material exchange between the pyroxenite units and their respective floor rocks.

Numerous studies have documented the use of immobile elements to monitor the intensity of alteration and metamorphism around ore deposits as well as magmatic fractionation processes and affinities of rocks. Examples of these applications towards improving lithostratigraphic correlation or chemostratigraphy through calculation of mass changes are in MacLean and Kranidiotis (1987); MacLean (1988); Richards et al. (1989); Elliott-Meadows and Appleyard (1991); and MacLean and Barrett (1993). Various techniques and approaches for determining whether certain elements have been immobile in metasomatism and alteration have been discussed, amongst others, by Gresens (1967), Babcock (1973), Finlow-Bates and Stumpfl (1981), Grant (1986), Kranidiotis and MacLean (1987), MacLean (1988, 1990) and Elliott-Meadows and Appleyard (1991).

5.3.2 Principles of the mass balance study

Mass balance calculations are achieved by defining a reference frame through various methods: the volume factor method (Gresens, 1967), the isocon method (Grant, 1986) and the immobile element method (MacLean and Kranidiotis, 1987). The method by Gresens (1967) included the gains and losses plots as a function of arbitrary volume factors in composition-volume diagrams. This reference frame proposed by Gresens (1967) was used to estimate the gains and losses of the rest of the mobile elements comparative to the immobile elements.

Gresens' mass balance equation was later readjusted by Grant (1986) into a linear relationship. This resulted into an isocon diagram which allows a straight comparison of mass transfer of the protolith and its altered product. In this isocon diagram the elemental abundances of the altered rock and its protolith are plotted on the X and Y-axis respectively. Grant (1986) proposed that all immobile elements would plot on a straight line through the origin in the diagram. This study uses the Grant method because of its simplicity and adaptability as reported by Mukherjee and Gupta (2008). This method also does not plot mass gains and losses as a function of arbitrary volume factors, and it does not consider only a single immobile element but instead considers all possible immobile elements.

Barrett and MacLean (1994) outline the principle underlying the immobile elements, and their usage in the mass balance calculations. The idea is that the mass of a sample after alteration (reconstructed composition) is calculated from the initial chemical analysis of precursor rocks, using immobile monitors. I.e. mass change calculations for an altered rock sample, is based on 100 units of precursor. Mass changes are calculated for each mobile element based on the dilution or concentration of an immobile component for the altered sample against those in the protolith (MacLean and Kranidiotis, 1987). Utami et al. (2006) mentions that the mass balance defines quantitatively the amount of a constituent that is lost or gained during the alteration process or changes in the amount of an element moved per unit volume or mass of rock relative to its initial content. Mukherjee and Gupta (2008) further mentioned that the quantifying mass balance can be applied in all alteration processes, providing the protolith and its altered product are known, and a reference frame about which mass balance calculations are made is defined.

The immobile elements are used to graphically define an isocon line (Selverstone et al., 1991; Leitch and Lentz, 1994; Kolb et al., 2005) as illustrated in the example of Figure 5.9. The isocon plot generally illustrates which elements are immobile during alteration stages, as the mass remains essentially conserved during the alteration process. The gradient of the isocons is defined by the mass ratio between the original samples and the altered samples. In this example the least altered pyroxenite (P-II) is plotted against the more altered pyroxenite (FP-II). The lines represent the constant mass (CM) and the constant volume (CV) respectively. Cf indicates the concentrations of the altered samples (FP-II) against Co which is the concentrations of the least altered samples.

The elements, which plot above the isocon are said to be enriched during alteration (gains). Elements plotted below the isocon have been depleted (losses) (Grant, 1986).

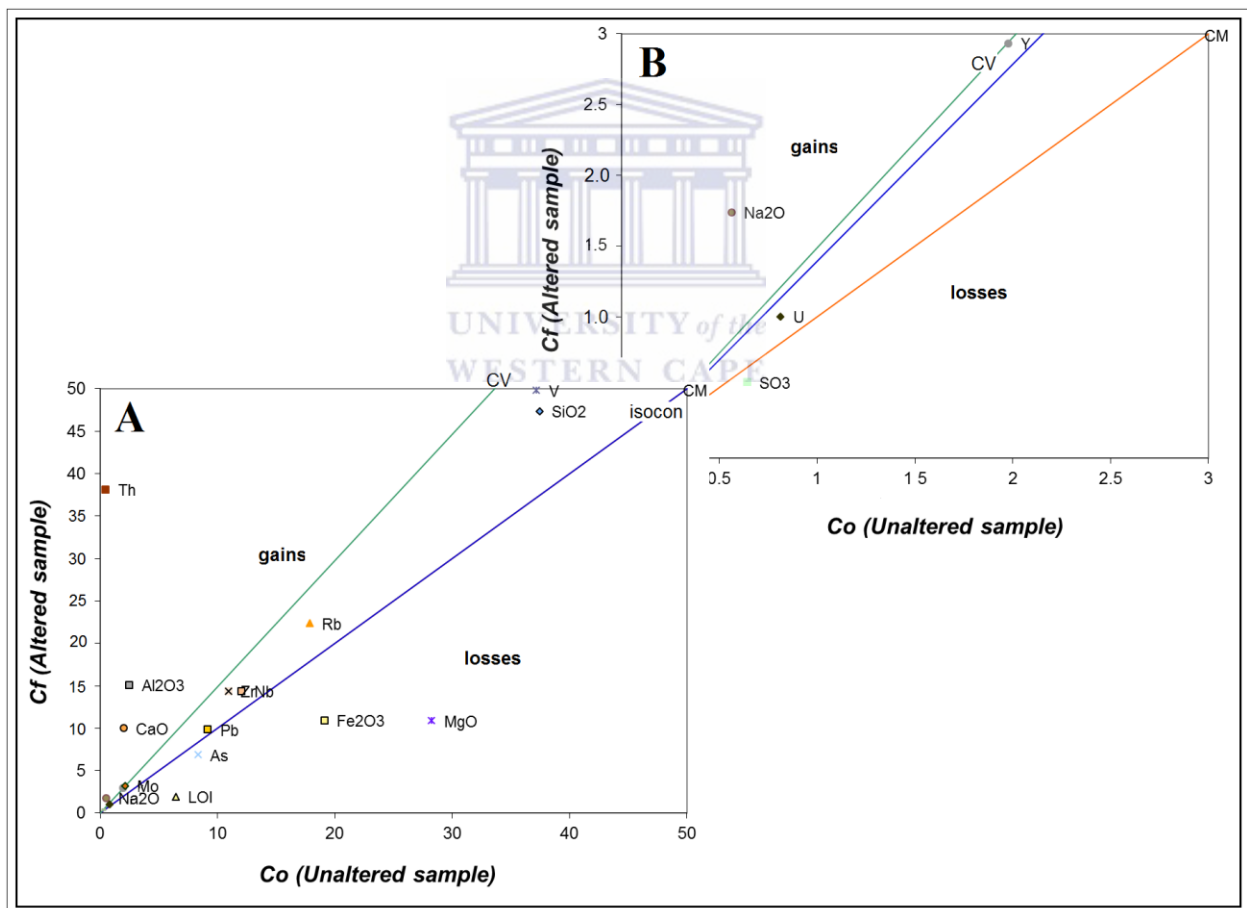


Figure 5.9: An example of the isocon diagram. Here the least altered pyroxenite (P-II) is plotted against the more altered pyroxenite (FP-II). The lines represent the constant mass (CM) and the constant volume (CV). The figure reflects two different scales: (A) the original view or scale; and (B) represents the extended view (in a stacked manner)

Table 5.5: Shows the median concentrations of hornfels and pyroxenite subunits from the samples of Tweefontein. This is together with the median concentrations of the calcsilicates and the pyroxenite subunits from samples at Sandsloot. All the oxides are in wt. % and trace elements in ppm.

	Tweefontein							Sandsloot						
	H-I	H-II	H-III	P-I	P-II	FP-I	FP-II	CS-I	CS-II	CS-III	P-I	P-II	FP-I	FP-II
SiO ₂	36.58	50.08	53.54	48.24	40.57	48.89	47.57	1.65	27.96	36.44	50.08	36.78	47.92	46.11
Al ₂ O ₃	8.85	3.69	0.01	7.10	2.67	5.43	15.47	0.01	3.30	4.19	9.89	2.84	3.65	12.53
Fe ₂ O ₃	35.57	24.31	36.53	14.26	21.25	13.61	10.63	0.18	4.58	8.36	13.17	14.00	14.98	11.68
MnO	0.26	0.33	0.18	0.19	0.21	0.21	0.16	0.79	1.14	0.23	0.19	0.19	0.21	0.16
MgO	6.28	5.20	3.07	20.77	23.77	23.70	10.83	20.11	31.76	10.71	18.75	29.69	24.81	10.70
CaO	6.32	10.81	3.46	5.93	2.07	4.84	9.69	39.92	17.04	32.97	6.13	4.85	3.99	12.76
Na ₂ O	0.66	0.50	0.16	1.08	0.48	0.79	1.71	0.73	0.46	0.96	0.97	0.90	1.05	2.33
K ₂ O	0.07	0.37	0.01	0.23	0.21	0.12	0.48	0.01	0.01	0.01	0.08	0.08	0.03	0.24
P ₂ O ₅	0.03	0.04	0.06	0.03	0.02	0.02	0.02	0.01	0.01	0.02	0.01	0.01	0.02	0.03
TiO ₂	0.45	0.24	0.06	0.20	0.20	0.17	0.17	0.04	0.18	0.12	0.17	0.09	0.16	0.27
SO ₃	0.51	0.28	0.20	0.93	0.85	0.49	0.54	0.10	0.11	0.44	0.01	0.51	0.67	0.64
LOI	1.10	1.00	0.55	1.20	6.48	1.60	1.80	32.00	9.80	6.00	0.55	4.11	1.69	2.58
As	26.94	18.18	20.63	0.50	15.51	0.50	3.68	105.34	0.50	24.95	2.48	1.84	0.83	11.59
Ba	73.75	91.51	58.73	92.80	77.72	77.24	109.59	53.93	48.75	54.00	78.41	78.41	65.49	162.85
Ce	356.76	271.66	524.55	126.43	224.32	96.58	89.93	202.71	78.12	107.41	133.29	133.29	128.04	83.91
Co	38.99	20.58	3.94	160.60	226.17	147.94	106.26	7.80	28.50	87.70	89.13	207.81	162.59	104.92
Cu	305.06	92.85	90.23	1076.18	797.31	684.71	463.65	43.99	78.54	670.26	27.03	1164.40	1536.77	1366.32
Nb	17.21	17.85	15.44	10.10	12.07	15.53	14.73	8.78	12.22	8.57	16.25	14.54	11.00	12.87
Ni	199.01	150.63	329.96	2389.35	2341.28	1675.18	1354.27	24.76	272.11	1468.56	583.62	3117.56	3283.15	2603.01
Pb	4.74	3.87	0.57	6.23	3.62	7.04	9.05	3.74	3.05	10.38	1.65	13.36	2.68	17.72
Rb	10.61	17.84	2.54	14.01	21.63	9.39	29.44	1.07	1.91	1.71	2.82	7.53	4.00	9.34
Sr	52.92	62.21	6.13	53.34	20.34	31.76	167.21	25.35	1.82	14.15	99.47	55.60	28.29	262.27
V	95.02	74.78	26.09	72.35	58.84	70.51	48.29	13.00	35.20	25.01	112.51	36.49	88.07	116.30
Y	5.47	3.28	2.40	2.66	1.31	3.81	2.14	7.18	7.12	3.20	5.66	2.59	4.41	9.45
Zn	96.25	55.52	44.77	86.34	109.87	86.47	67.26	32.04	42.54	56.07	131.80	131.80	111.52	80.44
Zr	20.71	12.72	9.46	13.19	14.68	11.86	16.04	31.62	12.28	13.90	7.22	3.14	4.98	12.70
Mo	5.78	5.84	8.13	4.28	2.13	4.62	3.33	0.80	0.80	2.50	3.66	3.66	2.81	1.93
U	0.63	0.63	0.92	1.00	0.82	1.00	1.00	0.50	0.50	0.50	0.50	0.50	0.50	0.50
Th	0.53	0.53	0.25	0.25	0.39	0.25	27.10	0.50	0.50	0.50	0.50	0.50	0.50	62.42

5.3.3 Mass-balance evaluation

In this chapter, mass-balance calculations are based on two goals: (1) to study the exchange of elements between the Platreef and their respective floor rocks, i.e. the least altered calcsilicate or hornfels relative to the pyroxenites at Sandsloot and Tweefontein respectively. And (2) to study the exchange of elements between the least altered pyroxenite relative to the more altered pyroxenites for comparison between the two farms.

Median values were calculated for each sample under their respective subunit, the average for these median values are then presented for each subunit at each farm. Table 5.5 shows the selected median data from drillcores TN754 and TN200. The mass balance calculations are based on the least altered hornfels (subunit H-I) against the more altered subunits H-II and H-III. Mass balance calculations also included using subunit H-I (least altered) against the pyroxenite lithologies found at Tweefontein; i.e. P-I, P-II, FP-I and FP-II. Thus, the median data in table 5.5 reflects values for all these subunits from Tweefontein. The reason for this was to assess the level of floor rock interaction with the Platreef where there is BIF floor rocks.

Mass balance calculations at Sandsloot are from drillcore SS339. Here the data included the least altered calcsilicates (CS-I) against the more altered calcsilicates (subunits CS-I and CS-III). Mass balance calculations also included using subunit CS-I (least altered) against the pyroxenite lithologies found at Sandsloot; i.e. P-I, P-II, FP-I and FP-II from drillcore SS339. Here it is to assess the level of floor rock interaction with the Platreef when there is a carbonate floor rock.

Mass balance calculations applied to data of the least metasomatised pyroxenites (P-II) relative to the more metasomatised pyroxenites (P-I, FP-I and FP-II) at each farm for comparison (i.e. separating the pyroxenites at Sandsloot from the Tweefontein pyroxenites). The goal here is to evaluate and compare the difference in pyroxenites between the two farms.

The median data include major and trace elements and these elements were used as the input values for mass balance calculations using the EASYGRESGRANT program.

(a) EASYGRESGRANT program

A significant number of mass-balance computer programs (e.g. Leitch and Day, 1990; Potdevin, 1993; Coelho, 2006) have been developed for the application of metasomatic systems. These programs were enabled by using the initial ideas by Gresens together with the isocon method of Grant (López-Moro, 2012).

The EASYGRESGRANT is a mass balance computer program in the form of a Microsoft Excel spreadsheet that is compatible with the Mac and Windows platforms (López-Moro, 2012). Other mass-balance programs often have the following problems: 1.) In order to find immobile elements, the graphical plots (e.g. the Grant's isocon diagram or Gresens's composition-volume diagram) are not useful tools when a large data set is being handled. This is because the large number of lines or symbols represented obstructs the good visualization and distinction of the elements themselves. 2.) Mukherjee and Gupta (2008) mentioned that the method of arbitrary scaling of compositional data proposed to mitigate this problem in the Grant's isocon diagram is inadequate. The reason for this is that the scaling influences the best fit isocon, yielding errors in the mass balance calculations. In contrast, the EASYGRESGRANT program permits correct selection of immobile elements from clusters of slopes, volume factors, improves the isocon diagram, and it provides an error free mass balancing of metasomatic systems (López-Moro, 2012).

The EASYGRESGRANT is also a user friendly program and it considers possible reference frames between the unaltered rocks and their altered counterpart. To establish the immobile elements, the following improved methods are used in EASYGRESGRANT: The composition-volume diagram; the isocon diagram ($C_a - C_o$ diagram) and the component-ratio diagram.

The choice of immobile elements was assessed by means of a regression method which calculates the regression index and typical error estimate. This process included an average of slope value equal or close to 1. It was combined with the regression index (equal or close to 1) and typical error (close to 0). This provides a best fit isocon from which mass-balance calculations could be performed. Three immobile elements were selected at each section, with slopes varying between 0.9 and 1.2. The regression index values range between 0.9 and 1, and with a typical error of 0.001 to 0.

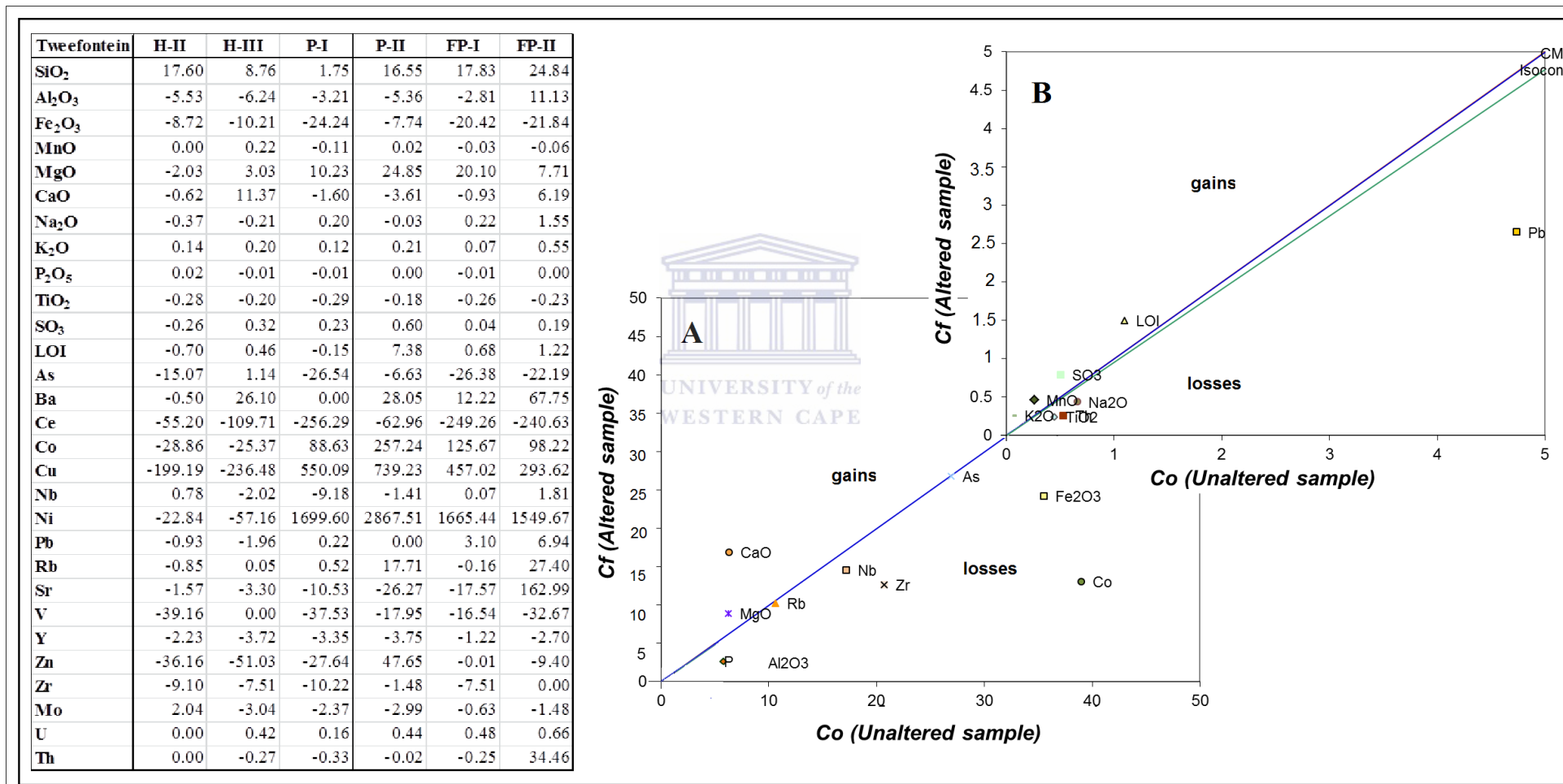
These median values presented above were used for the three parts of mass balance calculations. During the assessment using the EASYGRESGRANT program, the immobile elements were selected using the Grant method (explained in methodology section 5.3.2). This program mechanically calculated the slopes of the isocon diagrams using the calculated immobile elements. Mass gains and losses were also calculated from the isocon diagrams. The results are as follows: Table 5.8 presents the mass balance results (output by EASYGRESGRANT) for the hornfels metasomatic study. The table has values / percentages of the slopes for each major and trace element. These proportions are of mass loss and mass gained by each hornfels and pyroxenite subtype relative to the least altered hornfels subunit H-I. Figure 5.9 is an example of the isocon diagrams, and illustrates the mobility of elements in terms of their depletion and enrichment.

The mass balance output (i.e. results by EASYGRESGRANT) is presented in tables (e.g. 5.6, 5.7 and 5.8) together with the isocon figures (e.g. 5.9, 5.10 and 5.11). These results are briefly explained below: The proportions (in percentage) of mass loss and mass gained by each hornfels and pyroxenite subtype relative to the least altered hornfels (subunit H-I) is presented in table 5.6. This is supported by the isocon diagram which illustrates the mobility of elements in terms of their depletion and enrichment. The table includes values / percentages of the slopes for each major and trace element. A detailed description of these results and the mass balance study at Tweefontein is under section 5.3.4.

The proportions of mass loss and mass gained by each calcsilicate and pyroxenite subtype relative to the least altered calcsilicate (subunit CS-I) is presented in table 5.7. This is accompanied by the isocon diagram which illustrates the depleted or enriched elements. The table has values / percentages of the slopes for each major and trace element. A detailed description of these results and the mass balance study at Sandsloot is under section 5.3.5.

The proportions are of mass loss and mass gained by the pyroxenite subtypes relative to the least altered pyroxenite subunit P-II. The example were already given and explained in figure 5.9 under section 5.3.2. Table 5.8 presents the mass balance results for the pyroxenite metasomatic study at each farm. A detailed description of these results and the mass balance study of the pyroxenites are under section 5.3.6.

Table 5.6 (on the left): Shows the mass balance calculations for median concentrations for the hornfels and their accompanied pyroxenites (at Tweefontein) by using the clustering of slopes method (oxides are in wt. % and trace elements in ppm). Fig. 5.10 (on the right): Is an example of the isocon diagrams of the hornfels subunit H-I (least altered) relative to the more altered hornfels subunit H-III.



5.3.4 Mass balance in the hornfels and pyroxenite subunits at Tweefontein

Table 5.6 present the mass balance calculation results for hornfels and pyroxenite subunits. The mass balance results for the pyroxenites are presented in the order of their relative proximal occurrence in the sections under study. In addition, based on the petrography, a compositional progression in terms of changes in modal composition was also inferred. The results of the mass balance calculation are therefore presented in the sequence of change in their modal composition changes based on their increasing clinopyroxene relative to orthopyroxene contents as follows: P-II→FP-I→P-I→FP-II. The reference to mass loss and gain in the pyroxenites is therefore only used to contextualize the relative changes between the various subunits.

An isocon diagram illustrating the relative mass loss and gain in the hornfels unit H-II relative to unit H-I is given in as an example in Fig. 5.10. More examples are given in Appendix III. The isocon diagram shows a relative gain of SiO₂ (17.6%) and a loss of Al₂O₃ (-5.53%), Fe₂O₃ (-8.72), Cu (-199.2%), Ni (-22.8%) and Co (-28.9%). This corroborates the observed intense silicification in this layer, and the low contents of base metals.

In hornfels subunit H-III there is a relative gain of SiO₂ (8.76%), CaO (11.37%), MgO (3.0%) and a loss of Al₂O₃ (-6.24%), Fe₂O₃ (-10.21) as well as in the base metal contents: Cu (-236.5%), Ni (-57.2%) and Co (-25.4%). The above points and corroborates a much reduced silicification coupled with the occurrence of clinopyroxene in the hornfels subunit H-III. This layer also features a much subdued base metal content compared to the hornfels subunit H-I.

The pyroxenite subunit P-II has a relative gain of SiO₂ (16.55%), MgO (24.85%) and a loss of Al₂O₃ (-5.36%), CaO (-3.60), Fe₂O₃ (-7.74). The base metal enrichment in this subunit is highest with Cu (739.2%), and Ni (2867.5%) and Co (257.24%). The above, based on the CaO and Fe₂O₃ values is consistent with the mineralogical composition of the P-II pyroxenite that is dominated by orthopyroxene relative to clinopyroxene.

The pyroxenite subunit FP-I has a relative gain of SiO₂ (17.83%), MgO (20.1%) and a loss of Al₂O₃ (-2.81%), CaO (-0.93), Fe₂O₃ (-20.42). The base metal enrichment is less than P-II pyroxenites with Cu (457%), and Ni (1665.4%) and Co (125.7%). The FP-I unit therefore

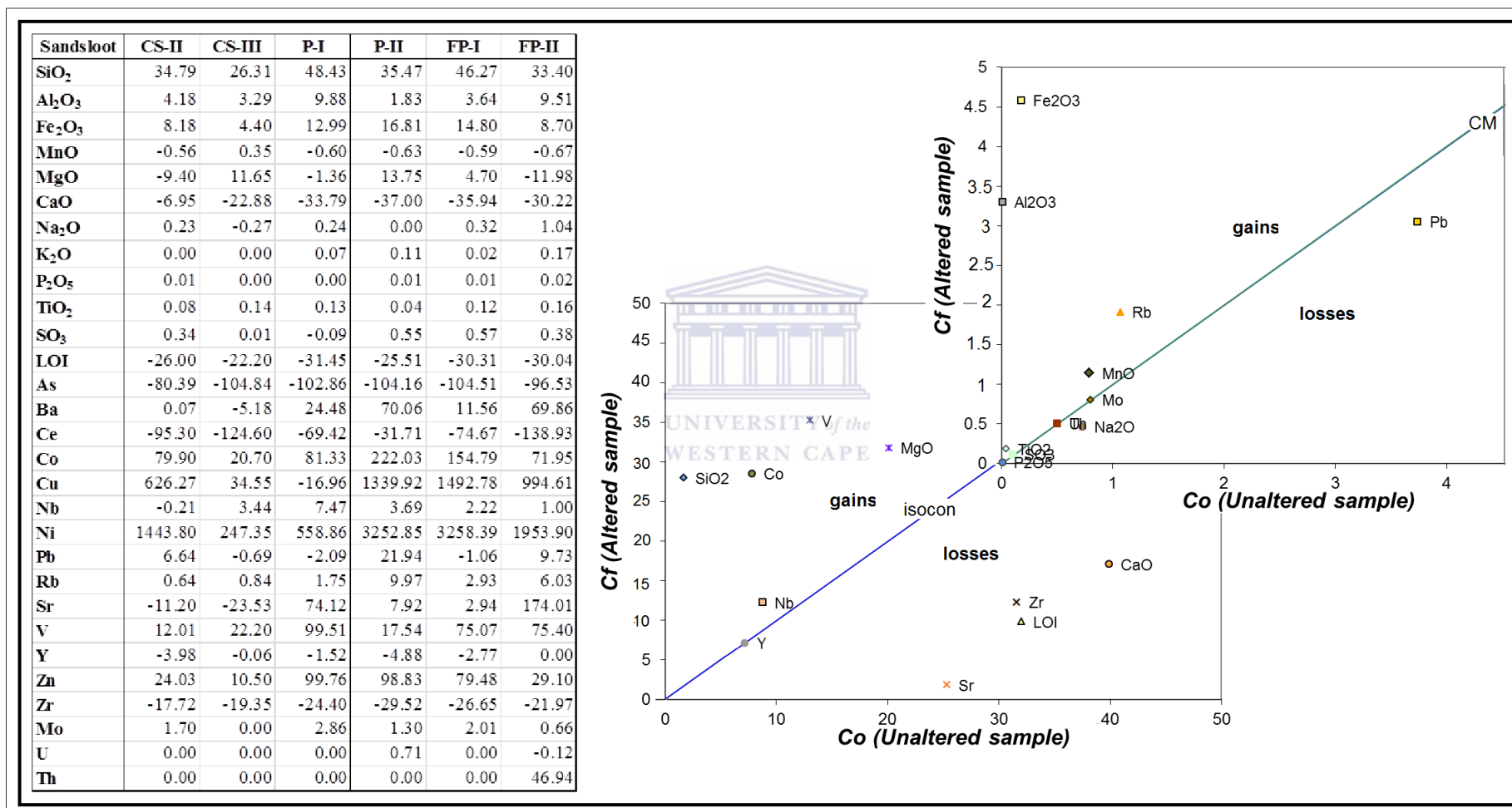
show a progressive enrichment of CaO, SiO₂, Al₂O₃ relative to the P-I unit that is coupled with more pronounced relative loss in Fe₂O₃, MgO and the base metals. Furthermore, this point to an increased feldspar and clinopyroxene content relative to the orthopyroxene content.

In the pyroxenite subunit P-I there is a relative gain of SiO₂ (17.5%), MgO (10.2%) and a loss of Al₂O₃ (-3.21%), CaO (-1.60), Fe₂O₃ (-24.24). The base metal enrichment is less than the subunits P-II and FP-I; with Cu 550.1%), and Ni (1699.6%) and Co (88.6%). The P-I pyroxenites, compared to the P-II and FP-II units shows weak changes in SiO₂, CaO and Al₂O₃. However, a significant change in a relative decrease in MgO, Fe₂O₃ corroborates an increase in clinopyroxene relative to orthopyroxene contents.

The pyroxenite subunit FP-II has a relative gain of SiO₂ (24.84%), MgO (7.71%), Al₂O₃ (11.13%), CaO (6.19%) and a loss of Fe₂O₃ (-21.84%). The base metals show the least enrichment compared to the other subunits; with Cu (293.6%), and Ni (1549.7%) and Co (98.22). The FP-II pyroxenite unit is therefore the most siliceous and feldspathic of the four units described. Pronounced enrichment in SiO₂, Al₂O₃, CaO coupled with reduced mass balance values for Fe₂O₃ and MgO are consistent with increased feldspathisation and increased clinopyroxene relative to orthopyroxene contents.

As presented on table 5.6, the mass balance results for the trace elements show an increasing trend from H-II to H-III for Ba, Rb, V and Co. The opposite decreasing trend is observed for Sr, Y, Cu, Ni and Zn. Sr is the trace element that shows a trend that is consistent with the sequence of change in modal composition (i.e. P-II→FP-I→P-I→FP-II) as it increases from P-II, to FP-I, to P-II to FP-II. The base metals do not follow this sequence, as Co and Zn show a decreasing trend in the order from P-II, P-I, FP-I to FP-II and Cu and Ni show a decreasing trend in the order from P-II, FP-I, FP-II to P-I.

Table 5.7 (on the left): Shows the mass balance calculations for median concentrations for the calcsilicates and their accompanied pyroxenites (at Sandsloot) by using the clustering of slopes method (oxides are in wt. % and trace elements in ppm). Fig. 5.11 (on the right): An example of the isocon diagrams of the calcsilicates subunit CS-I (least altered) relative to the more altered calcsilicate subunit CS-III.



5.3.5 Mass balance of the calcsilicates and pyroxenite subunits at Sandsloot

Table 5.7 presents the mass balance calculation results for calcsilicates and pyroxenites subunits. One example of an isocon diagram illustrating the relative mass loss and gain in the calcsilicates unit CS-II relative to unit CS-I is given in Fig. 5.11 (more examples are given in appendix III). The mass balance results are also presented as in the previous section, in the sequence modal composition changes of the pyroxenite units as follows: P-II→FP-I→P-I→FP-II.

The isocon diagram, which compares the calcsilicate subgroup CS-II with CS-I, in Fig 5.12 and Table 5.7 show pronounced relative gain in SiO₂ (34.79%), Al₂O₃ (4.18%) and Fe₂O₃ (8.18%), together with a loss of CaO (-6.95%) and MgO (-9.40%). The calcsilicate CS-II compared to the CS-I unit shows considerable enrichment in base metals; Cu (626.27%), Ni (1443.8%) and Co (79.9%). This is consistent with the petrography, where this layer has less carbonate minerals but higher contents of base metals relative to CS-I.

Calcsilicate subunit CS-III shows a relative gain in of SiO₂ (26.31%), Al₂O₃ (3.29%), Fe₂O₃ (4.40%) and MgO (11.65%), together with a loss of CaO (-22.88%). Base metal enrichment is less pronounced compared to the CS-II layer; Cu (34.6%), Ni (247.4%) and Co (20.7%). Significant drop in SiO₂, Fe₂O₃, CaO and Al₂O₃ enrichment corroborates a much reduced carbonate and higher pyroxene contents relative to CS-II.

The pyroxenite subunit P-II shows a relative gain in SiO₂ (35.47%), Al₂O₃ (1.83%), Fe₂O₃ (16.81%) and MgO (13.75%) coupled with a loss of CaO (-37%). The base metal enrichment in this pyroxenite unit is pronounced; Cu (1339.9%), and Ni (3252.9%) and Co (222%).

Pyroxenite subunit FP-I shows a relative gain in SiO₂ (46.21%), Al₂O₃ (3.64%), CaO (-35.94%) compared to the subunit P-II. The opposite is the case for Fe₂O₃ (14.8%), MgO (4.7%) and points to an increase in feldspar contents and more clinopyroxene relative to orthopyroxene in the FP-I pyroxenite unit. The base metal contents show a strong enrichment; Cu (1492.8%), and Ni (3258.4%) and Co (154.8%).

The pyroxenite subunit P-I is more enhanced in SiO₂ (48.43%), Al₂O₃ (9.88%) and Fe₂O₃ (12.99) when compared to the P-II and FP-I units and a pronounced relative loss in MgO (-1.36%) and CaO (-33.79%). The base metal enrichment is weaker compared to the subunits P-II and FP-I; Cu (-17%), and Ni (558.9) and Co (81.3%). Pronounced enrichment in SiO₂, Al₂O₃, and CaO coupled with reduced mass balance values for Fe₂O₃ and MgO are consistent with increased feldspathisation and increased clinopyroxene relative to orthopyroxene contents.

The pyroxenite subunit FP-II shows weaker gain in mass for SiO₂ (33.4%), Fe₂O₃ (8.7%) compared to the subunits P-II and FP-I and P-I that are coupled with a pronounced loss in MgO (-11.98%). Relative mass gain in Al₂O₃ (9.51) and an enrichment in CaO (-30.22%) points to an increase in feldspar contents and more clinopyroxene relative to orthopyroxene in the FP-II pyroxenite unit. The base metal show a weaker enrichment when compared to the P-II and FP-I pyroxenite units ; Cu (994.6%), and Ni (1953.9%) and Co (72).

As presented on table 5.7, the mass balance results for the trace elements show an increasing trend from CS-II to CS-III for Rb and V, and a decreasing trend is observed for Sr, Cu, Ni and Zn. This is similar to what has been proposed for the hornfels at Tweefontein (i.e. from H-II to H-III). The difference is that Ba and Co decreases from CS-II to CS-III whereas they increased from H-II to H-III. The opposite trends are also observed for Y.

At Sandsloot, Y is the trace element that shows a trend that is consistent with the sequence of change in modal composition (i.e. P-II→FP-I→P-I→FP-II) as it increases from P-II, to FP-I, to P-I to FP-II. The base metals do not follow this sequence, as Cu, Ni and Co shows a decreasing trend in the order from P-II, FP-I, FP-II and P-I at Sandsloot, which is consistent with the trend proposed at Tweefontein for Co. At Sandsloot Zn shows a decreasing trend from P-II, P-I, FP-I to FP-II (which is the trend proposed for Ni and Cu at Tweefontein).

Table 5.8: Shows the mass balance calculations for median concentrations for pyroxenites (at Tweefontein vs. Sandsloot) by using the clustering of slopes method (oxides are in wt. % and trace elements in ppm).

	TWEEFONTEIN			SANDSLOOT		
	P-I	FP-I	FP-II	P-I	FP-I	FP-II
SiO₂	6.70	16.36	2.97	12.48	10.61	7.50
Al₂O₃	4.29	3.66	11.49	7.90	1.78	10.20
Fe₂O₃	-7.27	-5.40	-11.52	-3.87	-2.02	-5.61
MnO	-0.02	0.03	-0.07	0.03	0.05	0.00
MgO	-3.41	3.83	-13.85	-15.10	-9.01	-23.27
CaO	3.75	3.57	6.80	3.14	1.05	9.36
Na₂O	0.58	0.44	1.08	0.23	0.32	1.52
K₂O	0.02	-0.07	0.22	-0.04	-0.09	0.12
P₂O₅	0.01	0.00	0.00	0.00	0.00	0.02
TiO₂	0.00	0.00	-0.04	0.09	0.08	0.18
SO₃	0.07	-0.27	-0.36	-0.64	0.01	-0.04
LOI	-5.30	-4.61	-4.83	-5.89	-4.76	-3.96
As	-15.02	-14.92	-12.14	1.27	-0.35	9.96
Ba	13.21	12.22	22.57	-45.70	-58.06	33.56
Ce	-100.43	-111.85	-142.01	-38.28	-42.77	-88.80
Co	-68.80	-53.90	-128.92	-140.00	-66.88	-126.90
Cu	257.22	0.00	-372.98	-1344.28	148.85	-58.71
Nb	-2.17	6.02	1.42	3.63	-1.48	0.00
Ni	0.00	-390.63	-1101.87	-2672.67	0.00	-746.91
Pb	2.49	4.58	4.66	-23.81	-22.78	-8.42
Rb	-7.90	-10.69	5.32	-8.16	-6.98	-1.97
Sr	31.93	16.64	132.68	64.88	-4.98	218.91
V	12.05	23.26	-14.65	80.42	56.84	81.44
Y	1.30	3.13	0.65	3.29	2.08	6.80
Zn	-25.27	-9.18	-48.31	0.00	-19.36	-52.39
Zr	-1.75	-0.86	0.00	5.02	2.84	10.12
Mo	2.06	3.25	0.91	1.52	0.69	-0.24
U	0.16	0.35	0.10	-0.71	-0.71	-0.72
Th	-0.15	-0.10	24.41	-0.01	-0.01	59.44

5.3.6 Mass balance in the pyroxenite subunits at Tweefontein and Sandsloot

Table 5.8 presents the mass balance calculation results for pyroxenite subunits at each farm respectively. One example of an isocon diagram illustrating the relative mass loss and gain in the pyroxenite unit FP-II relative to unit P-II is given in Fig. 5.9. The mass balance results are also presented as in the previous sections, in the sequence modal composition changes of the pyroxenite units as follows: FP-I→P-I→FP-II.

In table 5.8 and the isocon diagrams, the Tweefontein and Sandsloot mass balance calculation results for the pyroxenites are compared respectively (where subunit P-II is the least altered). The Tweefontein subunit FP-I show a relative gain of SiO₂ (16.36%), Al₂O₃ (3.66%), MgO (3.83%), CaO (3.57%) and a loss of Fe₂O₃ (-5.4%). The base metal contents show depletion; Cu (0%), and Ni (-390.6%) and Co (-53.9%). In the Sandsloot pyroxenite subunit FP-I there is a relative gain of SiO₂ (10.61%), Al₂O₃ (1.78%), CaO (1.05%) and a loss of MgO (-9.01%) and Fe₂O₃ (-2.02%). The base metal contents show enrichment in Cu and depletion in Co; where they are, Cu (148.85%), and Ni (0%) and Co (-66.88%).

The Tweefontein pyroxenite subunit P-I shows a relative gain of SiO₂ (6.7%), Al₂O₃ (4.29%), CaO (3.75%) and a loss of Fe₂O₃ (-7.27%) and MgO (-3.41%). The base metal contents show enrichment in Cu (257.2%), and Ni (0%) and a depletion of Co (-68.8%). In the Sandsloot pyroxenite subunit P-I there is a relative gain of SiO₂ (12.48%), Al₂O₃ (7.9%), CaO (3.14%) and a loss of Fe₂O₃ (-3.87%) and MgO (-15.1%). The base metal contents show depletion; Cu (-1344.3%), Ni (-2672.7%) and Co (-140%). At both farms, the subunit FP-I shows a pronounced increase of SiO₂, Al₂O₃, and CaO, and loss of Fe₂O₃ and MgO which corroborates with the petrography results. This points to the increase in feldspar and clinopyroxene contents relative to that of subunit P-II.

In the Tweefontein pyroxenite subunit FP-II, there is a relative gain of SiO₂ (2.97%), Al₂O₃ (11.47%), CaO (6.8%) and a loss of MgO (-13.85%) and Fe₂O₃ (-11.52%). The base metal contents show depletion; with Cu (-372.9%), and Ni (1101.9%) and Co (-128.92). In the Sandsloot pyroxenite subunit FP-II, there is a relative gain of SiO₂ (7.5%), Al₂O₃ (10.2%), CaO (9.36%) and a loss of MgO (-23.27%) and Fe₂O₃ (-5.61%). The base metal contents show depletion; with Cu (-58.7%), Ni (-746.9%) and Co (-126.9). At both farms, the subunit FP-II shows a pronounced increase of Al₂O₃ and CaO, and pronounced loss of Fe₂O₃ and

MgO compared to subunit P-II. This corroborates with the petrography results, and reflects the highly feldspathic nature of FP-II at both farms.

At both farms the mass balance calculation results show the same trend for certain elements. Al_2O_3 and CaO show an increase in values from FP-I, P-I and FP-II in that order. Conversely, Fe_2O_3 and MgO show a decrease in the same order. This also corroborates with the petrography results, as it shows that the rocks become more feldspathic and clinopyroxene-rich and less orthopyroxene-rich in the order from FP-I, P-I to FP-II.

The mass balance results included for the trace elements (see table 5.8) show an increase for Ba, Rb and Sr at both farms which is consistent with the sequence of modal composition changes, i.e. an increase from FP-I→P-I→FP-II. V and Y show the reverse trends at the two farms, e.g. V and Y increases (sequence of FP-I→P-I→FP-II) at Sandsloot and decreases at Tweefontein. The base metals show there is a decrease in Co and Zn at Tweefontein from FP-I, to P-I to FP-II.

At Sandsloot Co, Cu and Ni do not follow this sequence, as it decrease from FP-I, to FP-II to P-I. Ni and Cu from Tweefontein, together with Zn at Sandsloot also do not follow the sequence, as they show a decrease from P-I, to FP-I, to FP-II.

5.3.7 Summary

Relative to H-I, the altered hornfels subunit has a gain of SiO_2 and a loss of Al_2O_3 , Fe_2O_3 , Cu, Ni and Co. The more intense SiO_2 gain in H-II corroborates the observed intense silicification in this layer. H-III is a much reduced silicified layer and coupled with the occurrence of clinopyroxene. These layers also features a much subdued base metal contents compared to the hornfels subunit H-I. The mass balance results for the trace elements show an increasing trend from H-II to H-III for Ba, Rb, V and Co. The opposite decreasing trend is observed for Sr, Y, Cu, Ni and Zn.

Overall the pyroxenites comparative to H-I, are more enriched in SiO_2 , MgO, K_2O , SO_3 and depleted in Fe_2O_3 and TiO_2 . CaO and Al_2O_3 are also depleted for except in the highly enriched FP-II. This is consistent with the petrography as FP-II is most feldspathised; subunit P-II has the base metal enrichment in this subunit which is highest with Cu, Ni and Co and

dominated by orthopyroxene relative to clinopyroxene. The FP-I unit shows a progressive enrichment of CaO, SiO₂, Al₂O₃ relative to the P-I unit that is coupled with more pronounced relative loss in Fe₂O₃, MgO and the base metals. Furthermore, this point to an increase of feldspar and clinopyroxene relative to the orthopyroxene content. Pronounced enrichment in SiO₂, Al₂O₃, CaO coupled with reduced mass balance values for Fe₂O₃ and MgO are consistent with increased feldspathisation and increased clinopyroxene relative to orthopyroxene contents. Sr is the trace element that shows a trend that is consistent with the sequence of change in modal composition (i.e. P-II→FP-I→P-I→FP-II) as it increases from P-II, to FP-I, to P-II to FP-II.

Relative to CS-I, the altered calcsilicates subunits have a gain of SiO₂, Al₂O₃, Fe₂O₃, TiO₂ and SO₃, Cu, Ni, Zn and Co and a loss of CaO. This is consistent with the petrography, where CS-II has less carbonate minerals but higher contents of base metals relative to CS-I. CS-III has a significant drop in SiO₂, Fe₂O₃, CaO and Al₂O₃ enrichment; this corroborates a much reduced carbonate and higher pyroxene contents relative to CS-II. These layers also features a much extensive base metal contents compared to the hornfels subunit CS-I. Show an increasing trend from CS-II to CS-III for Rb and V, and a decreasing trend is observed for Sr, Cu, Ni and Zn. This is similar to what has been proposed for the hornfels at Tweefontein (i.e. form H-II to H-III). The difference is that Ba and Co decreases from CS-II to CS-III whereas it increased from H-II to H-III. The opposite trends are also observed for Y.

Overall the pyroxenites comparative to CS-I, are more enriched in SiO₂, Al₂O₃, Na₂O, K₂O, P₂O₅, TiO₂, Ni and Co and depleted of CaO, MnO and MgO.

The pyroxenite subunit P-II shows pronounced base metal enrichment in this pyroxenite unit. Pyroxenite subunit FP-I points to an increase in feldspar contents and more clinopyroxene relative to orthopyroxene in the P-II pyroxenite unit. Pronounced enrichment in SiO₂, Al₂O₃, and CaO coupled with reduced mass balance values for Fe₂O₃ and MgO are consistent with increased feldspathisation and increased clinopyroxene relative to orthopyroxene contents.

The mass balance results for the trace elements at Sandsloot, show Y as the trace element that has a trend that is consistent with the sequence of change in modal composition (i.e. P-II→FP-I→P-I→FP-II) as it increases from P-II, to FP-I, to P-II to FP-II. The base metals do

not follow this sequence, as Cu, Ni and Co show a decreasing trend in the order from P-II, FP-I, FP-II and P-I at Sandsloot, which is consistent with the trend proposed at Tweefontein for Co. At Sandsloot Zn shows a decreasing trend from P-II, P-I, FP-I to FP-II (which is the trend proposed for Ni and Cu at Tweefontein).

At both farms the pyroxenites are more enriched in SiO₂, Al₂O₃, CaO and Na₂O relative to the more pristine P-II. The subunit FP-I shows a pronounced increase of SiO₂, Al₂O₃, and CaO, and loss of Fe₂O₃ and MgO which corroborates the increase in feldspar and clinopyroxene contents relative to that of subunit P-II. The subunit FP-II shows a pronounced increase of Al₂O₃ and CaO, and pronounced loss of Fe₂O₃ and MgO compared to subunit P-II. This reflects the highly feldspathic nature of FP-II at both farms.

Al₂O₃ and CaO show an increase in values from FP-I, P-I and FP-II in that order. Conversely, Fe₂O₃ and MgO show a decrease in the same order. This also corroborates with the petrography results, as it shows that the rocks become more feldspathic and clinopyroxene-rich and less orthopyroxene-rich in the order from FP-I, P-I to FP-II.

Ba, Rb and Sr at both farms show a pattern which is consistent with the sequence of modal composition changes, i.e. an increase from FP-I→P-I→FP-II. V and Y show the reverse trends at the two farms, e.g. V and Y increase (sequence of FP-I→P-I→FP-II) at Sandsloot and decrease at Tweefontein. The base metals show there is a decrease in Co and Zn at Tweefontein from FP-I, to P-I to FP-II.

At Sandsloot Co, Cu and Ni do not follow this sequence, as it decrease from FP-I, to FP-II to P-I. Ni and Cu from Tweefontein, together with Zn at Sandsloot also do not follow the sequence, as it show a decrease from P-I, to FP-I, to FP-II.

5.4 Chemostratigraphy and Vectoring

5.4.1 Introduction

The study thus far has revealed that the rocks can be petrographically classified into subunits of calcsilicates, hornfels and pyroxenites. These rocks have unique mineralogical compositions and textures that are linked to alteration, magmatic processes and related contact metamorphism. A geochemical rock classification in section 5.1 mirrored the petrography results. The petrography was validated by the results of the cluster analysis, and the cluster analysis proved that there is a link between the mineralogy of the rock subunits and their major rock chemistry.

The rock characterisation in section 5.2 defined the compositional differences of the rock types and their subunits. For example a progressive decrease in the contents of Fe_2O_3 , Al_2O_3 , Ce, Co, Cu, Ni, Zn, Zr, Au, Pd and Pt from the hornfels subunits H-I, H-II to H-III and an increase in SiO_2 , Fe_2O_3 , TiO_2 , SO_3 , Co, Cu, Ni, Rb, V and Zn contents from CS-I, CS-II to CS-III. Hornfels subunit H-I and calcsilicate subunit CS-III are the main carriers of BMS and PGE at the floor rock pyroxenite interface/ reaction subunit. The pyroxenite subunit FP-I is most enriched in Cu, Ni and PGEs (Au, Pt and Pd).

All these results from the previous geochemical sections point to the fact that the hornfels and calcsilicate subunits may result from a gradational element loss or gain from the protolith. Mass balance calculations were used to define patterns of element mobility. The mass balance study has shown that Al_2O_3 , CaO, Na_2O , Ba, Rb and Sr show an increase in values from FP-I, P-I and FP-II in that order comparative to the least altered P-II. Conversely, Fe_2O_3 and MgO show a decrease in the same order. These trends corroborate the petrography results that shows increasing feldspathisation coupled with an increase in clinopyroxene contents relative to orthopyroxene from P-II, FP-I, P-I to FP-II pyroxenites.

This section now focuses on leading the investigation into establishing chemostratigraphy by delineating geochemical indices that provides geochemically distinct units. These indices will be derived from the element patterns observed in the geochemical characterisation and the

mass balance study. The mass balance study aimed at launching the lithological investigation by using immobile elements to calculate the mass changes that occurred within the alteration subunits.

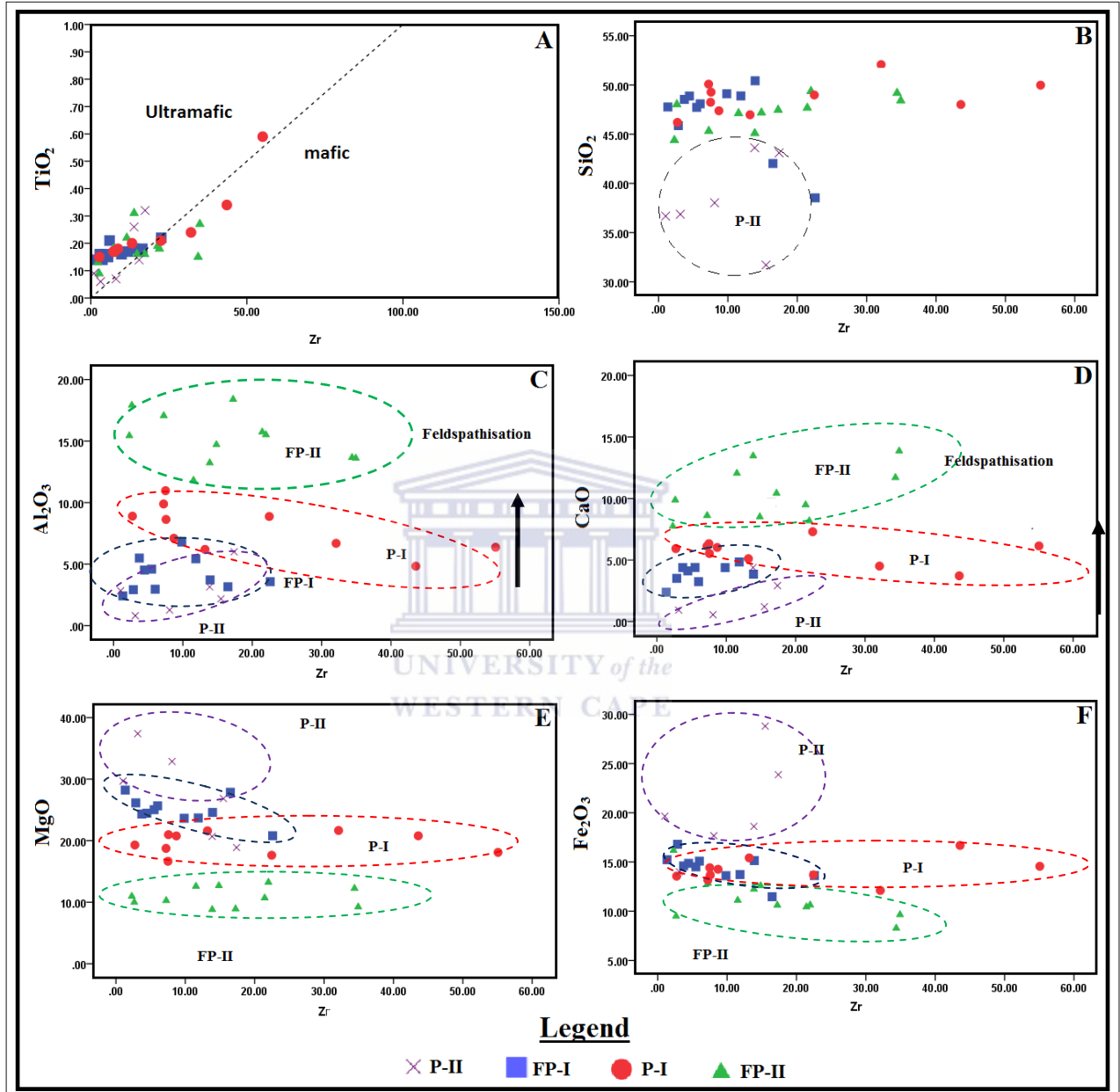


Figure 5.12: Bivariate plots of the immobile and mobile elements. (A) the immobile elements TiO₂ against Zr; (B-F) the immobile Zr against the mobile major elements; SiO₂, Al₂O₃, Fe₂O₃, MgO and CaO. It is evident how Al₂O₃ and CaO are clear indicatives of feldspathisation.

The cyclic occurrence of the pyroxenitic layers as documented in chapter 4 and the changes in their modal composition therefore point to an increasing degree of modal layering (McBirney and Nicolas, 1997) from TN754 through TN200 to SS339.

This section therefore attempts to investigate any underlying chemostratigraphic indices and their possible relationship with trace element fractionation. The ultimate objective is to establish as a possible link between the mechanism of the modal layering and the nature and style of the BMS/ PGE mineralisation. In order to establish the fractionation trends, due consideration was first made to the immobile element distribution in the pyroxenites as these yield precise hints of the precursor magmatic rock type and or affinity (Barrett and MacLean, 1994).

5.4.2 Geochemical Indices

According to Pearce et al. (2010) relative contents of the HFSE such as TiO_2 , Zr, Y and Nb remain unaffected in rocks that have suffered metasomatic alteration. When two HFSE are plotted against each other, it is expected that the data should create a linear trend where the slopes are close to unity (Cann, 1970). Fig. 5.12 (A) shows a single fractionation line or a linear relationship between TiO_2 vs Zr contents for the pyroxenite subunits. Thus, this point to a mafic to ultramafic nature of pyroxenite subunits, and also that these subunits derived from the same protolith or magma source.

Fig. 5.12 (B) displays a fairly uniform SiO_2 content relative to Zr for all the pyroxenite units except P-II.

Inverse trending relationships can be observed for the plots of Zr vs Al_2O_3 and CaO in Fig. 5.12 (C and D) respectively, when compared to those of Zr vs Fe_2O_3 and MgO in Fig. 5.12 (E and F) respectively. Both cases illustrate the feldspathisation as linked to an increase in the contents of Al_2O_3 and CaO, which is coupled with decreasing contents of Fe_2O_3 and MgO. This is well corroborated by the plot of Ba and Sr against Zr (Fig. 5.13), which also shows a progression from the P-II pyroxenites at the bottom of the plot to FP-I, P-I, and to FP-II. This corroborates with the mass balance study. However, Ba (not illustrated) does not show this clear trend.

The bivariate plots in the appendix IV illustrate the major elements against each other, and how they too can discriminate the pyroxenite subunits. The Al₂O₃ and MgO bivariate plot display a sequenced modal composition change of the pyroxenite subunits.

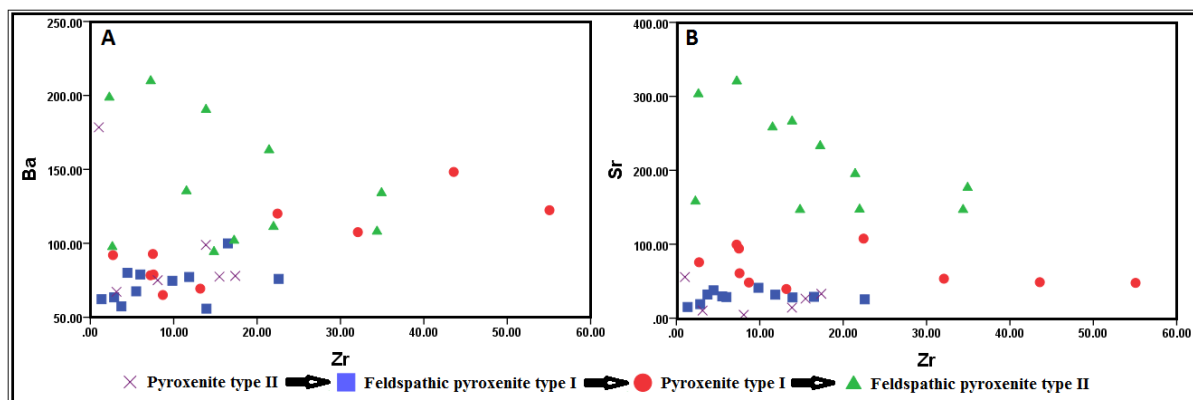


Figure 5.13: Illustrates bivariate plots of the Zr against Ba and Sr respectively. The arrows in this figure represents the sequence of change in modal composition (section 5.3.4)

5.4.3 Feldspathisation or metasomatic index

The information gathered in the previous subsections indicates that with increased feldspathisation, Fe₂O₃ and MgO were subdued relative to the addition of CaO, Na₂O₃ and Al₂O₃. Based on these elements patterns, an index was calculated to determine the enrichment of the added elements as follows:

$$\text{CaO} + 10\text{Na}_2\text{O} / \text{CaO} + 10\text{Na}_2\text{O} + \text{Fe}_2\text{O}_3 + \text{MgO}$$

The ensuing metasomatic index is lowest for the P-II pyroxenites and shows a progressive increase through FP-I, P-I to the highest values in FP-II. In Fig. 5.14, a plot of the metasomatic index (MI) versus Al₂O₃/SiO₂ ratio clearly demonstrates the feldspathisation process with increased Al₂O₃ relative to SiO₂. This confirms that P-II is the least metasomatised pyroxenite subunit. The plot also shows the pyroxenite subunits in the sequence of increasing feldspathisation, i.e. from P-II, FP-I, P-I to FP-II. Thus, it can be used to discriminate the pyroxenite subunits.

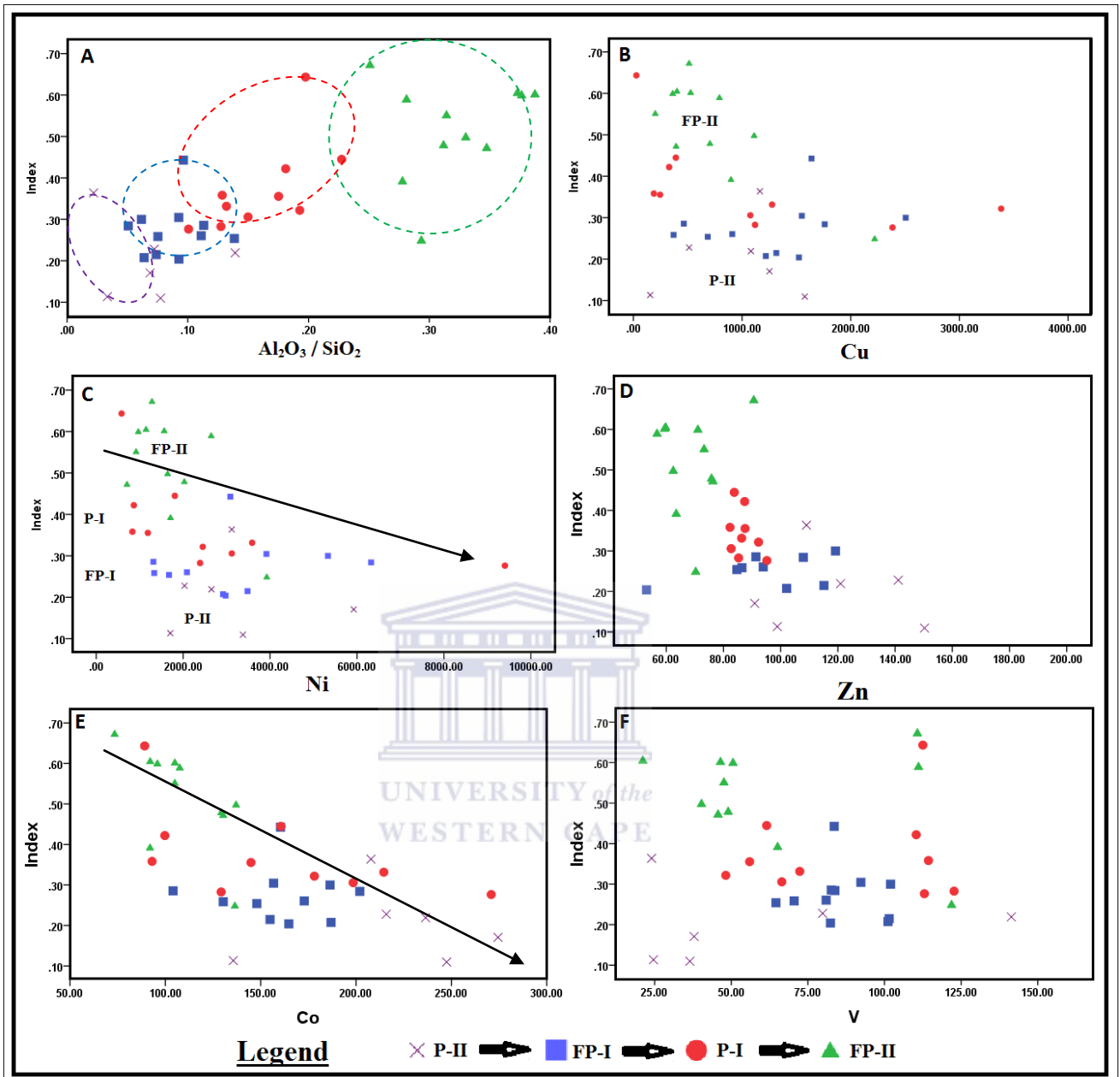


Figure 5.14: Illustrates the index $(CaO + 10Na_2O / CaO + 10Na_2O + Fe_2O_3 + MgO)$ against (A) SiO_2 ; (B) validation of the index against Al_2O_3 ; and (C-E) BMS mineralisation.

5.4.4 Relationships between the feldspathisation index and the BMS mineralisation

A relationship between the pyroxenitic subunits and the BMS contents was noted in the previous chapters, whereby the P-II pyroxenites are predominantly BMS rich while the FP-I

and FP-II are hinted to contain both BMS and PGE. These trends are however based on statistical summaries and therefore need to be spatially tested for chemostratigraphic purpose. A spatial pattern of the feldspathisation and the pyroxenitic units is conclusive from Fig. 5.14.

Fig. 5.14 (B-E) shows an inverse relationship between the metasomatism index and the base metals Cu, Ni, Co and Zn. The pyroxenitic units however show variable patterns of clustering within the inverse trending relationships. For example the plot of Cu, Ni and V versus the metasomatism index points to an inverse trend that is dominated by high Cu and Ni contents in the P-I and FP-I pyroxenitic units. The contents of Cu, Ni and V thus do not show useful patterns that can be related to feldspathisation. Zinc and to a great extent Co (Fig. 5.14 C-D) shows a clearly discernable inverse trend with increasing feldspathisation as expected.

5.4.5 Vectoring towards PGE mineralisation

Vectoring includes developing element ratios, pathfinder elements or trace element signatures, which are able to define a consistent gradient indicative of an ore subunit. This can potentially help to distinguish the mineralised from barren geological complexes (Eilu et al., 2001; Ames et al., 2007; Brand, 1999) and to identify geochemical trends (Rollinson, 1993).

The feldspathisation index has proven to have an inverse relationship with the base metals and also with the ratios. For example, in Fig 5.15 (A), the plot of the metasomatism index vs Co+Zn shows a progressive inverse trending curve, whereby the P-II pyroxenites show high Co+Zn and low metasomatism index. This grade through FP-I, P-I to FP-II, which contains a low Co+Zn contents against a high metasomatism index. In Fig. 15 (B-F), the plots of various base metals and their ratios show overwhelmingly an overlapping relationship between P-I and FP-I and a variable degree of separation of P-II and FP-II.

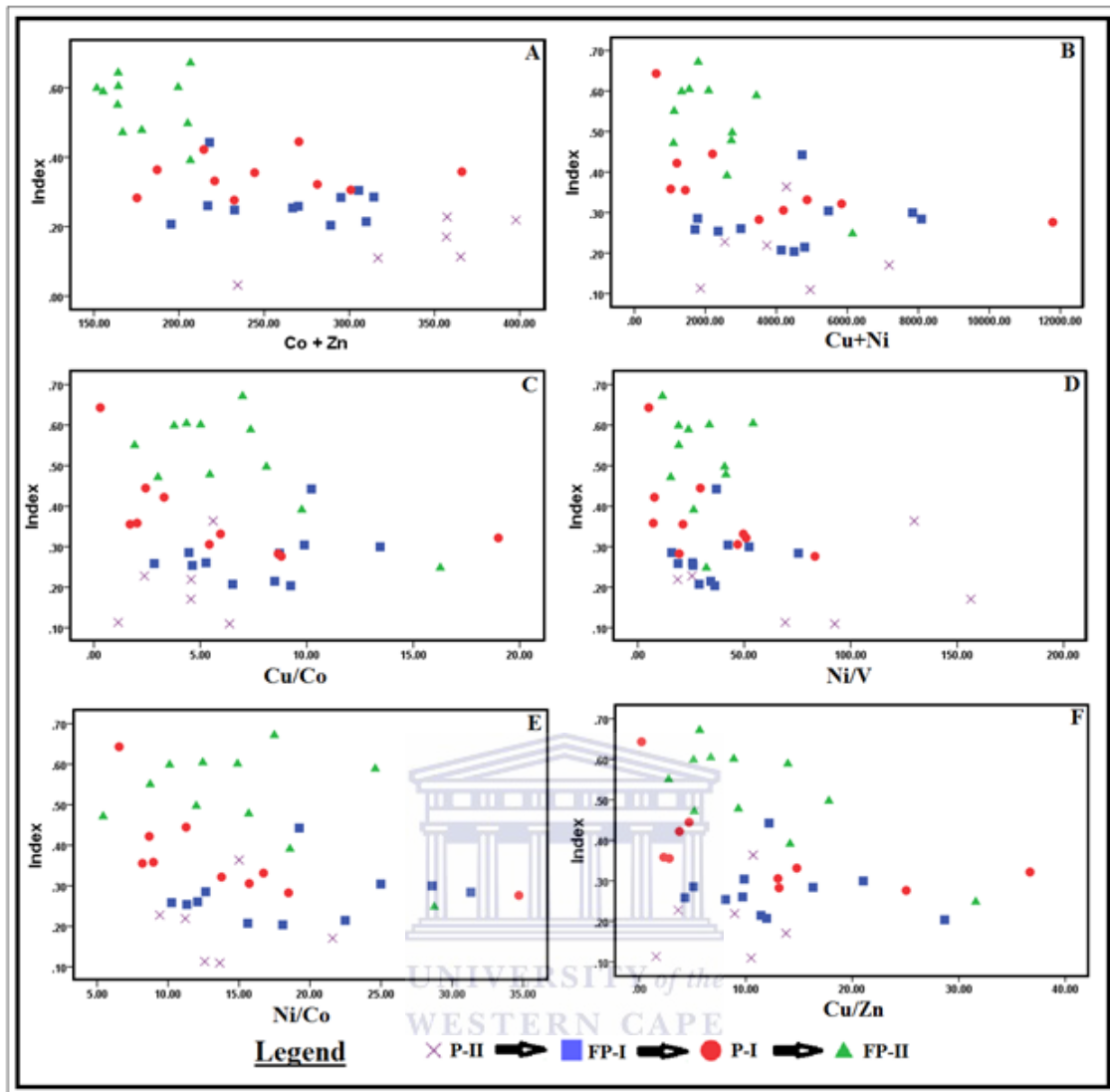


Figure 5.15: The feldspathisation index against ratios or indices of Co+Zn, Cu+Ni, Cu/Co, Ni/V, Ni/Co and Cu/Zn.

The plot of the base metals in Fig.5.16 (C, D and F) show a variable degree of overlapping relationships between the pyroxenite units and therefore may not serve as useful indices towards vectoring. Contrary, the plot of Co vs Ni and Cu vs Co in Fig 5.15 (E and A) respectively, show a greater extent of separation between the pyroxenite units and are therefore considered as potential indices towards vectoring.

Based on the foregoing results, Co+Zn has a positive correlation with the metasomatic index. The relationship between Co+Zn and Cu+Ni as well as Cu vs Ni is therefore looked into in Fig. 16 (B and G). The plot of Cu vs Ni shows a strong linear relationship between P-II, P-I and FP-II while FP-I is seemingly detached from the group.

The plot of Cu+Ni vs Co+Zn show three major groups comprising of FP-II with low Cu+Ni plus Co+Zn contents and P-II, which is characterised by high Cu+Ni and Co+Zn contents. A third group comprised of FP-I and PI are accompanied by moderate Cu+Ni and Co+Zn contents. The contents of Cu+Ni and Co+Zn in the P-II and FP-II are therefore linked to pyroxenites with high and low Fe₂O₃ and MgO contents respectively. The use of Ni/Co and Cu/Co ratios should therefore characterise the predominantly BMS rich P-II and separate it from the FP-I and FP-II pyroxenites, with moderate to low BMS and PGE as illustrated in Fig. 5.16 (H and J). The above trends will be validated in the ensuing downhole element plots.

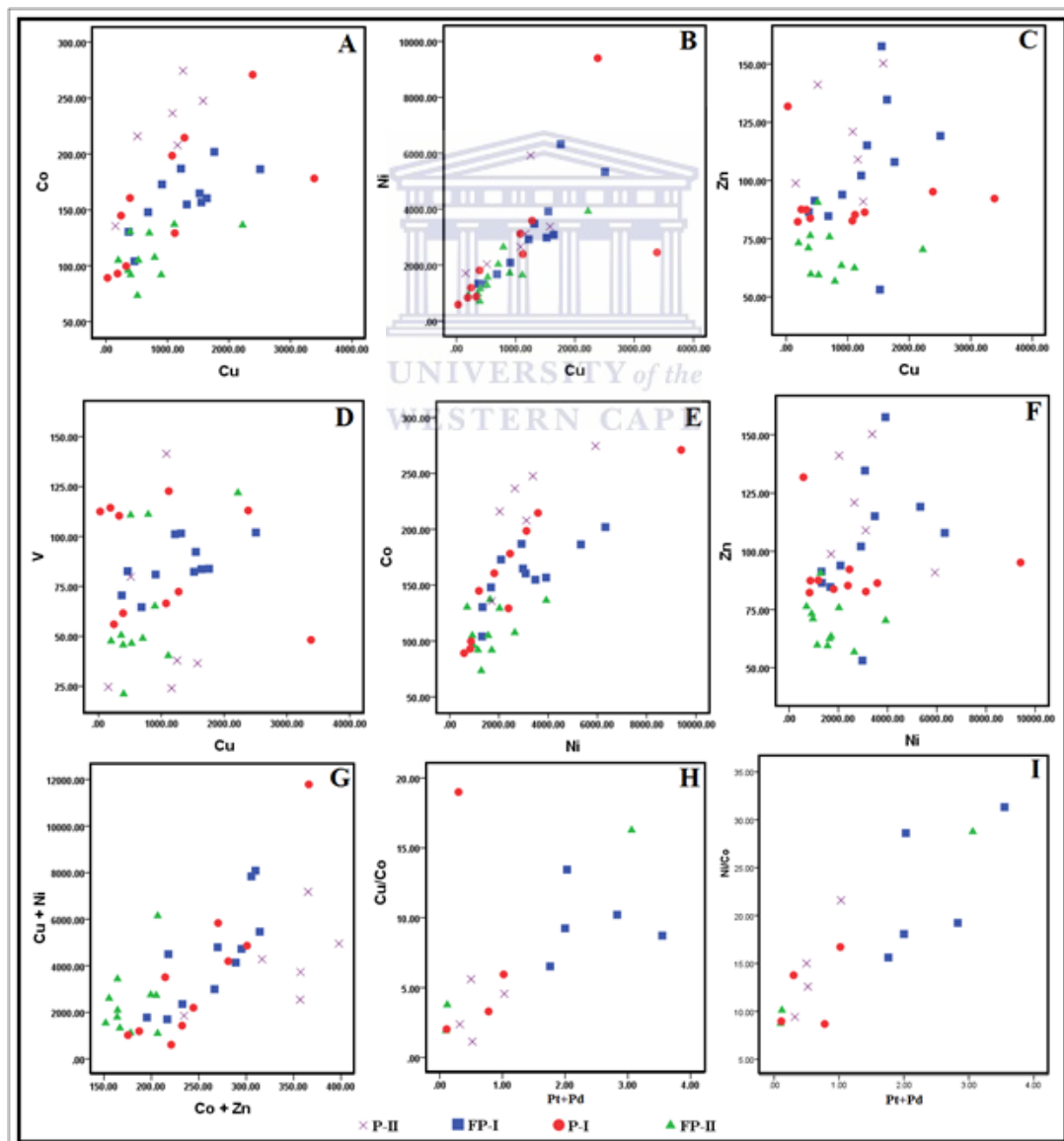


Figure 5.16: Ratios created against PGEs, with the aim of targeting the PGE mineralisation.

SS339



Figure 5.17: Downhole plot of drillcore SS339. This plot shows the down hole geochemical variations in this drillcore.

5.4.6 Downhole plots:

This subsection focuses on illustrating how Cu+Ni and Co+Zn content, the metasomatism index and other above mentioned indices reflect the lithologies and PGE distribution in the drillcores TN754, TN200 and SS339. The Co+Zn contents has a positive relationship with the variation patterns of the BMS (Cu+Ni) in the pyroxenite units outlined in this work. The metasomatic index ($\text{CaO} + 10\text{Na}_2\text{O} / \text{CaO} + 10\text{Na}_2\text{O} + \text{Fe}_2\text{O}_3 + \text{MgO}$) defines the modal variation in the pyroxenitic lithologies. The goal therefore is to relate these element patterns/indices and the metasomatic index to the nature and style of the PGE mineralisation. Figures 5.17, 5.18 and 5.19 present the down hole lithology and elements/indices plots for the drillcores SS339, TN754 and TN200 respectively.

Drill hole SS339 (Fig. 5.17) is located on a calcsilicate floor rocks and is capped by the hangingwall gabbronorite. In between these rocks is the Platreef package, which comprises of alternating layers of pyroxenite subunits; P-II, P-I, FP-II and predominantly FP-I. Platinum-group element mineralisations with Pt+ Pd grades of up to 3 ppm are distributed almost across the entire Platreef package.

The BMS (Cu+Ni) show similar patterns as the PGEs with grades hovering around 0.4-0.8% in the FP-I and FP-II pyroxenites. The metasomatic index in this section varies between 0.4 and 0.8 with peak contents over the gabbronorites FP-II pyroxenites and the calcsilicates as expected. Elevated Co+Zn contents of over 160 ppm occur throughout the entire pyroxenite package. The trends of the Ni/Co and Cu/Co ratios are similar to those of the metasomatic index but with spurious peaks coinciding with those of the PGE's.

Figure 5.18 and 19 illustrate the drillcores TN754 and TN200 respectively. These drillcores are located over a BIF/ shales or hornfels floor rocks and are also capped by the hangingwall gabbronorite. Drillcore TN200 intersects a Platreef package that is composed of alternating layers of P-I, P-II, FP-I and FP-II while TN754 mainly hosts the P-II subunit grading into P-I and FP-II subunits. This thus points to a decrease in the degree of feldspathisation from SS339 through TN200 to TN754.

In TN200 platinum-group element mineralisation, Pt+ Pd grades are subdued to less than 1.5 ppm while the BMS (Cu+Ni) are low and hover below 0.5%. The metasomatic index in TN

200 has a similar range of between 0.4 and 0.8 as in SS339 also with peak contents over the FP-II pyroxenites and the hornfels.

Similar elevated Co+Zn contents of over 160 ppm occur throughout the entire pyroxenite package. The trends of the Ni/Co and Cu/Co ratios are similar to those of the metasomatic index. In TN754 the PGE and Cu+Ni grades are highest in the hornfels and in the pyroxenite package both are subdued to less than 1.5 ppm and 0.5% respectively. Sharp drops in values of the metasomatic index, hovering below 0.4 and Co+Zn ~ 160 ppm occur in most of the pyroxenite package except the peak values in the FP-II subunit. Coincident peak contents of Cu/Co, Ni/Zn, Cu+Ni and Pt+Pd occur at various depths in the hornfels (H-I).





Figure 5.18: Downhole plot of drillcore TN754. This plot shows the down hole geochemical variations in this drillcore.

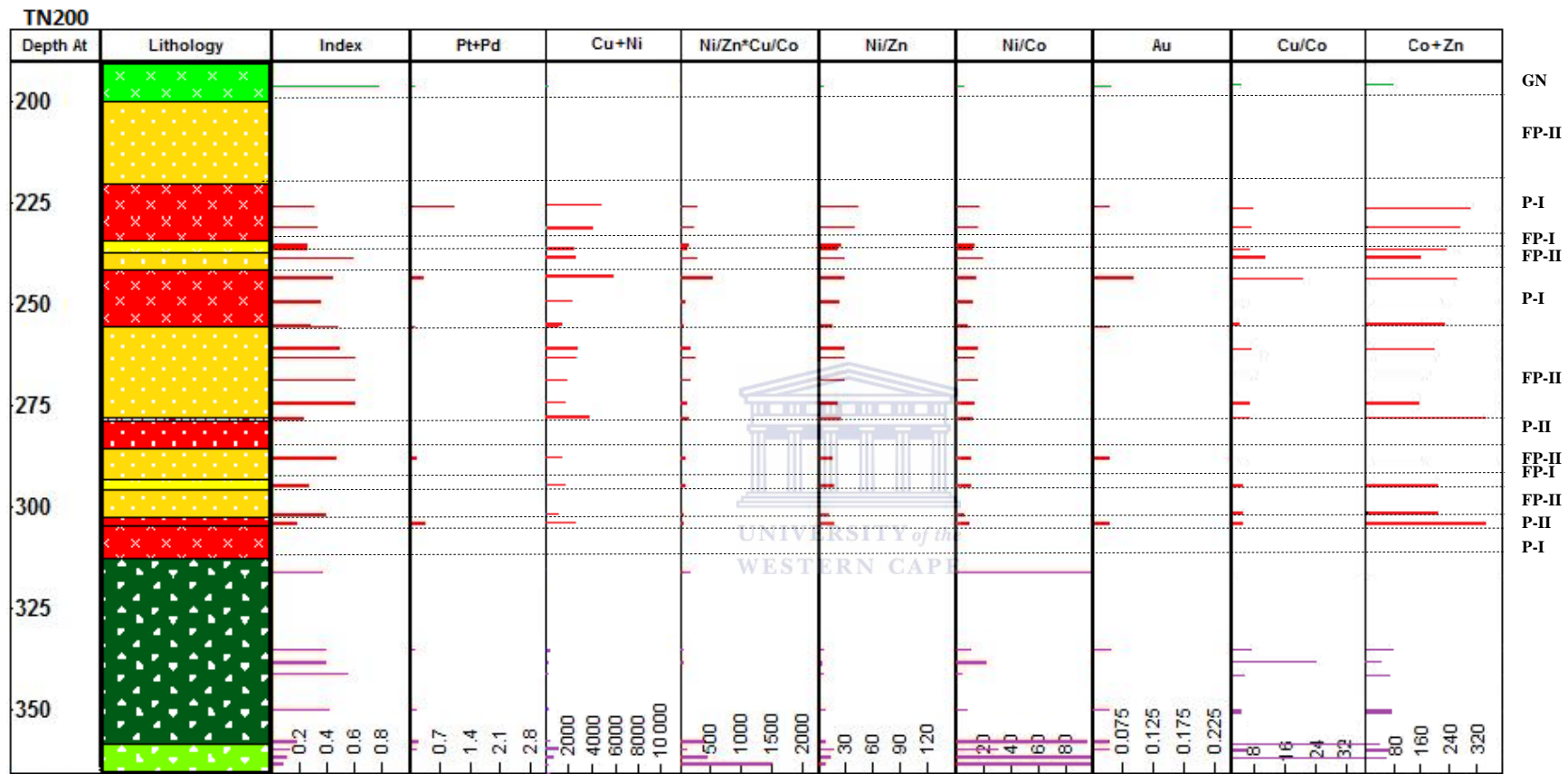


Figure 5.19: Downhole plot of drillcore TN200. This plot shows the down hole geochemical variations in this drillcore.

CHAPTER 6

6. DISCUSSION AND CONCLUSIONS

6.1 Discussion

6.1.1 Introduction

The preceding chapters have given an account of all the results for this thesis. In this chapter, further discussion and conclusions are given; together with the outcomes, short comings and recommendations of this work.

This thesis centred on finding a possible solution to challenges faced by exploration geologists, when locating the PGE mineralisation within the various lithologies of the Platreef. Traditional mineral exploration methods were hindered due to the uncertainty of the genesis of the Platreef; together with the major stratigraphic and mineralisation variations across the Platreef (laterally and vertically). These problems resulted in other issues such as; finding marker boundaries between the Platreef's heterogeneous lithologies, understanding the style and nature of the mineralisation, as well as having difficulty of targeting the irregular PGE and BMS mineralisation. Also, it can be difficult to identify the metasomatic aureole between the Platreef and its underlying floor rocks, and to find the marker boundaries of this aureole.

The aims of this thesis were to delineate geochemical indices (chemostratigraphy) and also to vector towards PGE mineralisation within the Platreef. This included the following objectives; 1) characterising the lithologies based on a petrographical foundation, enhanced with a geochemical based criteria; 2) create possible marker boundaries within the Platreef lithologies, and also find marker boundaries with the metasomatised aureole; 3) characterise the PGE and BMS mineralisation; 4) relate this to the various lithologies, mineralogy and other major, minor and trace elements.

The Platreef was studied at two farms; Tweefontein and Sandsloot. Generally, the underlying floor rocks to the Platreef package are the Penge BIF and the Duitschland shales at

Twefontein and the Malmani dolomite floor rocks at Sandsloot. The results are discussed below:

6.1.2 Chemostratigraphy

The potential of chemostratigraphy was investigated by using a petrographical classification, together with the geochemistry to identify the distinctive subunits within the pyroxenites, calcsilicates and/or hornfels at Sandsloot and Twefontein respectively. Emphasis is added by the author that the nature of the Platreef rocks is not homogeneous, and the criteria were used to characterise zones of greatest similarity to simplify the heterogeneity. It should also be noted that samples that included xenoliths or granitic veins were excluded from this study (as they were not representative and could not be used as training samples).

a. Platreef package

A cornerstone of this work is an attempt to revisit the classification of the pyroxenites in the Platreef package. In the past various classification approaches have been attempted, such as the subdivision of the Platreef in the central sector into three facies (A, B and C), based on texture and type of predominant pyroxene (e.g. White 1994; Lee 1996). Later, the focus on the modal percentages, cumulus phases and intercumulus assemblages (Kinnaird et al. 2005), whereby the rocks are named according to internationally- accepted classification schemes, e.g. the IUGS Rock Classification Scheme (see also Ch.2).

In this study, the heterogeneous pyroxenite package within the three drillcores was initially divided into three main layers: pyroxenite, and two distinctive feldspathic pyroxenites (FP-I and FP-II). However, the pyroxenites were also further separated as P-I and P-II (see Ch.4). This was because of a higher notable difference in the degree of alteration within P-I. This classification is compared and discussed to the existing available literature:

The pyroxenite subunit **P-I** is predominantly orthopyroxene (~56 %), clinopyroxene (~22%) and plagioclase (~15%); together with olivine (~2%), sulphides (~3%) and accessory minerals (~2%). These rocks are generally medium to coarse grained, and alteration includes fine grained chloritisation and sericitisation. These rocks are very similar to what Kinnaird et al. (2005); Reisberg et al. (2011); and Armitage (2011) have proposed as typical pyroxenites

in the southern sectors of the Platreef. The pyroxenite subunit **P-II** is predominantly orthopyroxene (~50%), clinopyroxene (~20%), olivine (~17%); together with plagioclase (~4%), sulphides (~6%) and accessory minerals (~3%). They are generally medium grained and are areas extensively serpentinised and sericitised. Sulphides occur as tiny disseminated blebs, stringers and veins.

The pyroxenite subunit **FP-I** was named in line with what was proposed by Kinnaird et al. (2005; as mentioned above, i.e. cumulus orthopyroxene and intercumulus plagioclase). These rocks are predominantly orthopyroxene (~77%), clinopyroxene (~10%) and plagioclase (~5%). Kinnaird et al. (2005) distinguishes the feldspathic pyroxenite (i.e. in this case FP-I) from the hanging wall norites, as these rocks will have cumulus orthopyroxene and intercumulus plagioclase; whereas the norites have both cumulus orthopyroxene and cumulus feldspars. Pronost et al. (2008) also describes these pyroxenites, with cumulus orthopyroxene and intercumulus plagioclase.

Whereas, the pyroxenite subunit **FP-II** is predominantly orthopyroxene (~17%), clinopyroxene (~25%), and plagioclase (~50%). They are generally medium to coarse grained with alteration by micas and carbonates, and with extensive sericitisation. Sulphide blebs are irregular, and have bigger blebs than other types, and are disseminated. These rocks are described by Reisberg et al. (2011), where they are called leuconorites. Harris and Chaumba (2001) and McDonald et al. (2005) refer to these rocks as possible equivalent to the main zone of the intrusion in the other limbs. The term “feldspathic pyroxenite” which connotes a lithology comprising of cumulus orthopyroxene with significant intercumulus feldspar was adopted and is commonly accepted amongst Platreef geologists (Kinnaird et al. 2005).

b. Cyclic layering and feldspathisation

Initially, there has been an observation of significant grain size and modal percentage variation of the feldspars in the pyroxenites (see Ch. 4). The cyclic layering as observed in the three drillcores is most prevalent in SS339, and least in TN754. The grain size and modal percentage variation of feldspars are significant and occurs in an increasing order from P-II, FP-I, P-I and FP-II. Feldspars changes from finer grained to coarser grained in the same sequence. Kinnaird et al. (2005) also mentions norite cycles, where the Platreef package is

composed of an upward succession of dunite, serpentinised peridotite, pyroxenite and feldspathic pyroxenite, to melanorite through leuconorite to anorthosite. Normally these include repetitive cycles of mafic-rich to mafic-poor layers that occur in the mid to upper portion of the Platreef.

In this study, there is a predominance of P-II and P-I in TN754. This grade into occurrences of interlayering subunits that are mostly P-I, P-II and FP-I in TN200. This is also coupled with an upward thickening of P-I layers in this drillcore. In SS339 there is a rhythmic interlayering of predominantly FP-I and FP-II. There appear to be a cyclic pattern of P-II, to FP-I to FP-II. Where P-I occurs, the pattern is P-II, FP-I, P-I and FP-II. Thus the layers generally grade from orthopyroxene and olivine; into predominantly orthopyroxene; then into orthopyroxene, clinopyroxene and plagioclase; and then into predominantly plagioclase rich (and clinopyroxene) layers.

This may relate possibly to the variation in floor rocks between the drillcores as SS339 has a dolomite floor rock, whereas TN200 and TN754 have the BIF and shales floor rocks. The carbonate rocks are naturally higher in Ca-contents comparative to the Fe-rich BIF rocks, and could explain the increase in feldspathisation in the pyroxenites along the strike from TN754, to TN200 to SS339. The reaction between the Platreef magma and the two floor rocks created unique set of metasomatism of the floor rocks at each farm. Wagner (1929) also recognised the formation of these rocks were a result of metamorphic / metasomatic processes. The metasomatised floor rocks at Sandsloot and Tweefontein were further characterised into three subunits of calcsilicates and hornfels respectively.

According to literature, cyclic modal layering may result from at least two categories of free convection which control crystallization regimes in the magma chamber (Brandeis and Jaupart, 1987). The first category is compositional convection driven by density contrasts due to fractional crystallization and the second category is thermal convection by temperature contrasts (Brandeis and Jaupart, 1987); these two regimes are important particularly in basic and ultrabasic magmas. The intermittent layering or rhythmic layering observed in SS339 could therefore result from the effects of convectional crystallization in the magma chamber as observed in the Skaergaard intrusion by McBirney and Noyes (1979).

c. Metasomatism index

Based on the progressive degrees of feldspathisation observed previously, it appears that the feldspathisation can distinguish the subunits in the Platreef package studied from the drillcores from TN754, to TN200 and to SS339. Many geochemical plots (corroborated by the petrographical and mass balance results) illustrated that the feldspathisation were linked to an increase in the contents of Al_2O_3 and CaO , and coupled with a decrease in contents of Fe_2O_3 and MgO . Together with other geochemical trends, geochemically distinct units of the Platreef package could be discriminated with a metasomatic index (MI; $\text{CaO} + 10\text{Na}_2\text{O} / \text{CaO} + 10\text{Na}_2\text{O} + \text{Fe}_2\text{O}_3 + \text{MgO}$). The ensuing MI is lowest for the P-II pyroxenite and shows a progressive increase through FP-I, P-I to the highest values in FP-II.

The sequence of these intrusive events that affects the Platreef and the Main Zone magma has been a subject of debate over the years (e.g. Harris and Chaumba, 2001; Hutchison and Kinnaird, 2005; Manyeruke et al., 2005; Kinnaird et al., 2005; Holwell and Jordaan, 2006; Howell and McDonald, 2007; and Pronost et al., 2008). Manyeruke et al. (2005) and Kinnaird et al. (2005) have suggested that the Platreef was intruded as a sill or series of sills (Pronost et al., 2008). Manyeruke et al. (2005), Kinnaird et al. (2005), Maier et al. (2008), and Yudovskaya and Kinnaird (2010) suggest that these sill-like intrusions are composed of three geochemically distinct pyroxenites. Yudovskaya and Kinnaird (2010) also used the chromitite correlation study to explain the relationship between the successions of these intrusive sills. Studies by McDonald and Holwell (2007) illustrated geochemical data showing trends appearing to be inconsistent with a single magma. McDonald and Holwell (2007) further concluded that the Platreef pyroxenite intruded as a crystal mush.

Annotated by various authors (Cawthorn and Davies, 1983; Sharpe et al., 1980; Eales et al., 1996; Kruger, 2005; Cawthorn and Walraven, 1998), the RLS did not result from the crystallization of a single magma, but was emplaced as multiple influxes (Yudovskaya et al., 2013). A possible explanation by Kinnaird et al. (2005) explains the earliest intrusive phase intruded within the Transvaal metasedimentary sequence as sills. This was followed by other pulses, which had some metasedimentary material being detached from the floor. Later magma flowed under or over these layers. Some of the later pulses also inter-fingered with the early Platreef pulses. The results obtained from this study do not point to a multiple magma injection model but accommodates 1.) an influx of magma, which subsequently

spread to the south to form the Merensky Reef above the Critical Subunit (Kruger, 2005) and 2.) that the Platreef pyroxenite intruded as a crystal mush and, at a given locality, the same country rock formed both the footwall and hanging wall (McDonald and Holwell, 2007).

Outside the Bushveld Complex literature, the formation of intermittent layering or rhythmic layering as defined by McBirney and Noyes (1979) observed in SS339 could occur as effects of convectional crystallization in the magma chamber. For example in the Skaergaard Layered Series, McBirney and Nicholas (1997) noted that such a system is accompanied by liquid fractionation, due to compaction and is augmented by compositionally driven convection. Products of the crystallization in an open system are elements that are introduced or removed by convective exchange (e.g. Morse, 1988), or by liquids (or fluids) expelled from lower levels by compaction (Shirley & McBirney, 1991; Sonnenthal & McBirney, 1998). This could also be possibly the case for the differences in feldspathisation in the sections studied.

The fluid fractionation process could be inferred from the distribution of the PGE. For example in drillcore TN754 the BMS are concentrated in the hornfels subunits, with weak mineralisation in its Platreef package. TN200 and SS339 have BMS concentrated in its Platreef packages, and not the hornfels / calcsilicate floor rocks. Beyond these, there is a positive correlation between high degree of feldspathisation in the pyroxenites and the BMS and PGE tenor or styles.

d. Floor rocks

Metasomatised floor rocks at Sandsloot have been described by Harris and Chaumba (2001), Armitage et al. (2002) and Ihlenfeld and Keays (2011), however, there has been no profound work done on the metasomatic rocks at Tweefontein. For example, according to Harris and Chaumba (2001) and Ihlenfeld and Keays (2011); this mixture of recrystallised and altered pyroxenites and highly altered calcsilicate rocks are locally referred to as ‘parapyroxenites’. Armitage et al. (2002) described these floor rocks as calcsilicate hornfels, serpentinite footwall lithologies and as skarns; where these rocks contain minerals that reflect a wide range of prograde and retrograde metamorphic reactions. Outside the Platreef vast descriptions have been made of the interaction between mafic to felsic magmas with

sedimentary floor rocks (e.g., Shand, 1930; Tilley, 1952; Sabine, 1975; Baker and Black, 1980; Del Moro et al., 2001; Ordonez-Calderon et al., 2008).

In this thesis, the main differences in the calcsilicates and their subunits can be described in the sequence of CS-I, to CS-II, to CS-III. In this sequence the carbonate minerals decrease; the minerals like orthopyroxene and clinopyroxene increase; the alteration increase; the rocks become finer grained and the BMS mineralisation increases. The main differences in the hornfels and their subunits can be described in the sequence H-I, to H-II, to H-III. In this sequence the oxide minerals and plagioclase decrease; the minerals clinopyroxene and quartz increase; the alteration increase; the texture becomes more coarser grained and the BMS and PGE mineralisation decreases. Ordonez-Calderon et al. (2008) also refers to the progression of lesser carbonate material towards a carbonate-magma interaction contact; where there is a progression of orthopyroxene, to plagioclase, to clinopyroxene from the distal calcsilicates to the proximal calcsilicates.

Gaeta et al., (2009) also added that during the assimilation of floor rock material by a mafic magma, this process favours the crystallization of clinopyroxene (Tilley, 1952; Joesten, 1977; Joesten et al., 1994; Cioni et al., 2013; Owens., 2000; Wenzel et al., 2002), whereas olivine is consumed.

The BMS and PGE mineralisation for the hornfels, is highest in the subunit H-I, whereas for the calcsilicates it is highest in the subunit CS-III. The subunit H-I, has the BMS and PGE coupled with Al_2O_3 , Fe_2O_3 , Na_2O , TiO_2 , SO_3 , LOI, As, Ba, Ce, Co, Cu, Ni, V and Sr. Whereas, the subunit CS-III has the BMS and Pd coupled with SiO_2 , Fe_2O_3 , Na_2O , TiO_2 , SO_3 , Co, Cu, Ni, Pb, Rb, V, Zn and Mo.

These calcsilicates show a decoupling of PGEs (Pt decoupled from BMS and Pd). Holwell and McDonald (2006) also reported that the BMS and the PGE were decoupled in the calcsilicate rocks. Ihlenfeld and Keays (2011), explains that the sulphides and the PGE do occur deep in the BIF footwall at Tweefontein (thus in H-I). Polat et al. (2007) suggests it is possible that these massive sulphides can be precipitated in a specific layer because of the driving force of intrusions where heavy metals are redistributed. Armitage et al. (2002) explains that the orthomagmatic processes have played a role in the initial development of the deposit, but these cannot be seen as the sole influence. The final distribution of the PGE in

the reef and footwall was strongly influenced by fluid activity, e.g. decoupling at Sandsloot. These played the dominant role in mobilizing and homogenizing PGE within the Platreef and carrying them into the footwall, where they formed irregular zones and regular layers containing high PGE concentrations.

Because the calcsilicate and hornfels are mineralised, they can be considered as skarn deposits. Numerous other studies involving skarn deposits have been documented before (Meinert, 1982). Yaxley et al. (1998) and Wenzel et al. (2002) outline similar subunits of skarn deposits in magma, and in a carbonate contact environment, whereas Guy (2010) outlines subunits of banded skarns. They are considered to be exoskarn because of its sedimentary protolith. This is confirmed by Armitage et al. (2002) who concluded that the calcsilicate footwall are indeed skarn deposits, and can be an 'exoskarn'.

In this study, the style of PGE mineralisation is consistent with what Armitage et al. (2002) proposed, which is a 'Pd-Pt-Au skarn'. And outside the Platreef, the occurrence of PGE is also reported in some skarns (e.g. Knopf, 1942).

Geochemical considerations suggest that PGEs could be transported by fluids under very acidic, oxidised conditions (Wood et al., 1989) which could possibly explain why TN754 has the BMS and PGEs concentrated in the hornfels subunits, with weak mineralisation in its Platreef package. Whereas TN200 and SS339 have BMS and PGEs concentrated in its Platreef packages, and not in the floor rocks. Thus, this is a result of the conditions brought about by the process of feldspathisation where mineralisation has been redistributed more extensively with higher feldspathisation.

6.1.3 Vectoring

In terms of geochemical vectoring, it was essential to establish a possible link between the metasomatism index and the nature and style of the PGE and/or BMS mineralisation.

The hornfels subunit H-I and calcsilicate subunit CS-III were the main carriers of BMS and PGE. There are two types of BMS mineralisation observed in this study. The first type is pronounced in pyroxenite subunit P-II and is associated with low contents of PGE and the other coincident with the pyroxenite subunit FP-I. The Platreef package can be further elaborated as: P-I (low PGE, low BMS); P-II (low PGE, high BMS); FP-II (high PGE, low BMS); and FP-I (high PGE, high BMS).

Armitage et al. (2002) relates the BMS mineralisation with weak PGE mineralisation to an orthomagmatic process. From this study, the BMS mineralisation with strong PGEs relates to increased feldspathisation process within the pyroxenite package. This corroborates earlier observations by Holwell and McDonald (2006), that the ‘noritic / feldspathic pyroxenite’ do carry the highest PGE and BMS. Kinnaird et al. (2005) also refers to the primary sulphides and PGE’s that were redistributed by several later processes. Hutchinson and McDonald (2008) stated that the Platreef formed by a complex interaction of magmatic, metasomatic and hydrothermal processes (e.g. Armitage et al., 2002; Hutchinson and Kinnaird, 2005; Manyeruke et al., 2005; McDonald et al., 2005; Holwell et al., 2006a; Holwell and Jordaan, 2006). Syn- and post-magmatic fluid alteration also occurred on a much greater scale (Buchanan et al. 1981; Holwell and McDonald 2006; Hutchinson and Kinnaird 2005).

6.1.4 Shortcomings and recommendations

a. Shortcomings

Only one drillcore was used at Sandsloot in comparative to the two drillcores used at Tweefontein. Thus, the three drillcores used in this study cannot be used solely to generalise the whole of the Platreef. Correlating the pyroxenites and feldspathic pyroxenites spatially from one drillcore to another were hindered, hence, chemostratigraphy were not completed spatially. However, it has been previously noted by Kinnaird et al. (2005) that the cyclic packages are limited to correlation at short segments.

b. Recommendations

The Platreef is complexed, therefore, future research can be undertaken to validate these findings across the Platreef, and with a bigger drillcore database.

6.2 Conclusions

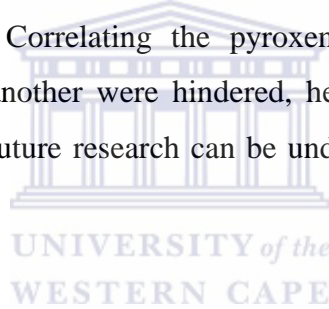
The use of chemostratigraphy and geochemical vectoring were investigated in this study to create geochemically distinct layers, and also to locate PGE mineralisation in the Platreef. The emphasis was on two farms; Tweefontein and Sandsloot, and included three drillcores (TN754, TN200 and SS339). The focus of this study was to aid mining geologists in potentially targeting the mineralisation irrespective of lithology, farm or the underlying differences in floor rocks. Based on the petrographical and geochemical studies, the conclusions are as follows:

Chemostratigraphy can be potentially favorable in the Platreef package as observed in the three drillcores studied. However, correlating the pyroxenites and feldspathic pyroxenites spatially from one drillcore to another were hindered, hence, chemostratigraphy could not be completed. Other reasons include variable differences in the cyclic layering. This could be related to the two distinctive floor rocks at the two different farms; i.e. the calcsilicates at Sandsloot and the hornfels at Tweefontein. There is also a progressive degree of feldspathisation in the Platreef package from Tweefontein to Sandsloot. The many geochemical plots that were corroborated by the petrographical and mass balance results, illustrated that the feldspathisation were linked to an increase in the content of Al_2O_3 and CaO , and coupled with a decrease in content of Fe_2O_3 and MgO . Together with other geochemical trends, geochemically distinct units of the Platreef package could be positively discriminated with a metasomatism index; $\text{CaO} + 10\text{Na}_2\text{O} / \text{CaO} + 10\text{Na}_2\text{O} + \text{Fe}_2\text{O}_3 + \text{MgO}$. The MI was lowest for the P-II pyroxenite and shows a progressive increase through FP-I, P-I to the highest values in FP-II. Geochemical layering were further observed in the calcsilicates and hornfels; e.g. a progressive decrease in the contents of Fe_2O_3 , Al_2O_3 , Ce, Co, Cu, Ni, Zn, Zr, Au, Pd and Pt from the hornfels subunits H-I, H-II to H-III and an increase in of SiO_2 , Fe_2O_3 , TiO_2 , SO_3 , Co, Cu, Ni, Rb, V and Zn contents from CS-I, CS-II to CS-III. The MI can also discriminate the calcsilicates.

Geochemical vectoring that locates PGE mineralisation has been made possible. There are two types of BMS mineralisation observed in this study; one relating to the orthomagmatic process, and the second to the feldspathisation process. The final distribution of the PGE in the reef and footwall is thought to be strongly influenced by the metasomatic fluid activity, and played the dominant role in mobilizing and homogenizing PGE within the Platreef and

carrying them into the footwall. The hornfels subunit H-I and calcsilicate subunit CS-III were the main carriers of BMS and PGE. The Platreef package were more complicated: P-I (low PGE, low BMS); P-II (low PGE, high BMS); FP-II (high PGE, low BMS); and FP-I (high PGE, high BMS). A link between the metasomatism index and the nature and style of the PGE and/or BMS mineralisation were observed. Therefore, the metasomatism (feldspathisation) index could be a strong indicator of high PGE and BMS, or ratios such as Cu/Co or Ni/Co can also be used.

In conclusion, the MI could also be a strong indicator of high PGE and BMS. Throughout the study, rocks were clustered together irrespective of farm. A validation process to assess the metasomatism index (MI), base metal indices and PGE distribution within the individual drillcores (TN754, TN200 and SS339) were undertaken. The results were that the MI ranges were similar in all drillcores, and discriminated the subunits of the Platreef package, gabbro-norites and even the calcsilicates. Limitations of this study included that the results only reflected three drillcores. Correlating the pyroxenites and feldspathic pyroxenites spatially from one drillcore to another were hindered, hence, chemostratigraphy were not completed spatially. Therefore, future research can be undertaken to validate these findings across the Platreef.



REFERENCES

- Ames, D., McClenaghan, M. & Averill, S. 2007, "Footwall-hosted Cu-PGE (Au, Ag), Sudbury Canada: towards a new exploration vector", *Exploration 07, Exploration in the New Millennium*. pp. 1013-1017.
- Armitage, P.E.B. 2011, *Development of the Platreef in the northern limb of the Bushveld Complex at Sandsloot, Mokopane District, South Africa*.
- Armitage, P., McDonald, I., Edwards, S. & Manby, G. 2002, "Platinum-group element mineralization in the Platreef and calc-silicate footwall at Sandsloot, Potgietersrus District, South Africa", *Applied Earth Science: Transactions of the Institutions of Mining and Metallurgy: Section B*, vol. 111, no. 1, pp. 36-45.
- Ashwal, L.D., Webb, S.J. & Knoper, M.W. 2005, "Magmatic stratigraphy in the Bushveld Northern Lobe: continuous geophysical and mineralogical data from the 2950 m Bellevue drillcore", *South African Journal of Geology*, vol. 108, no. 2, pp. 199-232.
- Babcock, R.S. 1973, "Computational models of metasomatic processes", *Lithos*, vol. 6, no. 3, pp. 279-290.
- Baker, C. & Black, P.M. 1980, "Assimilation and metamorphism at a basalt-limestone contact, Tokatoka, New Zealand", *Mineral Mag*, vol. 43, pp. 797-807.
- Barnes, S. & Maier, W.D. 2002, "Platinum-group element distributions in the Rustenburg layered suite of the Bushveld Complex, South Africa", *The Geology, geochemistry, mineralogy and mineral beneficiation of platinum-group elements*, vol. 54, pp. 431e458.
- Barrett, T.J. & MacLean, W.H. 1994, "Chemostratigraphy and hydrothermal alteration in exploration for VHMS deposits in greenstones and younger volcanic rocks", *Alteration and alteration processes associated with ore-forming systems. Geological Association of Canada, Short Course Notes*, vol. 11, pp. 433-467.
- Barrett, T. & MacLean, W. 1991, "Chemical, mass, and oxygen isotope changes during extreme hydrothermal alteration of an Archean rhyolite, Noranda, Quebec", *Economic Geology*, vol. 86, no. 2, pp. 406-414.
- Barton, J., Cawthorn, R.G. & White, J. 1986, "The role of contamination in the evolution of the Platreef of the Bushveld Complex", *Economic Geology*, vol. 81, no. 5, pp. 1096-1104.
- Boorman, S. & Boudreau, A. 2002, "Compaction in the Bushveld Complex and the nature of the Lower Zone-Critical Zone Transition", *9 th International Platinum Symposium, July 21-25*.
- Brand, N.W. 1999, "Element ratios in nickel sulphide exploration: vectoring towards ore environments", *Journal of Geochemical Exploration*, vol. 67, no. 1, pp. 145-165.

- Brandeis, G. & Jaupart, C. 1987, "The kinetics of nucleation and crystal growth and scaling laws for magmatic crystallization", *Contributions to Mineralogy and Petrology*, vol. 96, no. 1, pp. 24-34.
- Buchanan, D., Nolan, J., Suddaby, P., Rouse, J., Viljoen, M. & Davenport, J. 1981, "The genesis of sulphide mineralization in a portion of the Potgietersrus Limb of the Bushveld Complex", *Economic Geology*, vol. 76, no. 3, pp. 568-579.
- Buick, I.S., Maas, R. & Gibson, R. 2001, "Precise U–Pb titanite age constraints on the emplacement of the Bushveld Complex, South Africa", *Journal of the Geological Society*, vol. 158, no. 1, pp. 3-6.
- Bye, A. & Bell, F. 2001, "Stability assessment and slope design at Sandsloot open pit, South Africa", *International Journal of Rock Mechanics and Mining Sciences*, vol.38, no. 3, pp. 449-466.
- Cann, J. 1970, "Rb, Sr, Y, Zr and Nb in some ocean floor basaltic rocks", *Earth and Planetary Science Letters*, vol. 10, no. 1, pp. 7-11.
- Cawthorn, R.G., Barton, J. & Viljoen, M.J. 1985, "Interaction of floor rocks with the Platreef on Overysel, Potgietersrus, northern Transvaal", *Economic Geology*, vol. 80, no. 4, pp. 988-1006.
- Cawthorn, R.G. & Walraven, F. 1998, "Emplacement and crystallization time for the Bushveld Complex", *Journal of Petrology*, vol. 39, no. 9, pp. 1669-1687.
- Cawthorn, R. 2005, "Pressure fluctuations and the formation of the PGE-rich Merensky and chromitite reefs, Bushveld Complex", *Mineralium Deposita*, vol. 40, no. 2, pp. 231-235.
- Cawthorn, R. 1999, "The platinum and palladium resources of the Bushveld Complex", *South African Journal of Science*, vol. 95, no. 11/12, pp. 481-489.
- Cawthorn, R., Cooper, G. & Webb, S. 1998, "Connectivity between the western and eastern limbs of the Bushveld Complex", *South African Journal of Geology*, vol. 101, no. 4, pp. 291-298.
- Cawthorn, R. & Davies, G. 1983, "Experimental data at 3 kbars pressure on parental magma to the Bushveld Complex", *Contributions to Mineralogy and Petrology*, vol. 83, no. 1-2, pp. 128-135.
- Cawthorn, R., Eales, H., Walraven, F., Uken, R. & Watkeys, M. 2006, "The Bushveld Complex", *The Geology of South Africa*, vol. 691, pp. 261-281.
- Cawthorn, R. & Lee, C. 1998, "Field excursion guide to the Bushveld Complex", *8th international platinum symposium. Geol Soc South Africa and S African Inst Min Metall*.
- Cawthorn, R. G., and Webb, S. J., 2001, Connectivity Between the Western and Eastern Limbs of the Bushveld Complex: Tectonophysics, v. 330, p. 195-209.

- Cioni, R., D'Oriano, C., Bertagnini, A. & Andronico, D. 2013, "The 2nd to 4th century explosive activity of Vesuvius: new data on the timing of the upward migration of the post-AD 79 magma chamber", *Annals of Geophysics*, vol. 56, no. 4, pp. S0438.
- Coelho, J. 2006, "GEOISO—a Windows™ program to calculate and plot mass balances and volume changes occurring in a wide variety of geologic processes", *Computers & Geosciences*, vol. 32, no. 9, pp. 1523-1528.
- Del Moro, A., Fulignati, P., Marianelli, P. & Sbrana, A. 2001, "Magma contamination by direct wall rock interaction: constraints from xenoliths from the walls of a carbonate-hosted magma chamber (Vesuvius 1944 eruption)", *Journal of Volcanology and Geothermal Research*, vol. 112, no. 1, pp. 15-24.
- Dusel-Bacon, C., Wooden, J.L. & Hopkins, M.J. 2004, "U-Pb zircon and geochemical evidence for bimodal mid-Paleozoic magmatism and syngenetic base-metal mineralization in the Yukon-Tanana terrane, Alaska", *Geological Society of America Bulletin*, vol. 116, no. 7-8, pp. 989-1015.
- Eales, H., Botha, W., Hattingh, P., De Klerk, W., Maier, W. & Odgers, A. 1993, "The mafic rocks of the Bushveld Complex: a review of emplacement and crystallization history, and mineralization, in the light of recent data", *Journal of African Earth Sciences (and the Middle East)*, vol. 16, no. 1, pp. 121-142.
- Eales, H. & Cawthorn, R. 1996, "The Bushveld Complex", *Developments in Petrology*, vol. 15, pp. 181-229.
- Eilu, P. & Mikucki, E.J. 1998, "Alteration and primary geochemical dispersion associated with the Bulletin lode-gold deposit, Wiluna, Western Australia", *Journal of Geochemical Exploration*, vol. 63, no. 2, pp. 73-103.
- Eilu, P., Mikucki, E.J. & Dugdale, A.L. 2001, "Alteration zoning and primary geochemical dispersion at the Bronzewing lode-gold deposit, Western Australia", *Mineralium Deposita*, vol. 36, no. 1, pp. 13-31.
- Elliott-Meadows, S.R. & Appleyard, E.C. 1991, "The alteration geochemistry and petrology of the Lar Cu-Zn deposit, Lynn Lake area, Manitoba, Canada", *Economic Geology*, vol. 86, no. 3, pp. 486-505.
- Everitt, B.S. & Dunn, G. 2001, "Applied multivariate analysis", *Book 2nd.ed.London: Arnold*.
- Finlow-Bates, T. & Stumpfl, E.F. 1981, "The behaviour of so-called immobile elements in hydrothermally altered rocks associated with volcanogenic submarine-exhalative ore deposits", *Mineralium Deposita*, vol. 16, no. 2, pp. 319-328.
- Gaeta, M., Di Rocco, T. & Freda, C. 2009, "Carbonate assimilation in open magmatic systems: the role of melt-bearing skarns and cumulate-forming processes", *Journal of Petrology*, vol. 50, no. 2, pp. 361-385.

- Gain, S.B. & Mostert, A. 1982, "The geological setting of the platinoid and base metal sulphide mineralization in the Platreef of the Bushveld Complex in Drenthe, north of Potgietersrus", *Economic Geology*, vol. 77, no. 6, pp. 1395-1404.
- Good, N. & De Wit, M.J. 1997, "The Thabazimbi-Murchison lineament of the Kaapvaal craton, South Africa: 2700 Ma of episodic deformation", *Journal of the Geological Society*, vol. 154, no. 1, pp. 93-97.
- Grant, J.A. 2005, "Isocon analysis: a brief review of the method and applications", *Physics and Chemistry of the Earth, Parts A/B/C*, vol. 30, no. 17, pp. 997-1004.
- Grant, J.A. 1986, "The isocon diagram; a simple solution to Gresens' equation for metasomatic alteration", *Economic Geology*, vol. 81, no. 8, pp. 1976-1982.
- Gresens, R.L. 1967, "Composition-volume relationships of metasomatism", *Chemical Geology*, vol. 2, pp. 47-65.
- Guy, B. 2010, "Banded skarns, an example of geochemical dissipative structure".
- Hall, A.L. 1932, *The Bushveld igneous complex of the central Transvaal*, The Government printer.
- Harris, C. & Chaumba, J.B. 2001, "Crustal contamination and fluid-rock interaction during the formation of the Platreef, northern limb of the Bushveld Complex, South Africa", *Journal of Petrology*, vol. 42, no. 7, pp. 1321-1347.
- Hartigan, J.A. 1975, *Clustering algorithms*, John Wiley & Sons, Inc.
- Hatton, C. & Schweitzer, J. 1995, "Evidence for synchronous extrusive and intrusive Bushveld magmatism", *Journal of African Earth Sciences*, vol. 21, no. 4, pp. 579-594.
- Holwell, D., Armitage, P. & McDonald, I. 2005, "Observations on the relationship between the Platreef and its hangingwall", *Applied Earth Science: Transactions of the Institutions of Mining and Metallurgy: Section B*, vol. 114, no. 4, pp. 199-207.
- Holwell, D., Boyce, A. & McDonald, I. 2007, "Sulphur isotope variations within the Platreef Ni-Cu-PGE deposit: Genetic implications for the origin of sulphide mineralization", *Economic Geology*, vol. 102, no. 6, pp. 1091-1110.
- Holwell, D., Jones, A., Smith, J. & Boyce, A. 2013, "New mineralogical and isotopic constraints on Main Zone-hosted PGE mineralisation at Moorddrift, northern Bushveld Complex", *Mineralium Deposita*, vol. 48, no. 6, pp. 675-686.
- Holwell, D. & Jordaan, A. 2006, "Three-dimensional mapping of the Platreef at the Zwartfontein South mine: implications for the timing of magmatic events in the northern limb of the Bushveld Complex, South Africa", *Applied Earth Science: Transactions of the Institutions of Mining and Metallurgy: Section B*, vol. 115, no. 2, pp. 41-48.

- Holwell, D. & McDonald, I. 2010, "A review of the behaviour of platinum group elements within natural magmatic sulphide ore systems", *Platinum Metals Review*, vol. 54, no. 1, pp. 26-36.
- Holwell, D., McDonald, I. & Armitage, P. 2006, "Platinum-group mineral assemblages in the Platreef at the Sandsloot Mine, northern Bushveld Complex, South Africa", *Mineralogical Magazine*, vol. 70, no. 1, pp. 83-101.
- Holwell, D., McDonald, I. & Butler, I. 2011, "Precious metal enrichment in the Platreef, Bushveld Complex, South Africa: evidence from homogenized magmatic sulphide melt inclusions", *Contributions to Mineralogy and Petrology*, vol. 161, no. 6, pp. 1011-1026.
- Holwell, D. & McDonald, I. 2007, "Distribution of platinum-group elements in the Platreef at Overysel, northern Bushveld Complex: a combined PGM and LA-ICP-MS study", *Contributions to Mineralogy and Petrology*, vol. 154, no. 2, pp. 171-190.
- Holwell, D.A. & McDonald, I. 2006, "Petrology, geochemistry and the mechanisms determining the distribution of platinum-group element and base metal sulphide mineralisation in the Platreef at Overysel, northern Bushveld Complex, South Africa", *Mineralium Deposita*, vol. 41, no. 6, pp. 575-598.
- Hulbert, L. & Von Gruenewaldt, G. 1985, "Textural and compositional features of chromite in the lower and critical zones of the Bushveld Complex south of Potgietersrus", *Economic Geology*, vol. 80, no. 4, pp. 872-895.
- Hutchinson, D. & Kinnaird, J.A. 2005, "Complex multistage genesis for the Ni–Cu–PGE mineralisation in the southern region of the Platreef, Bushveld Complex, South Africa", *Applied Earth Science: Transactions of the Institutions of Mining and Metallurgy: Section B*, vol. 114, no. 4, pp. 208-224.
- Hutchinson, D. & McDonald, I. 2008, "Laser ablation ICP-MS study of platinum-group elements in sulphides from the Platreef at Turfspruit, northern limb of the Bushveld Complex, South Africa", *Mineralium Deposita*, vol. 43, no. 6, pp. 695-711.
- Ihlenfeld, C. & Keays, R.R. 2011, "Crustal contamination and PGE mineralization in the Platreef, Bushveld Complex, South Africa: evidence for multiple contamination events and transport of magmatic sulphides", *Mineralium Deposita*, vol. 46, no. 7, pp. 813-832.
- Ishikawa, Y., Sawaguchi, T., Iwaya, S. & Horiuchi, M. 1976, "Delineation of prospecting targets for Kuroko deposits based on modes of volcanism of underlying dacite and alteration haloes", *Mining Geology*, vol. 26, pp. 105-117.
- Joesten, R., Hill, J. & Van Horn, S. 1994, "Limestone assimilation and clinopyroxenite production along the contacts of a 9 metre alkali olivine basalt dike, Killala Bay, Ireland. Geological Society of America", *Abstracts with Program*, pp. 476.
- Joesten, R. 1977, "Mineralogical and chemical evolution of contaminated igneous rocks at a gabbro-limestone contact, Christmas Mountains, Big Bend region, Texas", *Geological Society of America Bulletin*, vol. 88, no. 10, pp. 1515-1529.

- Kaufman, L.R. & Rousseeuw, P. "PJ (1990) Finding groups in data: An introduction to cluster analysis", *Hoboken NJ John Wiley & Sons Inc.*
- Kaufman, L. & Rousseeuw, P.J. (2005) "Finding groups in data: an introduction to cluster analysis.
- Kinloch, E. 1982, "Regional trends in the platinum-group mineralogy of the critical zone of the Bushveld Complex, South Africa", *Economic Geology*, vol. 77, no. 6, pp. 1328-1347.
- Kinloch, E. & Peyerl, W. 1990, "Platinum-group minerals in various rock types of the Merensky Reef; genetic implications", *Economic Geology*, vol. 85, no. 3, pp. 537-555.
- Kinnaird, J. & Nex, P. 2003, "Mechanisms of marginal mineralisation in the Bushveld Complex", *TRANSACTIONS-INSTITUTION OF MINING AND METALLURGY*, vol. 112, no. B, pp. 206-207.
- Kinnaird, J.A. 2005, "Geochemical evidence for multiphase emplacement in the southern Platreef", *Applied Earth Science: Transactions of the Institutions of Mining and Metallurgy: Section B*, vol. 114, no. 4, pp. 225-242.
- Kinnaird, J.A., Hutchinson, D., Schurmann, L., Nex, P. & de Lange, R. 2005, "Petrology and mineralisation of the southern Platreef: northern limb of the Bushveld Complex, South Africa", *Mineralium Deposita*, vol. 40, no. 5, pp. 576-597.
- Kinnaird, J.A. & McDonald, I. 2005, "An introduction to mineralisation in the northern limb of the Bushveld Complex", *Applied Earth Science: Transactions of the Institutions of Mining and Metallurgy: Section B*, vol. 114, no. 4, pp. 194-198.
- Knopf, A. 1942, *Geology of the Seward Peninsula tin deposits, Alaska*, US Government Printing Office.
- Kolb, J., Rogers, A., Meyer, F.M. & Siemes, H. 2005, "Dominant coaxial deformation of veins during the interseismic stage of the fault-valve cycle: microfabrics of laminated quartz veins of the Hutti gold mine, India", *Journal of Structural Geology*, vol. 27, no. 11, pp. 2043-2057.
- Kranidiotis, P. & MacLean, W. 1987, "Systematics of chlorite alteration at the Phelps Dodge massive sulphide deposit, Matagami, Quebec", *Economic Geology*, vol. 82, no. 7, pp. 1898-1911.
- Kruger, F.J. 2005, "Filling the Bushveld Complex magma chamber: lateral expansion, roof and floor interaction, magmatic unconformities, and the formation of giant chromitite, PGE and Ti-V-magnetitite deposits", *Mineralium Deposita*, vol. 40, no. 5, pp. 451-472.
- Kruger, F. 1994, "The Sr-isotopic stratigraphy of the western Bushveld Complex", *S Afr J Geol*, vol. 97, no. 4, pp. 393-398.
- Large, R.R. & McGoldrick, P.J. 1998, "Litho-geochemical halos and geochemical vectors to stratiform sediment hosted Zn-Pb-Ag deposits, 1. Lady Loretta Deposit, Queensland", *Journal of Geochemical Exploration*, vol. 63, no. 1, pp. 37-56.

- Lee, C. 1996, "A review of mineralization in the Bushveld Complex and some other layered intrusions", *Developments in Petrology*, vol. 15, pp. 103-145.
- Lee, C. & Parry, S. 1988, "Platinum-group element geochemistry of the lower and middle group chromitites of the eastern Bushveld Complex", *Economic Geology*, vol. 83, no. 6, pp. 1127-1139.
- Leitch, C. & Day, S. 1990, "Newgres: a turbo pascal program to solve a modified version of gresens' hydrothermal alteration equation", *Computers & Geosciences*, vol. 16, no. 7, pp. 925-932.
- Leitch, C. & Lentz, D.R. 1994, "The Gresens approach to mass balance constraints of alteration systems: methods, pitfalls, examples", *Alteration and alteration processes associated with ore-forming systems: Geological Association of Canada, Short Course Notes*, vol. 11, pp. 161-192.
- Lomberg, K. 2014, "Best practice sampling methods, assay techniques, and quality control with reference to the platinum group elements (PGEs)", *Journal of the Southern African Institute of Mining and Metallurgy*, vol. 114, no. 1, pp. 53-62.
- López-Moro, F.J. 2012, "EASYGRESGRANT—A Microsoft Excel spreadsheet to quantify volume changes and to perform mass-balance modeling in metasomatic systems", *Computers & Geosciences*, vol. 39, pp. 191-196.
- MacLean, W. 1988, "Rare earth element mobility at constant inter-REE ratios in the alteration zone at the Phelps Dodge massive sulphide deposit, Matagami, Quebec", *Mineralium Deposita*, vol. 23, no. 4, pp. 231-238.
- MacLean, W. & Barrett, T. 1993, "Lithogeochemical techniques using immobile elements", *Journal of Geochemical Exploration*, vol. 48, no. 2, pp. 109-133.
- MacLean, W. & Kranidiotis, P. 1987, "Immobile elements as monitors of mass transfer in hydrothermal alteration; Phelps Dodge massive sulphide deposit, Matagami, Quebec", *Economic Geology*, vol. 82, no. 4, pp. 951-962.
- Maier, W., Barnes, S. & Groves, D. 2012, "The Bushveld Complex, South Africa: formation of platinum–palladium, chrome-and vanadium-rich layers via hydrodynamic sorting of a mobilized cumulate slurry in a large, relatively slowly cooling, subsiding magma chamber", *Mineralium Deposita*, vol. 48, no. 1, pp. 1-56.
- Maier, W., De Klerk, L., Blaine, J., Manyeruke, T., Barnes, S., Stevens, M. & Mavrogenes, J. 2008, "Petrogenesis of contact-style PGE mineralization in the northern lobe of the Bushveld Complex: comparison of data from the farms Rooipoort, Townlands, Drenthe and Nonnenwerth", *Mineralium Deposita*, vol. 43, no. 3, pp. 255-280.
- Manyeruke, T.D., Maier, W.D. & Barnes, S. 2005, "Major and trace element geochemistry of the Platreef on the farm Townlands, northern Bushveld Complex.", *South African Journal of Geology*, vol. 108, no. 3.

- McBirney, A.R. & Nicolas, A. 1997, "The Skaergaard layered series. Part II. Magmatic flow and dynamic layering", *Journal of Petrology*, vol. 38, no. 5, pp. 569-580.
- McBIRNEY, A.R. & NOYES, R.M. 1979, "Crystallization and layering of the Skaergaard intrusion", *Journal of Petrology*, vol. 20, no. 3, pp. 487-554.
- McCandless, T.E., Ruiz, J., Adair, B.I. & Freydier, C. 1999, "Re-Os isotope and Pd/Ru variations in chromitites from the Critical Zone, Bushveld Complex, South Africa", *Geochimica et Cosmochimica Acta*, vol. 63, no. 6, pp. 911-923.
- McCutcheon, S. 2012, *Platinum-group mineral assemblages in the Platreef on Tweefontein, Northern Bushveld complex, South Africa*.
- McDonald, I. & Holwell, D. 2011, "Geology of the northern Bushveld Complex and the setting and genesis of the Platreef Ni–Cu–PGE deposit", *Magmatic Ni–Cu and PGE deposits: geology, geochemistry, and genesis. Rev Econ Geol*, vol. 17, pp. 297-327.
- McDonald, I., Holwell, D. & Wesley, B. 2009, "Assessing the potential involvement of an early magma staging chamber in the generation of the Platreef Ni–Cu–PGE Deposit in the Northern Limb of the Bushveld Complex: a pilot study of the Lower Zone Complex at Zwartfontein", *Applied Earth Science: Transactions of the Institutions of Mining and Metallurgy: Section B*, vol. 118, no. 1, pp. 5-20.
- McDonald, I. & Holwell, D.A. 2007, "Did lower zone magma conduits store PGE-rich sulphides that were later supplied to the Platreef?", *South African Journal of Geology*, vol. 110, no. 4, pp. 611-616.
- McDonald, I., Holwell, D.A. & Armitage, P.E. 2005, "Geochemistry and mineralogy of the Platreef and "Critical Zone" of the northern lobe of the Bushveld Complex, South Africa: implications for Bushveld stratigraphy and the development of PGE mineralisation", *Mineralium Deposita*, vol. 40, no. 5, pp. 526-549.
- McDonough, W. & Sun, S. 1989, "Chemical and isotopic systematics of oceanic basalts: implications for mantle composition and processes", Geological Society, London, Special Publications, vol. 42, no. 1, pp. 313-345.
- McDonough, W.F. & Sun, S. 1995, "The composition of the Earth", *Chemical Geology*, vol. 120, no. 3, pp. 223-253.
- McLaren, C. 1982, "The Platinum-Group Minerals in the UG-2 Layer of the Bushveld Complex at Maandagshoek 254 KT", *Council for Mineral Technology*, , pp. 25.
- McLaren, C.H. 1980, *A mineralogical investigation of the platinum group minerals in the upper chromite layer (UG-2) of the Bushveld Complex*.
- Meinert, L.D. 1982, "Skarn, manto, and breccia pipe formation in sedimentary rocks of the Cananea mining district, Sonora, Mexico", *Economic Geology*, vol. 77, no. 4, pp. 919-949.

- Mitchell, A. 1990, "The stratigraphy, petrography and mineralogy of the Main Zone of the northwestern Bushveld Complex".
- Mitchell, A. & Scoon, R. 2012, "The Platreef of the Bushveld Complex, South Africa: a new hypothesis of multiple, non-sequential magma replenishment based on observations at the Akanani project, north-west of Mokopane", *South African Journal of Geology*, vol. 115, no. 4, pp. 535-550.
- Montero-Serrano, J.C., Palarea-Albaladejo, J., Martín-Fernández, J.A., Martínez-Santana, M. & Gutiérrez-Martín, J.V. 2010, "Sedimentary chemofacies characterization by means of multivariate analysis", *Sedimentary Geology*, vol. 228, no. 3, pp. 218-228.
- Morse, S.A. 1988, "Motion of crystals, solute, and heat in layered intrusions", *The Canadian Mineralogist*, vol. 26, no. 1, pp. 209-224.
- Mukherjee, P. & Gupta, P. 2008, "Arbitrary scaling in ISOCAN method of geochemical mass balance: An evaluation of the graphical approach", *Geochemical Journal*, vol. 42, no. 3, pp. 247.
- Myers, j. & Thorbjornsen, K. 2004, "Identifying metals contamination in soil: a geochemical approach", *Soil & Sediment Contamination*, vol. 13, no. 1, pp. 1-16.
- Naldrett, A., Wilson, A., Kinnaird, J. & Chunnett, G. 2009, "PGE tenor and metal ratios within and below the Merensky Reef, Bushveld Complex: implications for its genesis", *Journal of Petrology*, vol. 50, no. 4, pp. 625-659.
- Naldrett, A., Wilson, A., Kinnaird, J., Yudovskaya, M. & Chunnett, G. 2012, "The origin of chromitites and related PGE mineralization in the Bushveld Complex: new mineralogical and petrological constraints", *Mineralium Deposita*, vol. 47, no. 3, pp. 209-232.
- Nex, P.A. 2005, "The structural setting of mineralisation on Tweefontein Hill, northern limb of the Bushveld Complex, South Africa", *Applied Earth Science: Transactions of the Institutions of Mining and Metallurgy: Section B*, vol. 114, no. 4, pp. 243-251.
- Nichol, S.C. and Kinnaird, J.A. (2008). Platinum-Group Mineral Assemblages in the Platreef at Tweefontein North. 3rd Platreef Workshop, 11th-13th July 2008, Mokopane
- Norrish, K. & Hutton, J.T. 1969, "An accurate X-ray spectrographic method for the analysis of a wide range of geological samples", *Geochimica et Cosmochimica Acta*, vol. 33, no. 4, pp. 431-453.
- Nyama, N., Nex, P. and Yao, Y. (2005). Preliminary petrological studies of the Platreef on Tweefontein Hill, Bushveld Complex, South Africa. 2nd Platreef Workshop, 28th-30th October 2005, Mokopane.
- Ordóñez-Calderón, J., Polat, A., Fryer, B., Gagnon, J., Raith, J. & Appel, P. 2008, "Evidence for HFSE and REE mobility during calc-silicate metasomatism, Mesoarchean (~3075Ma) Ivisartoq greenstone belt, southern West Greenland", *Precambrian Research*, vol. 161, no. 3, pp. 317-340.

- Owens, B.E. 2000, "High-temperature contact metamorphism of calc-silicate xenoliths in the Kiglapait Intrusion, Labrador", *American Mineralogist*, vol. 85, no. 11-12, pp. 1595-1605.
- Pearce, T.J., Besly, B.M., Wray, D.S. & Wright, D.K. 1999, "Chemostratigraphy: a method to improve interwell correlation in barren sequences — A case study using onshore Duckmantian/Stephanian sequences (West Midlands, U.K.)", *Sedimentary Geology*, vol. 124, no. 1-4, pp. 197-220.
- Pearce, C.R., Coe, A.L. & Cohen, A.S. 2010, "Seawater redox variations during the deposition of the Kimmeridge Clay Formation, United Kingdom (Upper Jurassic): Evidence from molybdenum isotopes and trace metal ratios", *Paleoceanography*, vol. 25, no. 4.
- Penniston-Dorland, S.C., Mathez, E.A., Wing, B.A., Farquhar, J. & Kinnaird, J.A. 2012, "Multiple sulphur isotope evidence for surface-derived sulphur in the Bushveld Complex", *Earth and Planetary Science Letters*, vol. 337, pp. 236-242.
- Penniston-Dorland, S.C., Wing, B.A., Nex, P.A., Kinnaird, J.A., Farquhar, J., Brown, M. & Sharman, E.R. 2008, "Multiple sulphur isotopes reveal a magmatic origin for the Platreef platinum group element deposit, Bushveld Complex, South Africa", *Geology*, vol. 36, no. 12, pp. 979-982.
- Polat, A., Appel, P.W., Frei, R., Pan, Y., Dilek, Y., Ordóñez-Calderón, J.C., Fryer, B., Hollis, J.A. & Raith, J.G. 2007, "Field and geochemical characteristics of the Mesoarchean (~ 3075Ma) Ivisartoq greenstone belt, southern West Greenland: Evidence for seafloor hydrothermal alteration in supra-subduction oceanic crust", *Gondwana Research*, vol. 11, no. 1, pp. 69-91.
- Potdevin, J. 1993, "Gresens 92: a simple Macintosh program of the Gresens method", *Computers & Geosciences*, vol. 19, no. 9, pp. 1229-1238.
- Potts, P.J. 1987, *A handbook of silicate rock analysis*, Blackie Glasgow; London.
- Pronost, J., Harris, C. & Pin, C. 2008, "Relationship between footwall composition, crustal contamination, and fluid-rock interaction in the Platreef, Bushveld Complex, South Africa", *Mineralium Deposita*, vol. 43, no. 8, pp. 825-848.
- Ramkumar, M. & Sathish, G. 2006, "Integrated sequence and chemostratigraphic modelling: A sure-fire technique for stratigraphic correlation, petroleum exploration and reservoir characterization", *Mineral Exploration: Recent Strategies*. New India Publishers, , pp. 21-40.
- Ratcliffe, K., Wright, A., Montgomery, P., Palfrey, A., Vonk, A., Vermeulen, J. & Barrett, M. 2010, "Application of chemostratigraphy to the Mungaroo Formation, the Gorgon field, offshore northwest Australia", *APPEA Journal*, , pp. 371-388.
- Reczko, B., Oberholzer, J., Eriksson, P. & Schreiber, U. 1995, "A re-evaluation of the volcanism of the Palaeoproterozoic Pretoria Group (Kaapvaal craton) and a hypothesis on basin development", *Journal of African Earth Sciences*, vol. 21, no. 4, pp. 505-519.

- Reimann, C., Templ, M., & Filzmoser, P. 2008, "Cluster analysis applied to regional geochemical data: problems and possibilities", *Applied Geochemistry*, vol. 23, no. 8, pp. 2198-2213.
- Reisberg, L., Tredoux, M., Harris, C., Coftier, A. & Chaumba, J. 2011, "Re and Os distribution and Os isotope composition of the Platreef at the Sandsloot–Mogolakwena mine, Bushveld complex, South Africa", *Chemical Geology*, vol. 281, no. 3, pp. 352-363.
- Richards, H., Cann, J. & Jensenius, J. 1989, "Mineralogical zonation and metasomatism of the alteration pipes of Cyprus sulphide deposits", *Economic Geology*, vol. 84, no. 1, pp. 91-115.
- Rock, N.M. 1988, "Numerical geology: a source guide, glossary and selective bibliography to geological uses of computers and statistics", *Lecture Notes in Earth Sciences, Berlin Springer Verlag*, vol. 18.
- Rollinson, H. "1993, Using Geochemical Data: Evaluation, Presentation", *Interpretation: Longman Scientific & Technical, London*, , pp. 108-111.
- Sabine, P.A., 1975. "Metamorphic processes at high temperature and low pressure: the petrogenesis of the metasomatized and assimilated rocks of Carneal, Antrim." *Philosophical Transactions of the Royal Society of London* 280, 225–269.
- Schouwstra, R., Kinloch, E. & Lee, C. 2002, "A short review of the Bushveld Complex: Platinum Minerals Review, v. 44".
- Scoates, J.S. & Friedman, R.M. 2008, "Precise age of the platiniferous Merensky Reef, Bushveld Complex, South Africa, by the U-Pb zircon chemical abrasion ID-TIMS technique", *Economic Geology*, vol. 103, no. 3, pp. 465-471.
- Scoates, J.S., Wall, C.J., Friedman, R.M. & Chamberlain, K.R. 2011, "Revisiting the age of the Merensky Reef, Bushveld Complex", Abstract, Goldschmidt Conference 2011.
- Selverstone, J., Morteani, G. & STAUDE, J. 1991, "Fluid channelling during ductile shearing: transformation of granodiorite into aluminous schist in the Tauern Window, Eastern Alps", *Journal of Metamorphic Geology*, vol. 9, no. 4, pp. 419-431.
- Shand, S. 1930, "Limestone and the origin of felspathoidal rocks: an aftermath of the Geological Congress", *Geological Magazine*, vol. 67, no. 09, pp. 415-427.
- Sharpe, M.R., Bahat, D. & Von Gruenewaldt, G. 1980. *The concentric elliptical structure of feeder sites to the Bushveld Complex and possible economic implications*, Institute for Geological Research on the Bushveld Complex, University of Pretoria.
- Shirley, D. & McBirney, A. 1991, "Numerical modelling of crystallization of the Skaergaard intrusion", *Eos Trans AGU*, vol. 72, pp. 316.

- Sonnenthal, E.L. & McBirney, A.R. 1998, "The Skaergaard Layered Series. Part IV. Reaction–Transport Simulations of Foundered Blocks", *Journal of Petrology*, vol. 39, no. 4, pp. 633-661.
- Stevens, F.J. 2007, *Geology and Mineralisation of the Sheba's Ridge area, Eastern Bushveld Complex, South Africa*.
- Taylor, S.R. & McLennan, S.M. 1985, "The continental crust: its composition and evolution".
- Tilley, C. 1952, "Some trends of basaltic magma in limestone syntexis", *Am.J.Sci*, vol. 250, pp. 529-545.
- Urqueta, E., Kyser, T.K., Clark, A.H., Stanley, C.R. & Oates, C.J. 2009, "Lithogeochemistry of the Collahuasi porphyry Cu–Mo and epithermal Cu–Ag (–Au) cluster, northern Chile: Pearce element ratio vectors to ore", *Geochemistry: Exploration, Environment, Analysis*, vol. 9, no. 1, pp. 9-17.
- Utami, P., Browne, P.R.L., Simmons, S.F., Suroto. 2006, "Mass transfer during hydrothermal alteration at the Lahendong geothermal system, North Sulawesi", *Proceedings 28th, New Zealand, geothermal workshop*.
- van der Merwe, F., Viljoen, F. & Knoper, M. 2012, "The mineralogy and mineral associations of platinum group elements and gold in the Platreef at Zwartfontein, Akanani Project, Northern Bushveld Complex, South Africa", *Mineralogy and Petrology*, vol. 106, no. 1-2, pp. 25-38.
- van der Merwe, Mauritz J 2008, "The geology and structure of the Rustenburg Layered Suite in the Potgietersrus/Mokopane area of the Bushveld Complex, South Africa", *Mineralium Deposita*, vol. 43, no. 4, pp. 405-419.
- Van der Merwe, M. 1976, "The layered sequence of the Potgietersrus limb of the Bushveld Complex", *Economic Geology*, vol. 71, no. 7, pp. 1337-1351.
- Vermaak, C. 1976, "The Merensky Reef; thoughts on its environment and genesis", *Economic Geology*, vol. 71, no. 7, pp. 1270-1298.
- Vermaak, C. & Von Gruenewaldt, G. 1986, "Introduction to the Bushveld complex", *Mineral deposits of Southern Africa. Geol Soc S Afr, Johannesburg*, , pp. 1021-1029.
- Viljoen, M. & Schürmann, L. 1998, "Platinum-group metals", *The mineral resources of South Africa. Council for Geoscience, Pretoria*, , pp. 532-568.
- Wagner, P.A. 1929, *The platinum deposits and mines of South Africa*, Oliver and Boyd, Edinburgh, pp. 326.
- Walraven, F., Armstrong, R. & Kruger, F. 1990, "A chronostratigraphic framework for the north-central Kaapvaal craton, the Bushveld Complex and the Vredefort structure", *Tectonophysics*, vol. 171, no. 1, pp. 23-48.

- Webb, S.J., Cawthorn, R.G., Nguuri, T. & James, D. 2004, "Gravity modeling of Bushveld Complex connectivity supported by Southern African seismic experiment results", *South African Journal of Geology*, vol. 107, no. 1-2, pp. 207-218.
- Wenzel, T., Baumgartner, L.P., Brüggmann, G.E., Konnikov, e.g. & Kislov, E.V. 2002, "Partial melting and assimilation of dolomitic xenoliths by mafic magma: the Ioko-Dovyren intrusion (North Baikal Region, Russia)", *Journal of Petrology*, vol. 43, no. 11, pp. 2049-2074.
- White, J. 1994, "The Potgietersrus Prospect, geology and exploration history", *Proceedings XVth CMMI Congress*, pp. 173.
- Whitford, D.J. & Ashley, P. 1992, "The Scuddles volcanic-hosted massive sulphide deposit, Western Australia; geochemistry of the host rocks and evaluation of litho-geochemistry for exploration", *Economic Geology*, vol. 87, no. 3, pp. 873-888.
- Wilson, A. & Chunnett, G. 2006, "Trace element and platinum group element distributions and the genesis of the Merensky Reef, Western Bushveld Complex, South Africa", *Journal of Petrology*, vol. 47, no. 12, pp. 2369-2403.
- Wood, S.A., Mountain, B.W. & Fenlon, B.J. 1989, "Thermodynamic constraints on the solubility of platinum and palladium in hydrothermal solutions; reassessment of hydroxide, bisulphide, and ammonia complexing", *Economic Geology*, vol. 84, no. 7, pp. 2020-2028.
- Yaxley, G.M., Green, D.H. & Kamenetsky, V. 1998, "Carbonatite metasomatism in the southeastern Australian lithosphere", *Journal of Petrology*, vol. 39, no. 11-12, pp. 1917-1930.
- Yudovskaya, M.A. & Kinnaird, J.A. 2010, "Chromite in the Platreef (Bushveld Complex, South Africa): occurrence and evolution of its chemical composition", *Mineralium Deposita*, vol. 45, no. 4, pp. 369-391.
- Yudovskaya, M., Kinnaird, J., Naldrett, A.J., Rodionov, N., Antonov, A., Simakin, S. & Kuzmin, D. 2013, "Trace-element study and age dating of zircon from chromitites of the Bushveld Complex (South Africa)", *Mineralogy and Petrology*, vol. 107, no. 6, pp. 915-942.

APPENDIX I

WHOLE ROCK GEOCHEMISTRY DATA

Table 1: Whole rock data of Borehole TN754

LITHOLOGY	GN	P1	P1	P1	P1	P2	P2	FP2
SAMPLES ID	TN754-1	TN754-2	TN754-3	TN754-6	TN754-8	TN754-33	TN754-9	TN754-5
SiO ₂	65.85	42.95	46.19	43.62	31.71	58.72	38.03	43.10
Al ₂ O ₃	0.01	6.63	8.90	3.15	2.18	0.70	1.27	6.00
Fe ₂ O ₃	26.85	23.00	13.57	18.62	28.80	28.72	17.67	23.87
MnO	0.22	0.46	0.18	0.20	0.22	0.33	0.13	0.27
MgO	4.46	8.08	19.30	20.69	26.84	5.53	32.87	18.89
CaO	1.51	14.41	5.93	4.39	1.21	3.45	0.56	2.92
Na ₂ O	0.12	0.38	2.04	0.37	0.59	0.29	0.11	0.97
K ₂ O	0.00	1.25	0.23	0.15	0.08	0.28	0.53	0.27
P ₂ O ₅	0.02	0.01	0.03	0.03	0.02	0.02	0.02	0.02
TiO ₂	0.05	0.32	0.15	0.26	0.14	0.08	0.07	0.32
SO ₃	0.21	1.12	1.00	0.50	3.31	0.28	0.11	1.19
LOI	0.70	1.39	2.48	8.05	4.90	1.59	8.71	2.18
As	0.50	8.98	0.50	29.90	17.65	18.18	3.35	13.36
Ba	43.04	156.97	92.01	98.95	77.47	52.69	75.06	77.97
Ce	525.42	124.53	126.43	189.24	278.67	271.66	204.52	244.11
Co	0.25	0.07	178.15	215.87	274.44	10.13	135.61	236.46
Cu	62.61	18.90	3384.14	513.29	1251.92	111.89	154.94	1081.32
Mo	9.24	8.48	2.40	0.66	2.65	11.05	1.61	4.06
Nb	17.07	44.16	11.55	12.14	16.92	19.39	10.44	11.99
Ni	176.17	16.30	2451.53	2031.65	5924.50	524.91	1705.55	2650.90
Pb	0.50	9.74	14.77	1.60	2.22	0.50	19.69	5.01
Rb	0.55	49.72	14.01	21.38	8.57	6.11	165.99	21.87
Sr	10.01	12.33	75.55	14.26	26.42	1.67	4.52	32.92
Th	0.25	0.25	0.25	0.25	0.53	0.25	0.53	0.25
U	1.00	1.00	1.00	1.00	0.63	1.00	2.59	0.42
V	19.49	0.45	48.20	79.81	37.87	31.56	24.62	141.39
Y	2.78	92.61	1.11	9.74	0.63	0.50	0.54	1.99
Zn	30.20	28.38	92.25	141.12	90.91	44.40	98.81	120.93
Zr	0.13	270.07	2.72	13.86	15.49	0.83	8.08	17.38

Table 1: Whole rock data of Borehole TN754

LITHOLOGY	H1	H1	H1	H1	H1	H1	H2	H2
SAMPLES ID	TN754-17	TN754-22	TN754-24	TN754-32	TN754-35	TN754-42	TN754-19	TN754-21
SiO ₂	43.23	43.23	46.83	49.27	48.01	36.68	42.95	45.85
Al ₂ O ₃	2.55	1.00	3.69	8.63	4.83	2.84	2.43	2.34
Fe ₂ O ₃	24.46	23.07	26.43	13.68	16.68	19.65	23.90	15.11
MnO	0.48	0.35	0.44	0.22	0.19	0.22	0.47	0.32
MgO	9.01	10.28	5.47	20.97	20.79	29.69	8.73	9.47
CaO	17.02	18.24	15.22	5.53	3.72	4.85	16.70	21.53
Na ₂ O	0.43	0.53	0.43	0.77	1.72	0.90	0.42	0.69
K ₂ O	0.40	0.06	0.10	0.13	0.33	0.20	0.40	0.65
P ₂ O ₅	0.01	0.04	0.11	0.02	0.06	0.02	0.01	0.02
TiO ₂	0.24	0.20	0.23	0.17	0.34	0.09	0.24	0.31
SO ₃	0.79	1.41	0.05	0.51	1.23	0.78	0.78	0.44
LOI	1.39	1.59	1.00	0.10	2.11	4.11	2.97	3.40
As	21.92	29.82	28.94	0.50	7.29	1.84	24.60	28.53
Ba	106.00	91.51	50.84	78.92	148.23	178.43	98.89	75.65
Ce	190.15	195.28	312.28	154.68	227.54	224.84	275.81	146.23
Co	21.02	30.03	4.95	144.89	270.88	247.52	2.73	24.64
Cu	112.32	68.26	29.39	246.25	2384.56	1577.33	62.50	69.21
Mo	2.54	5.04	1.83	4.52	5.43	3.91	2.67	4.60
Nb	11.26	17.85	15.73	8.75	9.28	10.17	13.24	14.94
Ni	213.49	225.90	25.05	1187.31	9402.40	3375.89	56.99	105.75
Pb	13.58	2.78	2.51	8.14	4.02	37.51	0.50	5.84
Rb	58.80	11.03	9.29	7.91	22.08	14.34	8.77	10.70
Sr	134.01	63.09	31.52	60.74	48.62	55.60	12.51	49.32
Th	0.25	0.25	0.53	0.25	0.53	0.50	0.25	0.25
U	1.00	1.00	0.63	1.00	0.63	0.50	1.00	0.42
V	92.66	128.22	44.67	56.00	113.01	36.49	88.53	109.73
Y	0.62	1.81	7.41	1.77	10.22	2.59	1.51	2.09
Zn	53.11	43.30	42.60	87.54	95.17	150.28	42.93	43.76
Zr	0.02	39.71	21.45	7.57	43.58	1.02	3.72	21.80

Table 1: Whole rock data of Borehole TN754

LITHOLOGY	H2	H2	H2	H2	H2	H2	H2	H3
SAMPLES ID	TN754-26	TN754-27	TN754-29	TN754-31	TN754-36	TN754-37	TN754-41	TN754-40
SiO ₂	50.08	46.97	47.38	48.24	52.07	49.98	36.87	48.98
Al ₂ O ₃	9.89	6.20	7.10	10.97	6.69	6.37	0.81	8.87
Fe ₂ O ₃	13.17	15.42	14.26	14.42	12.11	14.56	14.00	13.69
MnO	0.19	0.20	0.19	0.19	0.18	0.25	0.09	0.21
MgO	18.75	21.61	20.77	16.65	21.66	18.10	37.39	17.63
CaO	6.13	5.11	6.02	6.33	4.51	6.15	0.93	7.30
Na ₂ O	0.97	1.12	1.06	1.08	0.88	1.77	0.54	1.06
K ₂ O	0.08	0.11	0.12	0.21	0.44	0.42	0.03	0.50
P ₂ O ₅	0.01	0.02	0.02	0.02	0.03	0.08	0.01	0.03
TiO ₂	0.17	0.20	0.18	0.17	0.24	0.59	0.06	0.21
SO ₃	0.01	1.18	1.01	0.93	0.08	0.53	0.51	0.31
LOI	0.55	1.89	1.89	0.79	1.10	1.20	8.75	1.20
As	2.48	0.50	0.50	3.34	0.35	7.36	0.50	8.07
Ba	78.41	69.35	65.06	92.80	107.56	122.37	67.22	120.10
Ce	133.29	148.75	87.61	119.58	110.93	186.42	113.93	106.33
Co	89.13	214.55	198.52	160.60	93.01	129.27	207.81	99.74
Cu	27.03	1276.18	1076.18	390.60	188.87	1119.22	1164.40	328.98
Mo	3.66	4.28	3.69	4.02	1.57	5.81	0.26	7.41
Nb	16.25	9.18	7.88	13.55	13.39	14.69	14.54	10.10
Ni	583.62	3586.75	3119.91	1809.35	833.47	2389.35	3117.56	865.06
Pb	1.65	5.87	6.23	10.73	0.09	4.94	13.36	13.91
Rb	2.82	8.55	8.73	11.02	25.35	19.45	7.53	35.62
Sr	99.47	39.45	48.23	94.17	53.34	47.65	10.31	107.54
Th	0.50	0.25	0.25	0.25	0.53	0.53	0.50	0.53
U	0.50	1.00	1.00	1.00	0.63	0.63	1.90	0.63
V	112.51	72.35	66.49	61.56	114.35	122.70	24.01	110.34
Y	5.66	2.58	4.36	2.66	0.54	10.07	1.97	5.46
Zn	131.80	86.34	82.70	83.76	82.29	85.29	109.00	87.41
Zr	7.22	13.19	8.70	7.50	32.09	55.07	3.14	22.45

Table 2: Whole rock data of Borehole SS339

LITHOLOGY	GN	GN	GN	P1	P2	P2	FP1	FP1
SAMPLES ID	SS339-2	SS339-1	SS339-3	SS339-4	SS339-7	SS339-18	SS339-8	SS339-9
SiO ₂	56.72	61.61	51.24	52.82	45.09	49.18	47.12	49.36
Al ₂ O ₃	6.65	2.25	0.37	17.76	13.23	13.66	11.82	15.51
Fe ₂ O ₃	18.84	24.31	36.20	8.38	12.24	8.28	11.12	10.64
MnO	0.33	0.20	0.40	0.11	0.15	0.13	0.17	0.17
MgO	2.31	1.89	3.03	4.77	8.80	12.25	12.59	13.24
CaO	12.70	9.15	7.46	11.03	13.46	11.70	12.05	8.18
Na ₂ O	0.62	0.25	0.24	2.30	2.96	1.77	1.70	1.37
K ₂ O	0.86	0.01	0.14	0.96	0.21	0.39	0.27	0.36
P ₂ O ₅	0.32	0.02	0.07	0.10	0.05	0.02	0.02	0.03
TiO ₂	0.25	0.12	0.07	0.35	0.31	0.15	0.22	0.18
SO ₃	0.01	0.01	0.57	0.02	1.03	0.47	0.24	0.36
LOI	0.40	0.20	0.20	1.40	2.47	1.99	2.68	0.60
As	3.35	12.04	34.39	11.41	6.80	0.50	16.38	0.50
Ba	193.95	47.87	73.37	252.20	190.38	107.97	135.31	111.20
Ce	211.68	243.93	428.99	87.22	101.36	24.99	66.46	58.27
Co	20.58	4.95	4.95	34.24	136.45	91.96	73.39	104.94
Cu	17.41	28.34	74.58	45.53	2220.16	898.01	512.48	201.00
Mo	6.93	8.13	7.01	4.00	1.19	1.41	2.66	3.14
Nb	12.30	18.39	6.06	17.38	11.96	15.04	13.77	14.25
Ni	38.40	25.80	63.46	93.54	3922.98	1708.85	1283.04	916.74
Pb	11.73	3.87	0.64	6.64	26.86	11.49	8.58	11.58
Rb	72.20	2.52	9.76	39.07	5.07	32.03	13.60	17.02
Sr	92.44	70.18	6.49	266.71	266.27	146.62	258.26	147.02
Th	16.94	4.53	0.53	73.43	54.84	23.41	69.99	17.77
U	-0.01	0.63	0.63	0.63	0.50	1.29	0.50	1.00
V	55.86	22.18	22.23	100.37	121.88	65.13	110.72	47.59
Y	9.34	6.88	1.84	9.43	12.43	1.86	6.47	0.50
Zn	68.90	55.52	48.49	65.88	70.28	63.47	90.59	73.21
Zr	12.72	5.67	9.31	54.83	13.87	34.38	11.53	21.97

Table 2: Whole rock data of Borehole SS339

LITHOLOGY	FP1	FP1	FP1	FP1	FP1	FP1	FP2	FP2
SAMPLES ID	SS339-11	SS339-12	SS339-14	SS339-16	SS339-5	SS339-6	SS339-13	SS339-15
SiO ₂	47.18	47.67	48.02	44.40	52.90	54.18	47.46	45.32
Al ₂ O ₃	14.71	15.74	17.91	15.43	0.01	0.01	18.39	17.06
Fe ₂ O ₃	12.59	10.45	9.49	16.19	39.09	36.85	10.62	12.84
MnO	0.16	0.13	0.15	0.21	0.14	0.05	0.14	0.18
MgO	12.69	10.70	9.99	10.96	2.93	3.10	8.90	10.26
CaO	8.51	9.49	9.88	7.75	4.07	2.85	10.43	8.62
Na ₂ O	1.65	2.24	1.92	0.97	0.17	0.14	1.94	1.20
K ₂ O	0.20	0.62	0.37	1.12	0.00	0.00	0.24	1.92
P ₂ O ₅	0.03	0.04	0.01	0.02	0.05	0.12	0.02	0.02
TiO ₂	0.16	0.19	0.09	0.13	0.08	0.01	0.16	0.18
SO ₃	0.93	0.74	0.36	1.04	0.18	0.12	0.69	0.25
LOI	1.19	1.99	1.80	1.80	0.40	2.60	1.00	2.20
As	0.50	0.50	6.86	7.09	43.75	6.86	0.02	21.70
Ba	94.20	163.05	97.61	198.66	97.59	44.08	101.89	209.76
Ce	127.93	129.47	39.69	148.39	764.86	523.68	63.73	104.64
Co	129.30	137.06	92.03	130.35	30.21	2.93	104.98	95.81
Cu	704.50	1111.03	400.64	392.82	185.42	105.87	526.65	361.43
Mo	4.81	3.41	4.76	4.21	2.14	13.30	2.91	1.63
Nb	13.72	16.99	15.44	7.05	18.94	13.80	14.42	15.39
Ni	2027.30	1642.77	1145.14	707.07	925.26	483.75	1563.39	968.19
Pb	4.94	6.14	7.00	11.43	1.87	0.32	13.29	7.06
Rb	7.43	27.52	17.09	40.98	3.75	1.32	9.48	69.30
Sr	146.69	195.18	303.03	157.89	5.76	4.19	232.85	320.45
Th	8.05	45.35	92.56	6.87	0.25	0.25	51.39	107.01
U	1.00	1.00	1.00	1.00	0.84	1.48	1.00	1.00
V	48.99	40.28	21.14	45.68	291.01	29.94	46.48	50.56
Y	5.24	3.44	0.50	0.26	3.24	2.01	3.55	0.50
Zn	75.81	62.43	59.76	76.31	60.09	41.05	59.41	71.05
Zr	14.83	21.44	2.64	2.28	35.35	9.60	17.24	7.24

Table 2: Whole rock data of Borehole SS339

LITHOLOGY	CS1	CS1	CS1	CS1	CS1	CS2	CS2	CS2
SAMPLES ID	SS339-25	SS339-26	SS339-36	SS339-37	SS339-38	SS339-22	SS339-24	SS339-28
SiO ₂	53.45	24.87	58.34	50.08	67.70	47.93	49.76	32.70
Al ₂ O ₃	19.88	0.83	5.71	9.73	3.32	18.66	22.99	10.32
Fe ₂ O ₃	6.47	55.41	28.40	23.38	13.78	5.70	3.69	26.02
MnO	0.09	0.28	0.14	0.26	0.21	0.10	0.05	1.74
MgO	4.39	6.26	4.57	5.20	2.52	8.63	2.74	5.94
CaO	10.86	8.95	1.87	8.65	10.81	12.69	14.60	10.51
Na ₂ O	2.87	0.38	0.22	1.03	0.50	2.29	2.62	1.55
K ₂ O	0.79	0.02	0.20	0.37	0.40	0.75	1.02	0.93
P ₂ O ₅	0.02	0.02	0.01	0.10	0.10	0.02	0.01	0.03
TiO ₂	0.48	1.48	0.33	0.54	0.17	0.16	0.07	0.18
SO ₃	0.01	0.31	0.01	0.25	0.28	0.01	0.26	5.07
LOI	0.70	1.20	0.20	0.40	0.20	3.04	2.20	5.00
As	3.32	25.76	11.87	9.10	7.65	18.30	0.50	18.39
Ba	246.66	70.68	73.25	150.18	136.31	174.25	197.71	262.82
Ce	19.52	265.39	355.56	301.56	114.28	32.63	5.00	361.03
Co	27.40	1.66	21.04	26.21	4.95	25.95	33.43	319.92
Cu	55.18	137.29	25.05	142.40	92.85	34.54	624.18	2330.64
Mo	5.00	4.88	7.81	5.84	11.05	0.65	2.08	7.22
Nb	21.03	15.74	14.72	22.32	9.79	15.09	14.05	13.99
Ni	140.14	184.51	150.63	110.03	67.98	116.88	1531.71	8805.97
Pb	6.38	4.74	2.96	3.81	6.86	8.10	8.32	11.92
Rb	25.53	6.46	17.84	30.93	31.31	33.55	37.40	76.26
Sr	290.36	17.28	38.30	143.46	51.35	354.48	334.04	99.56
Th	76.43	0.25	0.53	34.23	0.53	118.84	112.25	15.73
U	1.00	1.00	0.63	6.47	0.63	0.61	0.50	0.59
V	91.08	46.04	89.61	112.82	42.06	70.22	40.89	46.00
Y	9.51	6.90	3.28	43.69	11.64	7.46	4.54	3.18
Zn	54.40	37.67	97.47	119.73	51.09	64.59	44.71	61.46
Zr	62.82	25.32	34.21	73.62	35.54	11.01	4.77	21.68

Table 2: Whole rock data of Borehole SS339

LITHOLOGY	CS2	CS2	CS2	CS2	CS2	CS3	CS3	CS3
SAMPLES ID	SS339-29	SS339-32	SS339-33	SS339-34	SS339-27	SS339-21	SS339-23	SS339-31
SiO ₂	41.39	35.85	37.08	48.50	51.77	48.41	50.61	42.70
Al ₂ O ₃	12.97	8.07	0.20	7.78	10.09	13.61	14.13	5.04
Fe ₂ O ₃	29.45	39.13	51.32	29.57	15.89	9.65	8.67	40.72
MnO	0.20	0.24	0.27	0.29	0.50	0.14	0.12	0.27
MgO	7.21	6.29	1.14	6.52	2.86	9.23	11.69	6.19
CaO	5.62	7.01	8.93	3.28	15.17	13.86	11.16	2.23
Na ₂ O	0.89	0.21	0.31	0.83	1.02	2.02	1.32	0.97
K ₂ O	0.10	0.01	0.03	0.69	0.98	0.56	0.34	0.20
P ₂ O ₅	0.02	0.04	0.22	0.05	0.11	0.04	0.02	0.04
TiO ₂	0.45	0.44	0.02	0.20	0.38	0.27	0.21	0.30
SO ₃	0.70	0.11	0.29	1.40	0.02	0.60	0.01	1.15
LOI	1.00	2.62	0.20	0.89	1.20	1.61	1.70	0.20
As	14.21	59.38	40.59	20.75	11.63	9.70	14.99	27.19
Ba	63.48	76.81	37.09	93.34	178.38	134.03	143.90	61.03
Ce	322.01	447.69	659.55	318.91	223.96	75.22	60.47	413.66
Co	46.49	12.27	4.95	115.81	29.80	107.54	49.17	82.35
Cu	500.57	37.13	256.52	1431.81	25.96	791.61	37.06	1959.85
Mo	4.82	8.60	3.87	0.38	3.63	6.21	1.14	6.67
Nb	17.73	20.41	16.25	20.58	17.53	16.21	14.53	16.97
Ni	206.14	89.93	371.45	3534.69	61.75	2644.88	217.13	3273.57
Pb	0.49	2.72	2.96	10.46	10.08	6.06	6.10	11.50
Rb	13.50	7.72	3.45	77.91	77.41	31.96	16.96	25.99
Sr	114.44	49.02	6.65	62.21	107.12	176.52	246.10	56.81
Th	20.83	0.53	0.53	11.77	22.76	30.79	65.73	0.53
U	0.63	0.63	0.63	0.63	0.63	0.63	0.50	0.63
V	118.67	101.58	15.70	86.03	38.33	111.10	65.85	88.46
Y	12.96	4.03	3.63	0.54	23.17	2.42	1.73	8.62
Zn	141.28	63.26	52.68	117.86	67.81	56.77	67.82	129.24
Zr	29.84	9.35	1.93	11.61	31.48	34.92	16.39	20.62

Table 2: Whole rock data of Borehole SS339

LITHOLOGY	CS3	CS3
SAMPLES ID	SS339-30	SS339-35
SiO ₂	36.08	51.73
Al ₂ O ₃	9.63	9.45
Fe ₂ O ₃	32.01	25.89
MnO	0.25	0.33
MgO	9.23	4.30
CaO	4.89	5.69
Na ₂ O	1.06	0.57
K ₂ O	0.01	0.46
P ₂ O ₅	0.15	0.06
TiO ₂	0.70	0.24
SO ₃	1.26	0.29
LOI	4.71	1.00
As	58.60	8.77
Ba	83.93	70.96
Ce	352.48	253.04
Co	44.63	37.10
Cu	353.59	600.91
Mo	1.83	4.28
Nb	21.59	17.99
Ni	153.28	745.40
Pb	4.73	8.26
Rb	5.30	48.45
Sr	78.59	102.72
Th	8.44	28.20
U	0.63	0.63
V	175.34	74.78
Y	14.26	2.13
Zn	138.22	86.15
Zr	20.79	5.66

Table 3: Whole rock data of Borehole TN200

LITHOLOGY	GN	P1	P1	P1	P1	P1	P2	P2
SAMPLES ID	TN200-1	TN200-2	TN200-3	TN200-7	TN200-8	TN200-9	TN200-16	TN200-24
SiO ₂	0.01	28.38	36.44	42.02	48.89	49.10	20.99	31.28
Al ₂ O ₃	0.01	8.43	6.35	3.16	5.43	6.80	0.01	2.97
Fe ₂ O ₃	3.71	8.19	14.27	11.47	13.73	13.61	0.01	0.68
MnO	0.79	1.17	0.20	0.18	0.21	0.21	2.10	1.51
MgO	23.04	30.31	8.67	27.86	23.70	23.63	42.03	25.47
CaO	39.35	12.24	27.94	9.65	4.84	4.39	18.66	31.69
Na ₂ O	0.72	0.52	1.98	0.42	0.79	0.79	0.34	0.57
K ₂ O	0.01	0.01	0.01	0.14	0.11	0.12	0.01	0.01
P ₂ O ₅	0.01	0.01	0.02	0.02	0.02	0.02	0.01	0.02
TiO ₂	0.01	0.18	0.26	0.18	0.17	0.16	0.03	0.21
SO ₃	0.23	0.92	1.70	0.25	0.49	0.58	0.09	0.02
LOI	32.00	9.63	2.20	4.66	1.60	0.60	16.00	5.56
As	102.93	0.50	24.95	0.50	0.27	0.50	0.50	0.50
Ba	53.93	47.66	53.78	99.93	77.24	74.66	39.94	49.84
Ce	250.09	103.77	141.11	96.58	96.56	111.30	40.05	47.82
Co	7.80	78.49	255.59	130.37	172.81	147.94	1.04	9.45
Cu	38.54	659.21	2990.40	369.63	909.96	684.71	66.89	24.75
Mo	0.80	0.80	10.99	4.62	2.01	6.76	0.40	0.80
Nb	13.64	12.14	15.03	16.29	11.30	15.53	11.79	15.21
Ni	27.65	946.26	5337.36	1335.52	2087.14	1675.18	54.55	80.89
Pb	9.39	5.47	19.84	18.32	7.04	1.73	2.00	3.00
Rb	1.00	1.30	1.58	12.54	9.39	6.52	3.17	2.02
Sr	48.82	1.00	6.62	28.86	31.76	41.08	7.54	1.00
Th	45.41	0.50	0.50	0.25	0.25	0.25	0.50	0.50
U	0.50	0.50	0.50	1.00	1.00	1.00	0.50	0.50
V	13.00	44.83	164.09	70.51	80.96	64.59	13.00	11.56
Y	168.36	10.35	8.93	6.26	0.50	3.81	2.68	1.39
Zn	37.64	72.19	77.50	86.47	93.88	84.70	37.63	26.74
Zr	36.13	5.74	13.90	16.50	11.86	9.84	3.17	25.46

Table 3: Whole rock data of Borehole TN200

LITHOLOGY	FP1	FP1	FP1	FP2	FP2	FP2	FP2	FP2
SAMPLES ID	TN200-20	TN200-4	TN200-5	TN200-10	TN200-11	TN200-12	TN200-13	TN200-14
SiO ₂	33.74	38.53	47.76	11.02	9.64	1.65	0.35	28.16
Al ₂ O ₃	0.15	3.57	2.42	0.01	0.11	0.76	0.01	6.23
Fe ₂ O ₃	0.01	13.62	15.24	2.06	0.01	0.18	0.01	10.26
MnO	1.93	0.29	0.19	0.31	0.96	1.29	0.39	0.38
MgO	27.02	20.80	28.23	15.82	20.67	20.11	3.72	37.80
CaO	25.99	16.35	2.39	39.92	38.59	41.44	54.93	13.63
Na ₂ O	0.48	1.10	0.95	0.73	0.70	0.77	1.01	0.62
K ₂ O	0.01	0.01	0.01	0.01	0.01	0.01	0.01	0.01
P ₂ O ₅	0.01	0.02	0.02	0.01	0.01	0.01	0.01	0.04
TiO ₂	0.06	0.22	0.14	0.04	0.08	0.20	0.03	0.18
SO ₃	0.04	1.19	1.04	0.01	0.10	0.17	0.02	0.65
LOI	11.00	4.29	1.60	30.30	29.00	33.44	40.00	2.09
As	0.50	12.75	0.50	105.96	100.75	105.34	169.00	0.50
Ba	51.09	75.94	62.22	50.76	64.84	88.97	42.04	45.22
Ce	39.17	121.01	158.09	230.61	158.02	197.57	202.71	72.79
Co	2.89	164.77	201.94	13.38	9.72	16.15	6.91	56.54
Cu	23.02	1523.08	1760.56	36.16	43.99	60.73	50.14	785.62
Mo	2.59	2.41	5.23	0.80	0.80	0.80	0.80	0.04
Nb	12.52	7.12	9.52	19.88	8.78	6.35	1.77	12.97
Ni	45.01	2977.63	6324.83	12.25	24.76	53.52	12.56	1275.71
Pb	0.65	2.00	0.55	1.33	0.40	3.74	7.08	8.01
Rb	1.80	3.56	3.96	1.07	0.84	2.97	2.68	0.61
Sr	2.56	25.46	15.11	25.35	13.66	19.67	87.94	8.48
Th	0.50	0.50	0.50	0.50	0.50	0.50	0.50	0.50
U	0.50	0.50	0.50	0.50	0.50	0.23	22.54	0.50
V	18.51	82.35	83.83	13.00	1.43	23.02	13.00	48.98
Y	1.64	5.89	1.51	7.18	8.55	3.23	0.19	9.88
Zn	27.46	53.13	107.93	24.48	32.04	39.86	20.65	78.02
Zr	9.17	22.59	1.35	12.87	31.62	41.10	28.79	17.49

Table 3: Whole rock data of Borehole TN200

LITHOLOGY	FP2	FP2	FP2	H1	H2	H2	H2	H2
SAMPLES ID	TN200-18	TN200-22	TN200-6	TN200-36	TN200-37	TN200-38	TN200-39	TN200-40
SiO ₂	27.76	17.15	50.42	48.08	48.88	48.53	45.87	47.73
Al ₂ O ₃	6.14	3.63	3.72	2.96	4.52	5.49	2.93	4.60
Fe ₂ O ₃	7.29	1.88	15.15	15.09	14.86	14.60	16.80	14.51
MnO	1.11	0.85	0.21	0.20	0.20	0.21	0.22	0.20
MgO	32.40	38.93	24.58	25.66	24.46	24.33	26.14	25.04
CaO	14.27	15.42	3.85	3.24	4.12	4.39	3.51	4.40
Na ₂ O	0.44	0.29	1.00	1.46	1.16	0.58	0.75	1.13
K ₂ O	0.01	0.01	0.05	0.17	0.09	0.03	0.01	0.02
P ₂ O ₅	0.01	0.01	0.03	0.02	0.02	0.02	0.02	0.02
TiO ₂	0.26	0.16	0.18	0.21	0.16	0.14	0.16	0.15
SO ₃	0.38	0.11	0.41	0.82	0.62	0.11	0.71	0.43
LOI	9.97	21.60	0.40	2.10	0.90	1.49	2.78	1.78
As	0.50	1.56	11.16	0.50	0.50	2.20	1.16	0.50
Ba	42.62	56.60	55.82	78.92	80.04	57.36	63.45	67.53
Ce	94.61	83.44	146.45	127.87	138.22	103.83	128.21	106.41
Co	43.86	30.23	154.88	186.37	156.78	104.03	186.91	160.41
Cu	406.36	73.26	1315.30	2506.22	1550.45	464.13	1218.97	1639.06
Mo	1.77	0.80	2.54	2.75	2.99	3.28	2.86	2.66
Nb	12.29	11.60	12.48	13.02	7.64	13.42	8.52	12.56
Ni	694.80	352.82	3480.78	5331.45	3916.41	1316.16	2918.24	3085.52
Pb	3.10	2.00	1.98	3.36	10.32	2.00	16.40	6.79
Rb	2.66	0.83	6.06	10.92	5.66	3.46	4.03	3.48
Sr	1.00	3.42	28.03	28.55	37.65	31.98	18.98	29.45
Th	0.50	0.50	0.50	0.50	0.50	0.50	0.50	0.50
U	0.50	0.50	0.50	0.50	0.50	0.50	0.50	0.50
V	62.28	34.10	101.53	102.00	92.30	82.62	101.14	83.60
Y	14.74	4.36	9.17	6.15	2.65	5.65	3.17	0.60
Zn	49.86	29.72	115.11	119.14	157.59	91.32	102.08	134.67
Zr	14.21	25.59	13.93	6.00	4.45	3.73	2.86	5.50

Table 3: Whole rock data of Borehole TN200

LITHOLOGY	H3	H3	H3	H3	H3
SAMPLES ID	TN200-28	TN200-31	TN200-32	TN200-34	TN200-35
SiO ₂	25.36	37.54	32.62	28.39	41.09
Al ₂ O ₃	2.69	3.19	4.28	4.19	0.02
Fe ₂ O ₃	7.28	8.36	5.26	12.07	0.01
MnO	0.85	0.20	0.23	0.30	1.08
MgO	31.12	10.67	10.71	13.44	15.36
CaO	22.69	21.96	38.92	32.97	35.59
Na ₂ O	0.44	0.80	0.96	2.32	0.69
K ₂ O	0.01	0.01	0.01	0.01	0.01
P ₂ O ₅	0.01	0.02	0.01	0.02	0.02
TiO ₂	0.19	0.37	0.05	0.07	0.12
SO ₃	0.11	0.44	0.26	1.76	0.03
LOI	9.29	16.47	6.70	4.47	6.00
As	0.50	15.20	37.05	52.57	23.57
Ba	59.84	64.82	46.39	58.93	54.00
Ce	131.24	107.41	73.86	193.77	87.35
Co	26.77	87.70	34.34	108.68	12.03
Cu	83.82	670.26	534.72	3466.15	55.90
Mo	0.98	9.19	0.80	0.89	2.50
Nb	8.44	7.31	7.91	8.57	14.38
Ni	191.40	1468.56	838.25	4546.75	81.30
Pb	3.96	0.33	10.38	20.08	2.60
Rb	3.66	1.70	2.93	2.52	1.71
Sr	1.08	14.15	62.82	52.26	10.66
Th	0.50	0.50	0.50	0.50	0.50
U	0.50	0.50	0.50	0.50	0.73
V	36.29	256.95	15.35	25.01	13.00
Y	19.27	11.83	2.14	3.20	2.83
Zn	47.44	47.93	56.07	69.59	29.39
Zr	10.34	31.62	3.20	4.58	16.54

APPENDIX II

FIRE ASSAY (PGE) DATA

BOREHOLE	SAMPLES ID	LITHOLOGY	Au	Pd	Pt
SS339	SS339-25	CS1	0.05	0.05	0.05
SS339	SS339-26	CS1	0.05	0.05	0.10
SS339	SS339-24	CS2	0.09	0.35	0.28
SS339	SS339-28	CS2	0.15	0.93	0.14
SS339	SS339-29	CS2	0.05	0.05	0.05
SS339	SS339-34	CS2	0.08	1.05	0.39
SS339	SS339-31	CS3	0.16	1.28	0.88
SS339	SS339-30	CS3	0.05	0.05	0.05
SS339	SS339-35	CS3	0.13	0.59	0.31
SS339	SS339-9	FP1	0.05	0.05	0.05
SS339	SS339-5	FP1	0.05	0.05	0.05
SS339	SS339-15	FP2	0.05	0.07	0.05
SS339	SS339-7	P2	0.15	1.63	1.43
TN200	TN200-4	FP1	0.19	1.12	0.88
TN200	TN200-5	FP1	0.24	1.93	1.62
TN200	TN200-14	FP2	0.14	0.39	0.45
TN200	TN200-36	H1	0.12	1.13	0.90
TN200	TN200-39	H2	0.07	0.95	0.81
TN200	TN200-40	H2	0.20	1.53	1.30
TN200	TN200-3	P1	0.08	0.75	0.23
TN200	TN200-16	P2	0.05	0.32	0.26
TN754	TN754-17	H1	0.05	0.05	0.05
TN754	TN754-22	H1	0.05	0.05	0.05
TN754	TN754-24	H1	0.05	0.05	0.05
TN754	TN754-27	H2	0.05	0.60	0.42
TN754	TN754-36	H2	0.05	0.03	0.08
TN754	TN754-41	H2	0.05	0.28	0.22
TN754	TN754-40	H3	0.05	0.35	0.43
TN754	TN754-3	P1	0.09	0.16	0.14
TN754	TN754-6	P1	0.05	0.20	0.12
TN754	TN754-8	P1	0.16	0.79	0.24
TN754	TN754-33	P2	0.05	0.06	0.05
TN754	TN754-9	P2	0.05	0.28	0.24

APPENDIX III: ISOCON DIAGRAMS (additional examples)

